NATIONAL AERONAUTICS AND SPACE ADMINISTRATION

Space Programs Summary No. 37-34, Volume III

for the period May 1, 1965 to June 30, 1965

The Deep Space Network

JET PROPULSION LABORATORY
CALIFORNIA INSTITUTE OF TECHNOLOGY
PASADENA, CALIFORNIA

July 31, 1965

NATIONAL AERONAUTICS AND SPACE ADMINISTRATION

Space Programs Summary No. 37-34, Volume III

for the period May 1, 1965 to June 30, 1965

The Deep Space Network

JET PROPULSION LABORATORY
CALIFORNIA INSTITUTE OF TECHNOLOGY
PASADENA, CALIFORNIA

July 31, 1965

Preface

The *Space Programs Summary* is a six-volume, bimonthly publication that documents the current project activities and supporting research and advanced development efforts conducted or managed by JPL for the NASA space exploration programs. The titles of all volumes of the *Space Programs Summary* are:

Vol. I. The Lunar Program (Confidential)

Vol. II. The Planetary–Interplanetary Program (Confidential)

Vol. III. The Deep Space Network (Unclassified)

Vol. IV. Supporting Research and Advanced Development (Unclassified)

Vol. V. Supporting Research and Advanced Development (Confidential)

Vol. VI. Space Exploration Programs and Space Sciences (Unclassified)

The *Space Programs Summary*, Vol. VI consists of an unclassified digest of appropriate material from Vols. I, II, and III; an original presentation of technical supporting activities, including engineering development of environmental-test facilities, and quality assurance and reliability; and a reprint of the space science instrumentation studies of Vols. I and II.

W. H. Pickering, *Director*
Jet Propulsion Laboratory

Space Programs Summary No. 37-34, Volume III

Prepared under Contract No. NAS 7-100, National Aeronautics & Space Administration

Contents

I. Introduction

1. General

The Deep Space Network (DSN) is a precision communication system which is designed to communicate with, and permit control of, spacecraft designed for deep space exploration. The DSN consists of the Deep Space Instrumentation Facility (DSIF), the Space Flight Operations Facility (SFOF), and the DSN Ground Communication System (GCS).

The DSN is a NASA facility, managed by JPL through a contract between NASA and the California Institute of Technology. The Office of Tracking and Data Acquisition is the cognizant NASA office.

It is the policy of the DSN to continuously conduct research and development of new components and systems and to engineer them into the DSN to maintain a state-of-the-art capability.

The DSN has facilities for simultaneously controlling a newly launched spacecraft and a second one already in flight. Within a few months, it will be able to control simultaneously either two newly launched spacecraft plus two in flight or the operations of four spacecraft in flight at the same time. The DSIF is equipped with 85-ft antennas having gains of 53 db at 2300 Mc and a system temperature of 55°K, making it possible to receive significant data rates at distances as far as the planet Mars. To improve the data rate and distance capability, a 210-ft antenna is under construction at the Goldstone Mars station and two additional antennas of this size are planned for installation at overseas stations.

The DSIF utilizes large antennas, low-noise phase-lock receiving systems, and high-power transmitters located at stations positioned around the Earth to track, command, and receive data from deep space probes. Overseas stations are generally operated by personnel of the respective countries. The DSIF stations are:

I.D. No.	Name	Location
11	Goldstone, Pioneer	Goldstone, California
12	Goldstone, Echo	Goldstone, California
13	Goldstone, Venus (R&D)	Goldstone, California
14	Goldstone, Mars (under construction)	Goldstone, California
41	Woomera	Island Lagoon, Australia
42	Tidbinbilla	Canberra, Australia
51	Johannesburg	Johannesburg, South Africa
61	Madrid (under construction)	Madrid, Spain
71	Spacecraft Monitoring	Cape Kennedy, Florida
72	Spacecraft Guidance and Command (under construction)	Ascension Island

The SFOF is located in a three-story building at the Jet Propulsion Laboratory in Pasadena, California, and utilizes operations control consoles, status and operations displays, computers, data processing equipment for analysis of spacecraft performance and space science experiments, and communication facilities to control space flight operations. This control is accomplished by generating trajectories and orbits, and command and control data, from tracking and telemetry data received from the DSIF in near real-time. The SFOF also reduces the telemetry, tracking, command and station performance data recorded by the DSIF into engineering and scientific information for analysis and use by the scientific experimenters and spacecraft engineers.

The DSN Ground Communication System consists of voice, normal and high data rate teletype circuits provided by the NASA World-Wide Communications Network between each overseas station and the SFOF; teletype and voice circuits between the SFOF, Goldstone Stations, and Cape Kennedy; and a microwave link between the SFOF and Goldstone, provided by the DSN.

2. DSN Utilization Scheduling System

The DSN Utilization Scheduling System has been developed for management and control of DSN usage. This comprehensive and integrated scheduling process provides the means for maximizing the use of the DSN, the equitable allocation of limited facilities in accordance with the established policies and priorities, and the defining in detail of the commitments to the various users.

a. Description. The basic DSN Utilization Scheduling System is one of request, review, and allocation. (Fig. 1). Potential users of DSN facilities define their requirements on special forms and submit them at established intervals to the DSN. The DSN consolidates the various requests, compares the requirements with available capabilities, and makes an allocation of the facilities. A composite schedule is prepared which indicates these allocations, and it is released by the DSN to all requestors and elements of the DSN. It will be the only document authorizing use of the facilities, and as such, will provide a comprehensive set of common guidelines for all operating elements of the DSN.

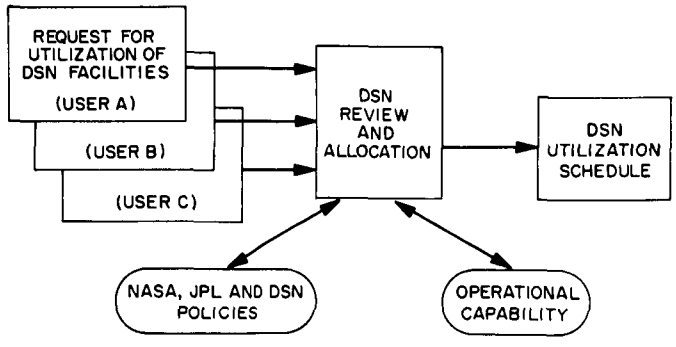

Fig. 1. DSN utilization scheduling system

Three different time bases and level of detail are employed in this system in order to provide a degree of resolution consistent with the accuracy of the requirements and the needs for scheduling specifics. For the long-range scheduling a time base of months is used, intermediate scheduling is by weeks, and the immediate activities are reflected on a daily basis. The three resultant schedules are: (1) 16-mo, (2) 12-wk, and (3) 10-day.

The 16-mo schedule provides a broad, long-range view of DSN utilization. It has a minimum number of line items which are scheduled on a days-per-month basis. It provides a gross allocation of facilities and guidance for the development of the more detailed 12-wk schedule.

The 12-wk schedule provides a detailed view of forthcoming activities. It has sufficient line item detail to permit interleaving of several users at one time and employs a time base of hours per week. This schedule provides the guidelines for the 10-day schedule and is a primary document for use and operation of the DSN.

The 10-day schedule is the sequence of events for the immediate weekly period. It specifies the exact periods of use in hours and minutes and is in sufficient detail to define all operational activities.

These three schedules are phased and sequenced in a manner which will allow the step-by-step movement into greater detail as needed. It should be noted that the 16-mo schedule does not cover the immediate two to three months which are part of the 12-wk schedules, but, rather, it is associated with the monthly periods beyond 12 wk.

b. Schedule organization. The DSN Utilization Schedules are divided into three parts: SFOF, DSIF, and GCS. These parts, in turn, are subdivided into various categories and line items which are consistent with the composition of these elements and their mode of operation.

II. Tracking Stations Engineering and Operations

A. Goldstone Operations

The tracking of the *Mariner IV* spacecraft was the primary activity at Goldstone after the successful completion of the *Ranger* Program. The Echo Station, which had maintained full operation status in the L-band system for the *Ranger* Program, concentrated on the installation of the S-band system for additional backup to the Pioneer Station during the Mars encounter and subsequent tracking. In addition, the Venus Station halted its planetary radar experiments and stood by for high-power command backup to the Pioneer Station.

1. Mariner IV Operations

a. Pioneer Station. In May and June the *Mariner IV* tracking progressed satisfactorily. The prototype S-band system, installed in the east annex building (*SPS 37-27*, Vol. III, pp. 5–11), was in continual operation since the launch of *Mariner IV*, except for the brief time the antenna was in use with the L-band system for tracking *Ranger VIII* (*SPS 37-32*, Vol. III, pp. 4–5), and *Ranger IX*. Early in the *Mariner* track, the operation settled into a routine procedure, and periodically, as the distance to the spacecraft increased, a command loop between DSIF-11 and the spacecraft was established for training and for providing a continuous tracking capability.

b. Venus Station. Since May 1, 1965, the Venus Station was operational in a transmit-command capacity for *Mariner IV* backup. During scheduled weekly operations, two-way coherent doppler and three-way noncoherent doppler was established between the Pioneer Station and the Venus Station, and three-way noncoherent doppler between the Pioneer, Venus, and Tidbinbilla Stations. Although original plans called for a high-power command capability for *Mariner IV* backup (*SPS 37-28*, Vol. III, pp. 12–13), the Venus Station modified its 100-kw cone transmitter assembly to include a 2295-Mc traveling wave maser. With associated conversion equipment, the Venus Station had the additional capability of receiving *Mariner IV* signals with the standard 2388-Mc receiver. Operation was limited to transmitting only, or to a receiving only operation pending development of a 100-kw diplexer.

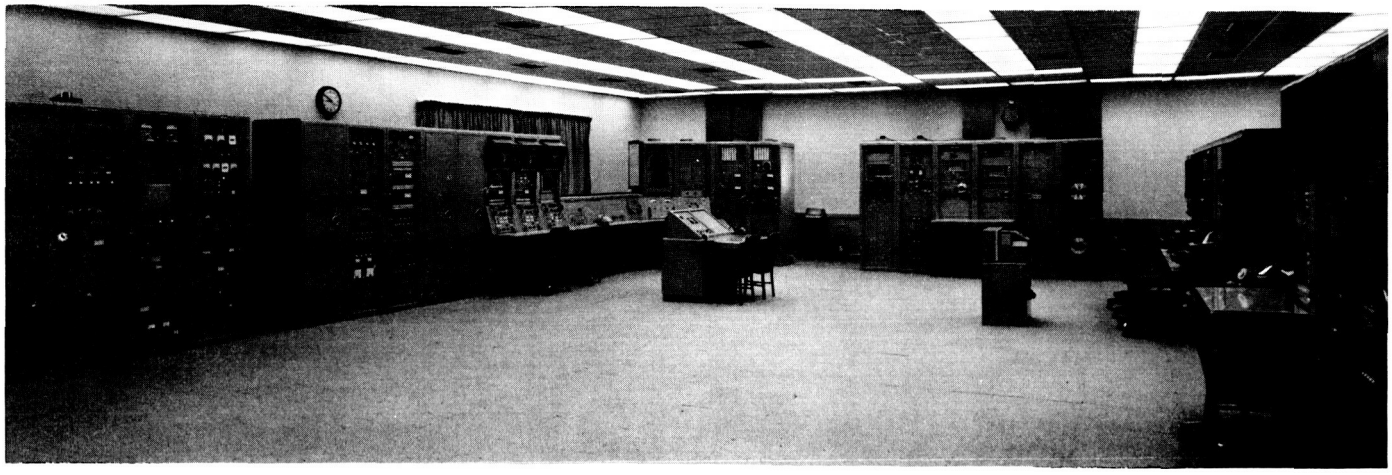

Fig. 1. The Echo S-band control room

c. Echo Station. The installation of the Echo S-band system (Fig. 1) was completed in June except for some interfaces with the digital instrumentation equipment. System tests were to be performed until approximately July 6, at which time the Echo Station would operate as a backup station for *Mariner IV*.

During the conversion from L-band to S-band, all cabling associated with the L-band was removed from the control room and the antenna. New cable trays were installed from the basement of the new control room, through the interconnecting tunnel to the hydromechanical building, and then overhead to and on the antenna. The recabling included the S-band klystron coolant lines, the traveling wave maser cryodyne lines, and all electronic signal and control lines.

Because time requirements for *Mariner IV* backup precluded installation of the standard Dec wheel equipment room, one of the old equipment cages on the antenna was reworked for the receiver assemblies, and the transmitter was mounted in the same location as the L-band transmitter. Otherwise, the antenna remained unchanged. The new S-band electronics equipment was installed in its permanent configuration in the control room. The maser and the parametric amplifier received extensive inspection, cleaning, and testing before being installed in the S-band cone. All cryodyne lines were pressure tested with a series of sustained operations in both static and dynamic conditions. The maser was installed in the antenna-mounted cone and cooled down in mid-June for an operational test, holding steady at 4.5°K.

2. Station Activities and Projects

a. Pioneer Station. Three S-band systems have been tested: the original system used by Pioneer for the *Mariner IV* track, the Tidbinbilla system, and the Madrid system. Two additional systems, one for Ascension Island and one for Woomera, are in process of installation and testing.

Personnel from Australia who will install and operate the Woomera S-band equipment are at Goldstone receiving training in the installation, operation, and maintenance of the system. The training in the S-band system was to be augmented by practical operation with the Pioneer *Mariner IV* operations during a scheduled track of the spacecraft.

The Ascension Island Station will provide additional early tracking of a spacecraft after launch from Cape Kennedy and prior to its acquisition by one of the standard DSIF Stations. Equipment for the station is being assembled and tested at Pioneer by the Ascension Island personnel. This station is primarily a receiving station; however, a full 10-kw, 2115-Mc transmitting capability utilizing a 30-ft azimuth-elevation antenna is incorporated. No *read-write-verify* command equipment nor telemetry demodulation equipment is required at this station. Received spacecraft telemetry and antenna tracking data will be transmitted to Cape Kennedy and then to the SFOF in real-time.

Continuing at the Pioneer Station is the ground support system installation for the *Surveyor* Program. Tests

have been conducted on the command and data handling console, and the interfaces with the Pioneer digital instrumentation equipment. Compatibility tests between the *Surveyor* equipment and the S-band system were conducted during the times the Pioneer Station was not involved in actual *Mariner* tracking. The former *Ranger* control room was prepared with a raised floor for installation of the *Surveyor* spacecraft TV ground data-handling equipment. In addition, a darkroom was prepared for processing of film. An enlarged screen room (Fig. 2) was erected at the Goldstone Microwave Test Facility for installation of a *Surveyor* test model, which will be used in simulated flight, lunar landing, and postlanding tests. For these tests, the Pioneer Station S-band equipment and the *Surveyor* ground control equipment will be used.

b. Echo Station. Installation of the Pioneer probe ground control equipment was completed in the Echo Station control building. Interface tests between the Pioneer Mission Dependent Equipment (MDE), the digital instrumentation equipment, and the analog instrumentation equipment were conducted. These included a test run of a taped, simulated *Pioneer* tracking mission. Additional testing with the S-band system was scheduled for those times between system tests, *Mariner IV* testing, and backup tracking.

Implementation of a Goldstone Primary and Secondary Standards Laboratory has begun at the Echo Station. Traceable to the National Bureau of Standards, the Primary facility will perform calibrations of inspection, testing, and laboratory working level equipment, tools, and devices. Standards equipment used by the overseas DSIF stations and the Cape Kennedy facility will be certified by the Goldstone Laboratory.

The Goldstone Laboratory is being implemented in a building block program to provide for acquisition of the recommended standards over a period of 12 to 18 mo, yet provide a facility capable of functioning as a certification source at inception. Twelve hundred square feet in the west end of the Administration and Engineering building have been allocated for the laboratory's location, and preliminary installation of the Standards hardware has begun.

3. Construction

a. Pioneer Station. The 30-ft Az-El mockup antenna is nearing completion (Fig. 3). Static equipment installations will be performed on this antenna for determination of mounting and location.

b. Echo Station. Construction of the two prefabricated steel supply storage buildings (Fig. 4) is essentially completed. Building G-41 (the larger building) is being used as a supply warehouse, and building G-42 (the smaller building) is being used for maintenance and storage.

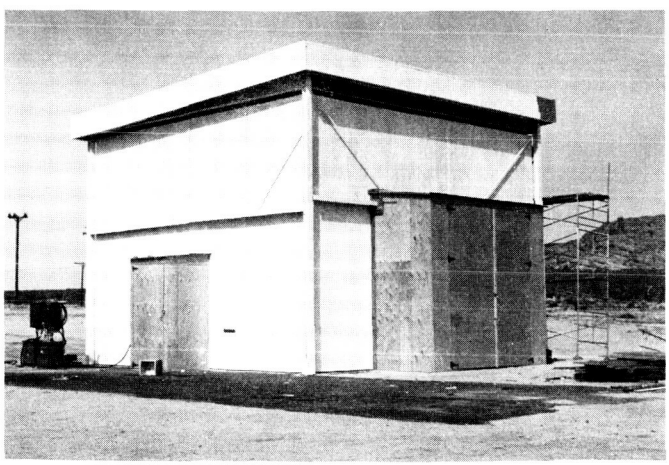

Fig. 2. Spacecraft screen room

Fig. 3. Pioneer 30-ft Az-El antenna

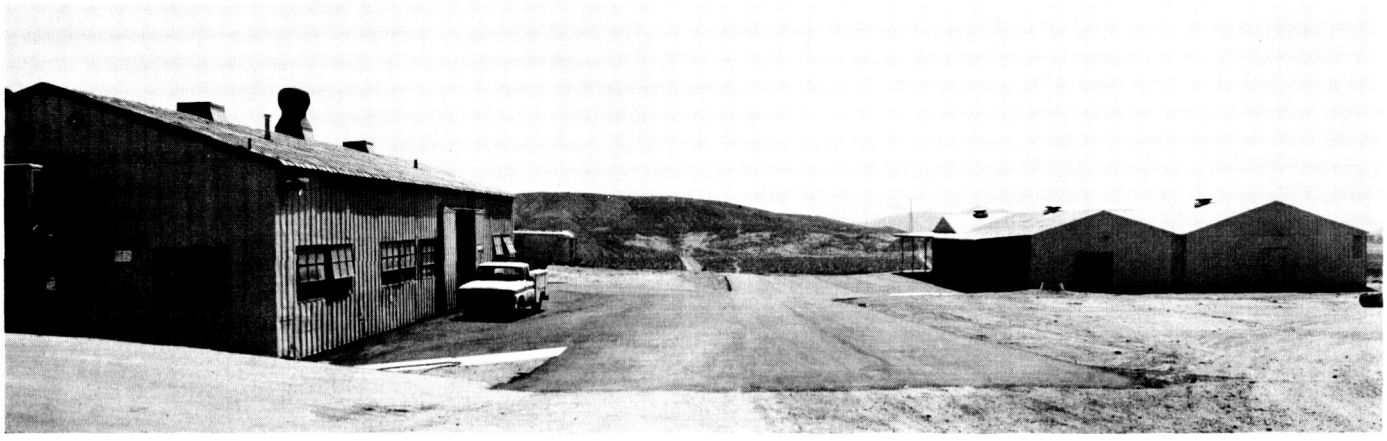

Fig. 4. Echo supply and storage buildings

B. Advanced Antenna System

1. Construction

Construction of the 210-ft D advanced antenna system (AAS) is continuing at the Goldstone Mars Station. Work progress has been reported regularly in the *SPS*, with a series of discussions concerning major components of the system. Progress toward completion of the project continues in a satisfactory manner, and indications are that the scheduled project completion date of June 1, 1966 will be met. Fig. 5 shows the on-site construction progress as of May 19, 1965.

Fabrication and on-site installation of the antenna structure and drives are being accomplished under subcontract to Rohr Corp., Chula Vista, Calif. All major components of the structure have been delivered to the Mars Station except the feed cone and subreflector. The fabrication of the panels for the primary 210-ft D reflector is nearing completion, and progressive deliveries to the site are being made.

Structural steel has been erected to a point including the intermediate ribs of the primary reflector structure. Erection of the cantilever, or outer, ribs is in progress.

Procurement and fabrication actions are being taken for the S-band electronic subsystems required for space operations of the antenna. The fabrication of the precision angle data subsystem (master equatorial) is under way at various locations. Installation of the electronic components is scheduled to begin in November 1965, upon completion of the AAS structure and drives.

Fig. 5. On-site construction, May 19, 1965

Fig. 6 is a photograph of the center hub of the AAS being lifted into place. The erected center hub rests directly on the tie truss between the two elevation bearings. This hub will support the feed cone and will house the optical instrument for monitoring the reflector surface. The primary reflector rib trusses radiate from the center hub.

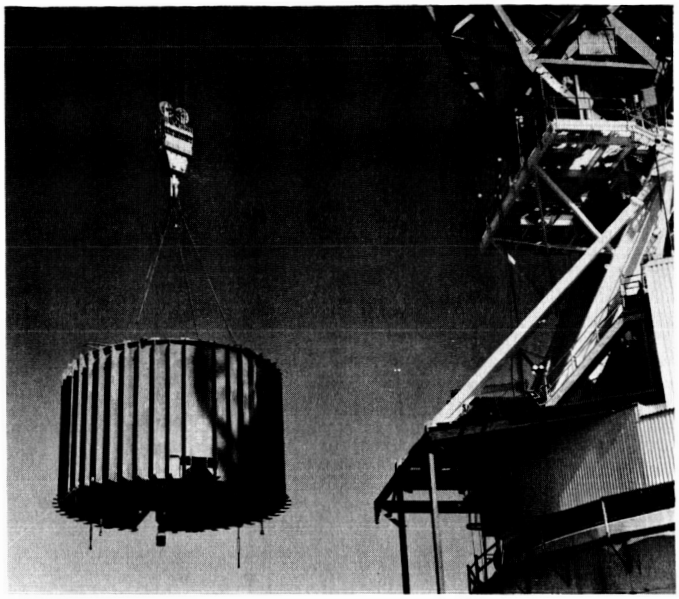

Fig. 6. AAS primary reflector center hub

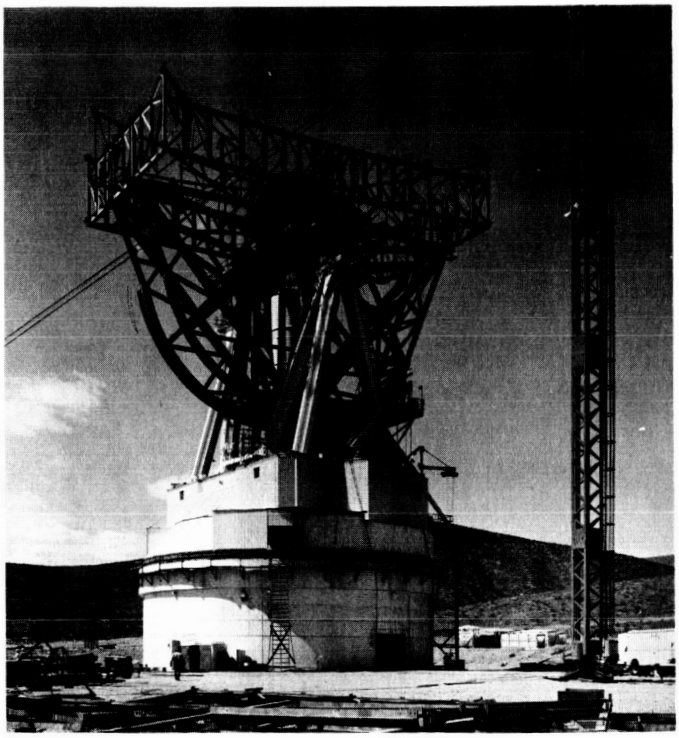

Fig. 7. AAS rectangular girder of the primary reflector structure

Fig. 7 shows the AAS with the center hub and rectangular girder of the primary reflector installed. The rectangular girder supports the primary reflector rib trusses. The vertical members of the girder are also vertical members of the rib trusses. The AAS quadripod, which supports the subreflector, will be attached at the corners of the rectangular girder.

The installation of the inner and intermediate ribs of the primary reflector structure is shown in Fig. 8. The inner ribs are that portion from center hub to the rectangular girder. The intermediate ribs extend from the rectangular girder to the 56-ft radius of the reflector structure.

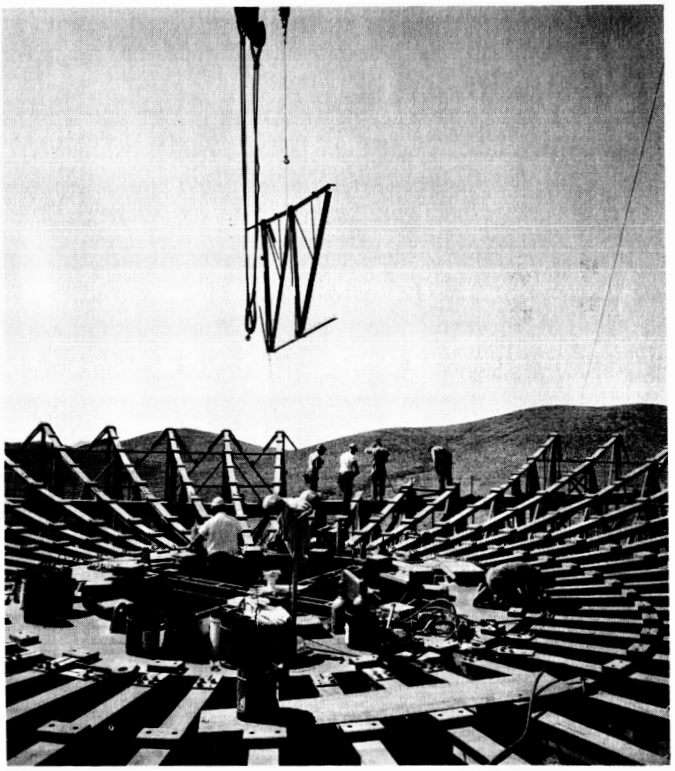

Fig. 8. Primary reflector inner and intermediate ribs

Sections of the cantilever, or outer, ribs were assembled on the ground and are now being installed as part of the reflector structure. Fig. 9 is a photograph of an assembly of three cantilever ribs being prepared for erection. The cantilever ribs will extend the reflector radius to 105 ft. For safety of personnel working on the structure, safety nets are being installed below the cantilever ribs.

2. *Primary Reflector Surface Panels*

The reflector surface is composed of 552 aluminum panels. These panels extend from a radius of 10.25 to 105.0 ft. The inner four rows of panels are solid, and the outer four rows are 51% porous. Fig. 10 is a plan view

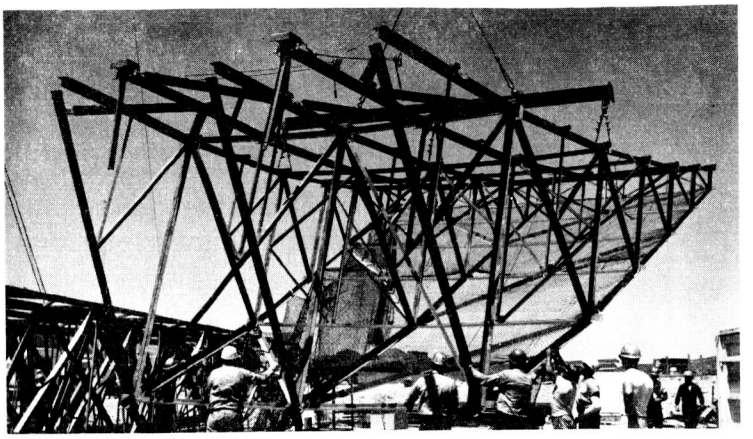

Fig. 9. Section of AAS cantilever ribs

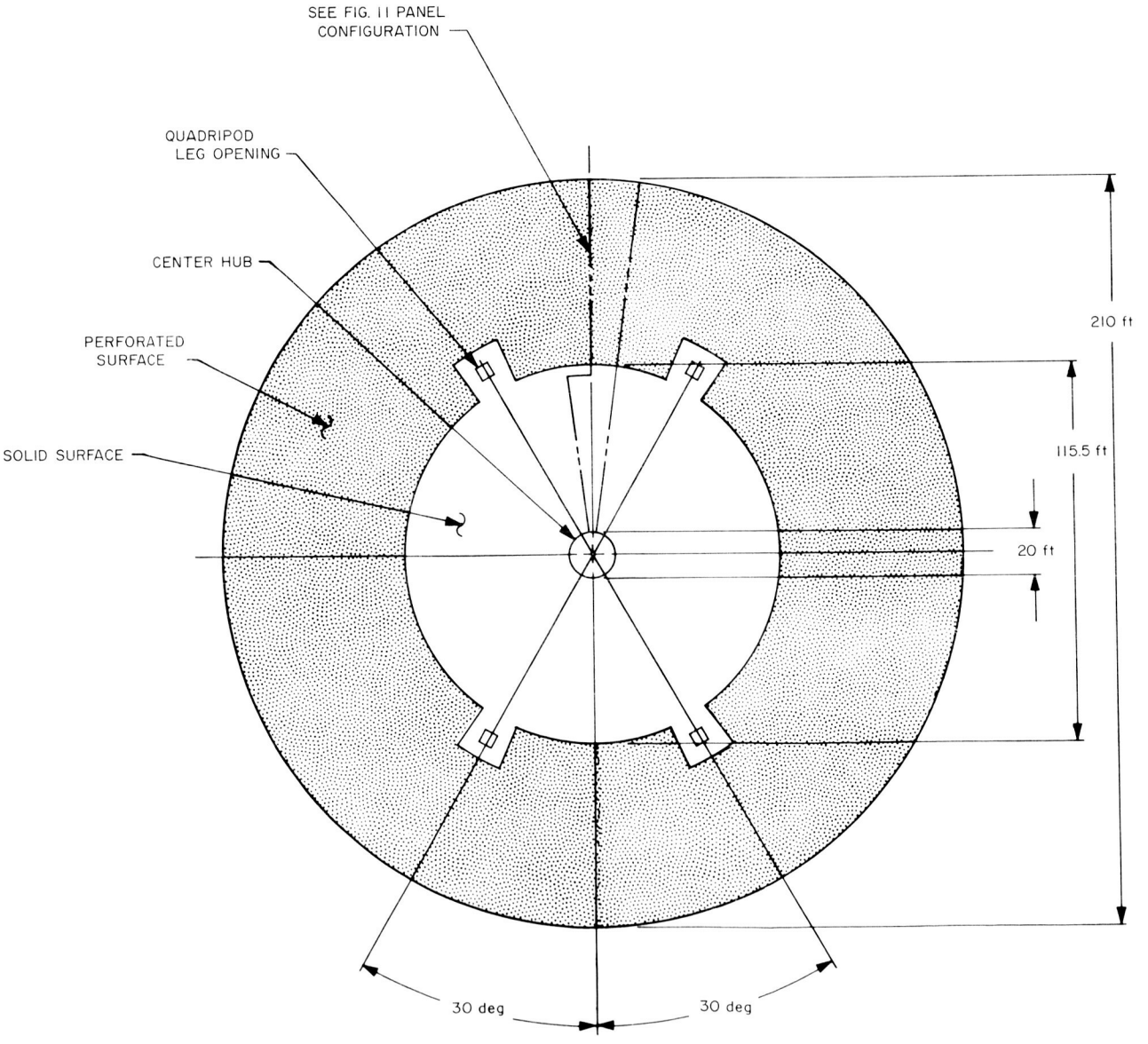

Fig. 10. Reflector plan

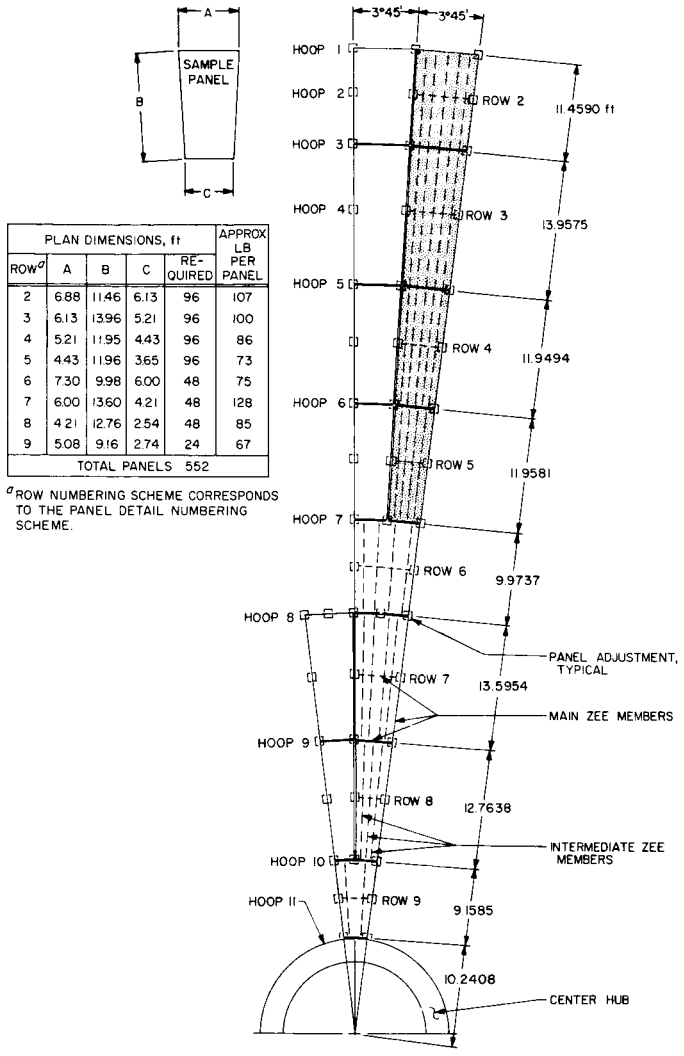

PLAN DIMENSIONS, ft					APPROX LB PER PANEL
ROW[a]	A	B	C	RE-QUIRED	
2	6.88	11.46	6.13	96	107
3	6.13	13.96	5.21	96	100
4	5.21	11.95	4.43	96	86
5	4.43	11.96	3.65	96	73
6	7.30	9.98	6.00	48	75
7	6.00	13.60	4.21	48	128
8	4.21	12.76	2.54	48	85
9	5.08	9.16	2.74	24	67
TOTAL PANELS 552					

[a]ROW NUMBERING SCHEME CORRESPONDS TO THE PANEL DETAIL NUMBERING SCHEME.

Fig. 11. Detail panel configuration

of the 210-ft reflector surface, and Fig. 11 is a 7°30′ angular segment, showing the panel numbering scheme and approximate panel sizes.

The surface panels utilize 6061-T6 aluminum "zee" members riveted together with angle brackets. The 6061-T6 aluminum skin is riveted to the zee framing members. Fig. 12 shows a typical panel cross section. The panels are attached to the reflector structure by ball-socket adjustment screws. The panel attachment points are reinforced by an aluminum alloy casting with a threaded insert. The adjustment screw is attached to the reflector structure by a panel support clip that is welded to the top chord of the reflector rib truss. Fig. 13 details the relationship of the panel, panel adjustment screw, and the reflector structure.

The surface panels were manufactured on special assembly fixtures contoured by numerical control machining. The skins were placed on the assembly fixture and the stretch-formed zee framing members were clamped and temporarily affixed to the skin. The riveting of the zee members and the skin is done on the Drivematic riveting machine. The panels are cleaned, primed, and painted before crating and shipment to the site.

The surface panels are carefully checked for surface accuracy after the riveting is complete. A Cincinnati Milling Machine has been instrumented to read the surface panel deviations from a perfect panel surface, taking one error reading for every 100 in.^{2} of panel surface. The number and magnitude ranges of the recorded errors are set for each panel and are the basis for quality control acceptance of each panel.

Panel adjustment in the field will be achieved by rotating the adjustment screw from the dish surface. The small hand tool shown in Fig. 12 will be used to raise or lower the panel, as required.

3. Feed for AAS

a. Introduction. Reports of the 16-Gc 1/7-scale model program for the Advanced Antenna System feed development have appeared in previous issues of *SPS*, Vol. III. Discussions included the feedhorn and Cassegrain radiation characteristics (*SPS 37-29*, Vol. III, pp. 109–112; *SPS 37-32*, Vol. III, pp. 75–80) and the secondary radiation patterns and far-field gain of the Goldstone Venus 30-ft reflector (*SPS 37-30*, Vol. III, pp. 110–115). During the month of May 1965, the 30-ft reflector was used for Phase II studies of the AAS model. Phase II studies include the use of a carefully modeled quadripod structure on the 30-ft reflector, intended to duplicate the complex scattering structure present on the 210-ft prototype (*SPS 37-31*, Vol. III, p. 99).

During the May 1965 test period a far-field absolute gain measurement using the high-efficiency low-noise dual mode listening feed was performed, and a large number of far-field radiation patterns for both the listening feed and the monopulse tracking feed were obtained.

This reporting will update the reader on recent modifications to the 30-ft reflector, as significant to RF performance, as well as discuss the Tiefort Mountain Venus Station propagation path and will describe the absolute gain measurement.

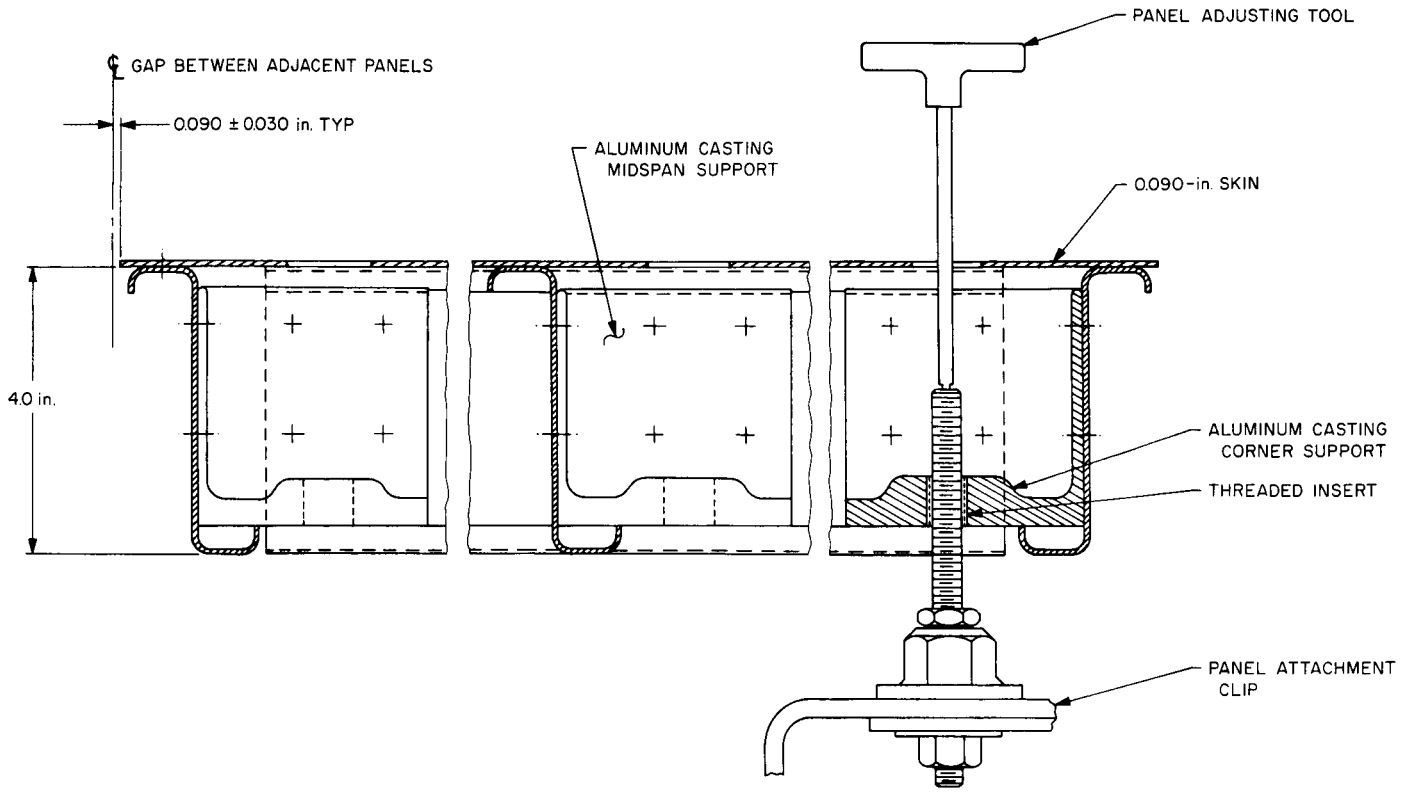

Fig. 12. Typical section of panel and adjustment screw

b. Antenna configuration modifications. Among several modifications made on the Goldstone Venus Station 30-ft reflector recently (see Sect. D), the two most important, in terms of RF performance, are: (1) the installation of an accurately scaled model quadripod, and (2) the adjustment of the parabolic surface to provide a horizon-look perfect surface.

Model quadripod. The quadripod has been installed on the Venus 30-ft reflector in order to provide RF performance (radiation patterns and gain) identical to that of the 210-ft AAS. Figs. 14 and 15 are photographs of the reflector, before and after installation. Four holes in the reflector panels previously used with the old quadripod have been patched, using subpanels of appropriate contour. Figs. 16 and 17 are photographs of the apex region showing the precision Cassegrain hyperboloid positioner capable of remote axial and tilt motions for focussing and boresighting. In these figures, the beamshaping flange is attached, and the vertex region shows the location for mounting optical equipment or vertex matching plates. Fig. 18 is a closeup photograph of one of the truss-type quadripod members, showing the size and complexity of construction.

Parabolic surface. As documented in the last issue, the 30-ft reflector panel positions have, in the past, been optically adjusted to provide a true paraboloid at zenith attitude. If one considers a plane normal to the reflector aperture plane and at right angles to the two hard attach points, i.e., the elevation bearings, it becomes apparent that the deflections in this plane with the reflector at the zenith attitude are likely to be greater than those in an orthogonal plane across the elevation bearings. This is precisely the case with the 30-ft reflector, causing the zenith attitude perfect surface adjustment of the panels to produce variations in spacing between the backup structure and the panel attach points. In other words, there is a 1-cycle circumferential variation in the dZ direction for the backup structure but not for the surface panels.

With the reflector oriented to the horizon-look attitude, the above-mentioned circumferential variation in dZ becomes apparent because of orthogonal gravity loading.

Because collimation tower data are obtained at essentially the horizon (less than 1-deg elevation), the behavior of the backup structure-surface combination, which

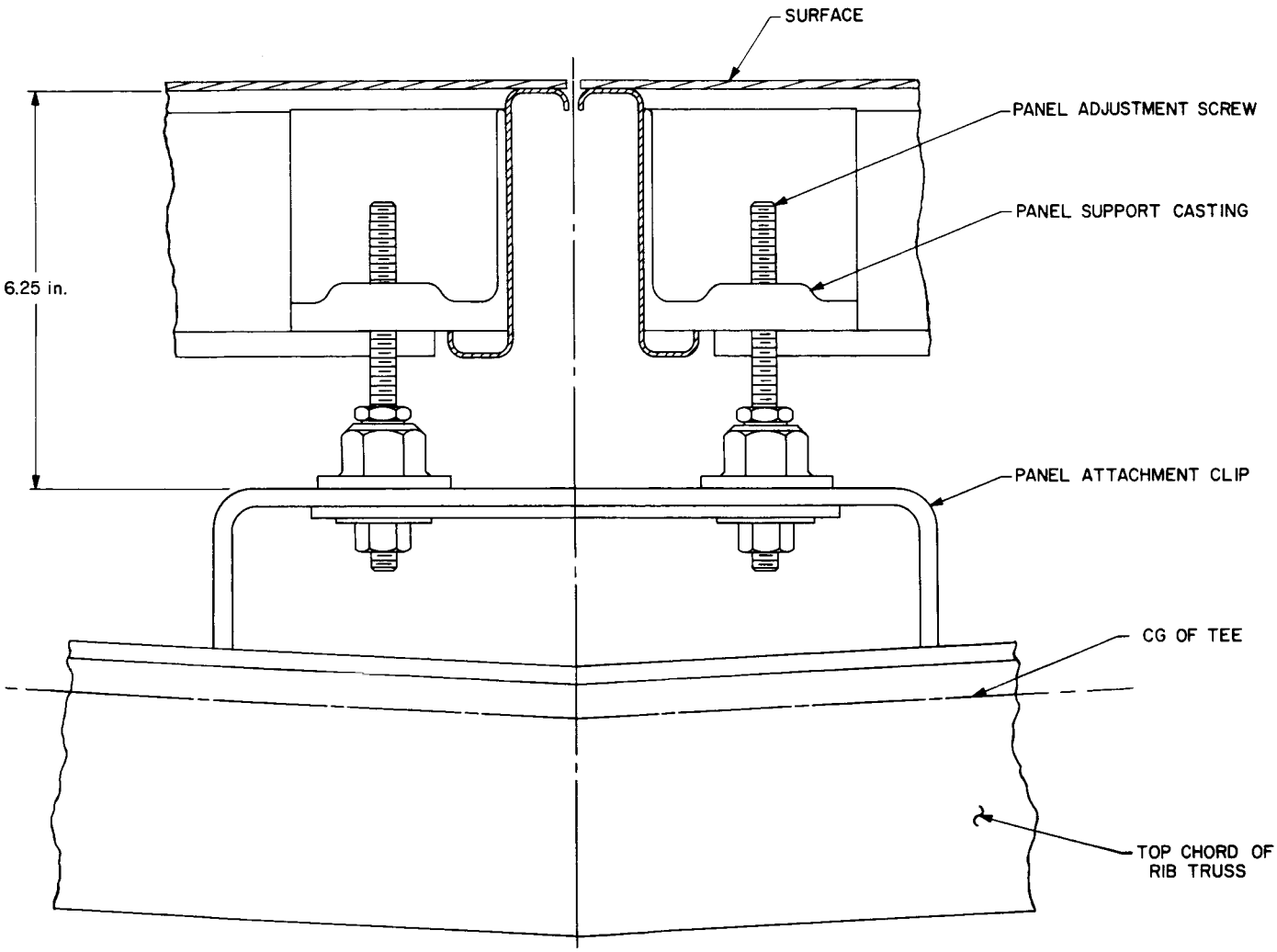

Fig. 13. Relationship of surface panels to rib trusses

produces an astigmatic surface, must be considered. Recently available data have been provided by Dr. C. Lawson's elliptic cross section best-fit paraboloid computer program.[1] Using the elliptic best-fit it was found that a 0.200-in. difference exists between the horizontal and vertical plane focal lengths for the contour maps presented in *SPS 37-33*, Vol. III. A value of 0.200 in. represents an increment $\delta = 0.28\lambda$ at the model frequency. If we assume a virtual (focal point) feed at the paraboloid foci, best-fitted between the azimuth and elevation planes, the approximate path length error at the rim is given by

$$\Delta\lambda = \pm \frac{\delta}{2} \cos \Psi$$

where Ψ is the aperture edge angle. For a 62-deg-edge angle this becomes $\pm 0.066\lambda$ or ± 0.048 in. at the model frequency. In *SPS 37-33*, Vol. III, ± 0.045-in. half path-length peaks were reported.

It should be mentioned that the 30-ft reflector experience reported previously is to be considered the extreme case of circumferential deflections. This is because of the full 90-deg change in elevation angle between panel adjustment attitude and horizon attitude surveys and/or RF data. Better all-attitude performance can be effected by panel adjustments performed at some intermediate elevation angle, 45 deg for example.

In order to obtain more readily interpretable data using the AAS model at the horizon-look attitude, i.e., avoid

[1]A. C. Ludwig, private communication.

the astigmatism found previously, the decision to adjust panels for a true paraboloid at horizon was made. While not discussed in this reporting, all indications show that an extremely close-tolerance setting was realized. Indicators of high-quality paraboloidal surface characteristics are taken to be the simultaneous occurrence of deep nulls in the far-field ($> 4D^2/\lambda$) radiation patterns with maximum far-field gain, as the system was focussed during the RF test period.

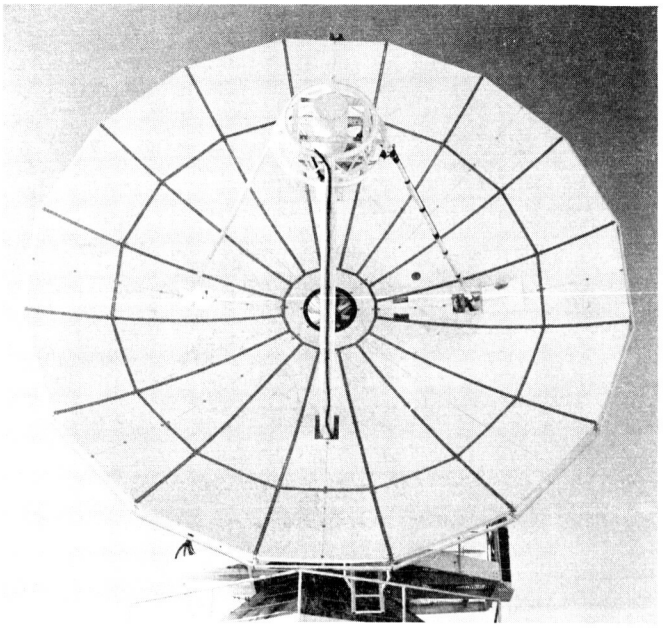

Fig. 14. 30-ft reflector before modification

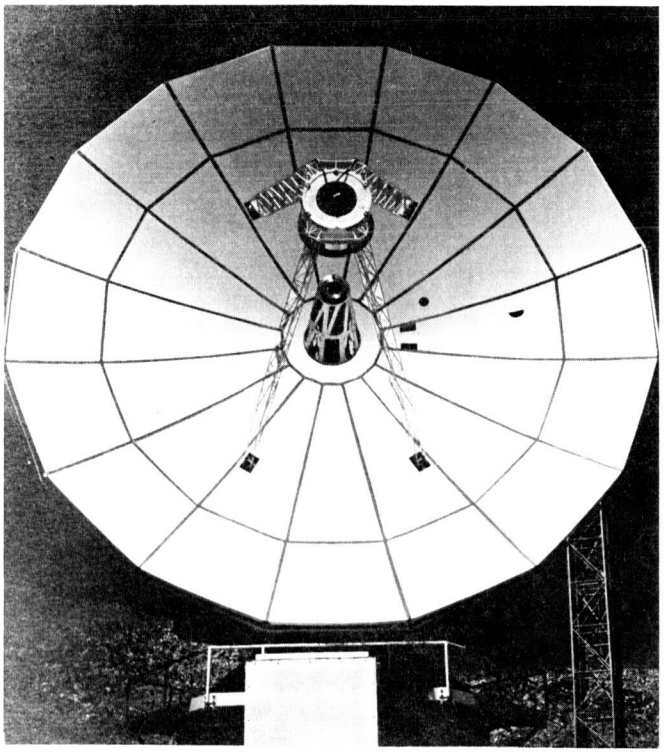

Fig. 15. 30-ft reflector after modification

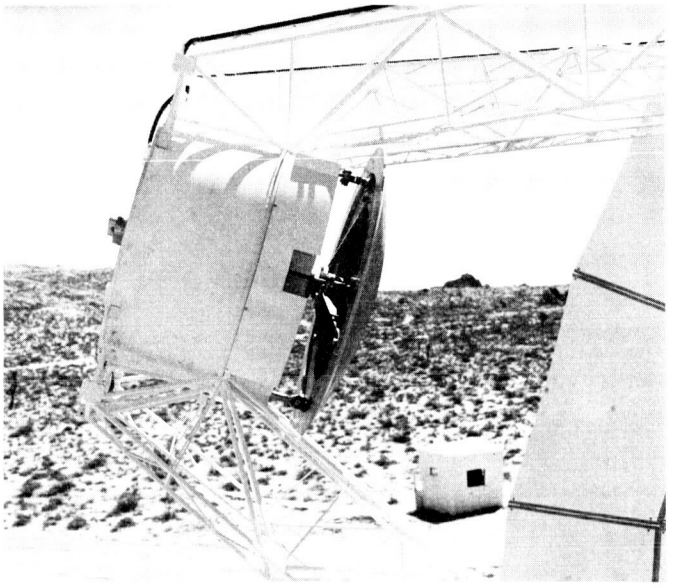

Fig. 16. Scale quadripod apex region

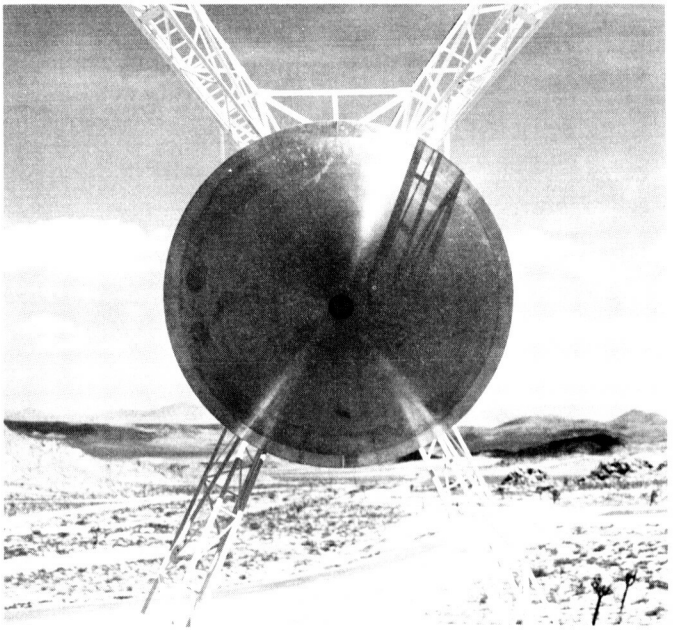

Fig. 17. Scale hyperboloid

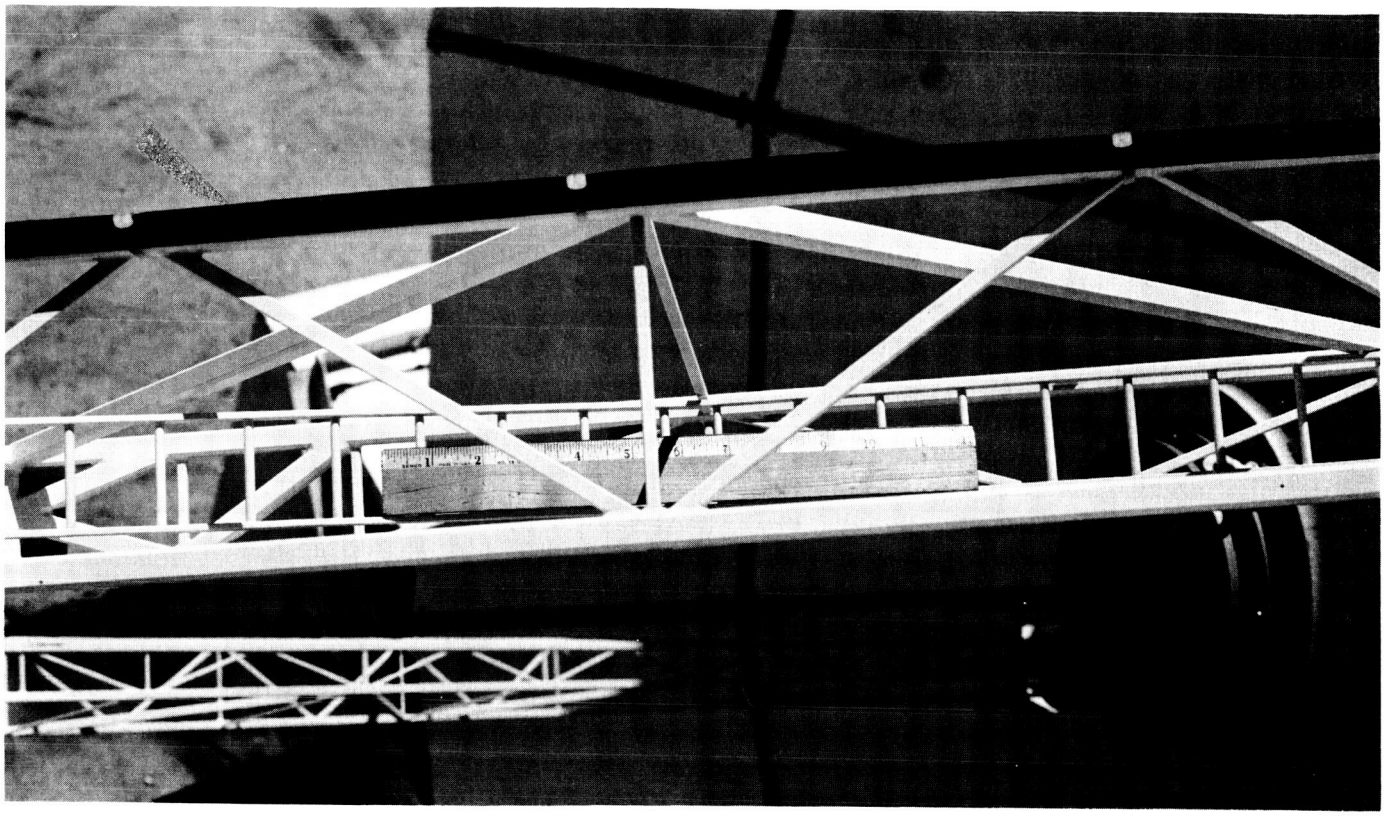

Fig. 18. Scale quadripod truss section

Following quadripod installation and paraboloidal surface adjustment at the horizon attitude, the Cassegrain hyperboloid was centered and autocollimated in the horizon-look attitude, using the same reference plane as the paraboloid survey. In summary, it is felt that an extremely accurate, horizon-look optimized system was made available for test.

c. Tiefort Mountain Venus Station. The Goldstone Venus Station–Tiefort Mountain path profile, based on a flat Earth, and exaggerated vertically, is shown in Fig. 19. The receiver site, at 3500 ft above sea level, is separated from the transmitter, at 4600 ft, by a depressed region containing Bicycle Lake (dry). Access to Tiefort Mountain is accomplished by helicopter only. Because of the depression, the averaged path altitude is in excess of 1000 ft. Generalized weather conditions for this area of the high desert for this time of year (April and May) include warm sunny days (80 to 90°F), moderate nights (50 to 60°F), with prevailing westerly moderate to gusty ground winds (0 to 40 knots). Relative humidity is typically low during daylight (10 to 20%) and moderate at night (30 to 50%).

Experience gained over the past 3 yr with the Tiefort Mountain-Venus path using the 30-ft reflector at 8.5, 16.3 and 22 Gc includes occasional difficulty with signal scintillation. In the past these difficulties have been generally attributed to equipment instabilities. During the last test period, instrumentation problems were eliminated as a possibility. This was accomplished by increased experience in using an amplitude leveling feedback loop within the signal source, crystal control of the source frequency, a variety of receiver schemes, and by a comparison of low-gain and high-gain illuminator antenna performance during gusty winds. In addition, critical items have been battery-operated. Mechanical (e.g., antenna pointing) and electrical instabilities at the Mount Tiefort facility were, in this case, insignificant. Pointing stability of the 30-ft antenna at 16 Gc was also eliminated as a significant factor.

Figs. 20 and 21 are strip chart recordings, using a 1-cps response recorder, of the 16-Gc received signal at the Venus Station on May 11, 1965. Fig. 20 at 13:00 PDT, shows approximately 0.15 db peak-to-peak fluctuations, while Fig. 21, at 20:00 PDT, shows quiescient behavior, approximately 0.05 db peak-to-peak. Either case is considered a quite useful signal for most purposes. Unfortunately, this behavior is not always available; indeed, 3.0-db peak-to-peak scintillations have been observed, at

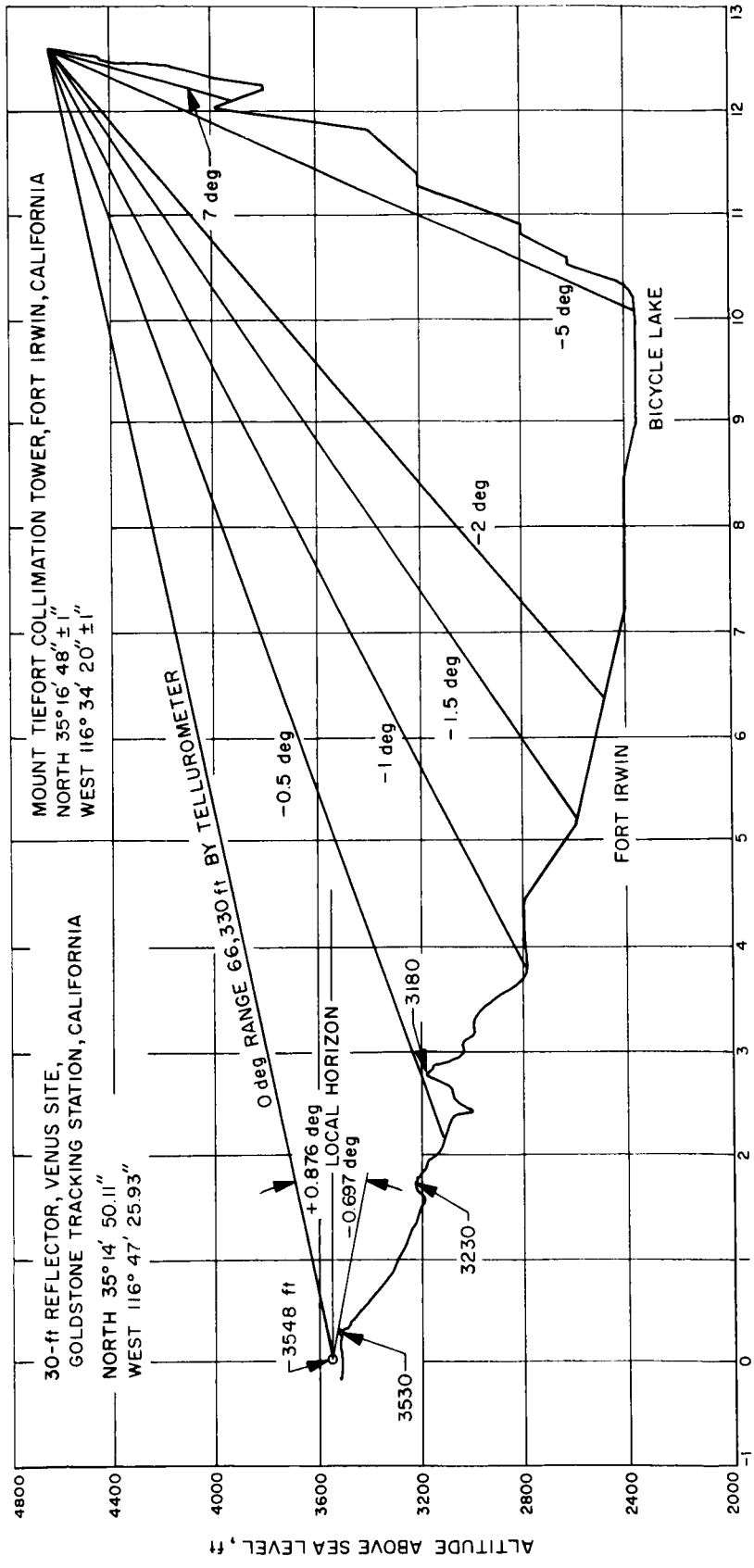

Fig. 19. Goldstone Venus Station, Tiefort Mountain path profile

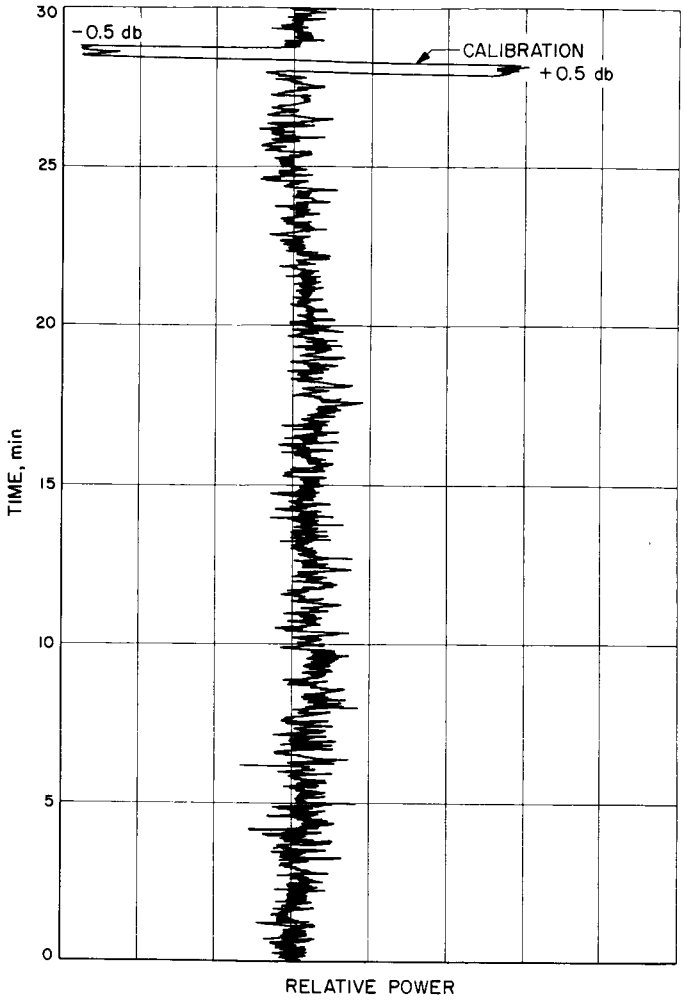

Fig. 20. Received signal level, 16 Gc, 13:00 PDT

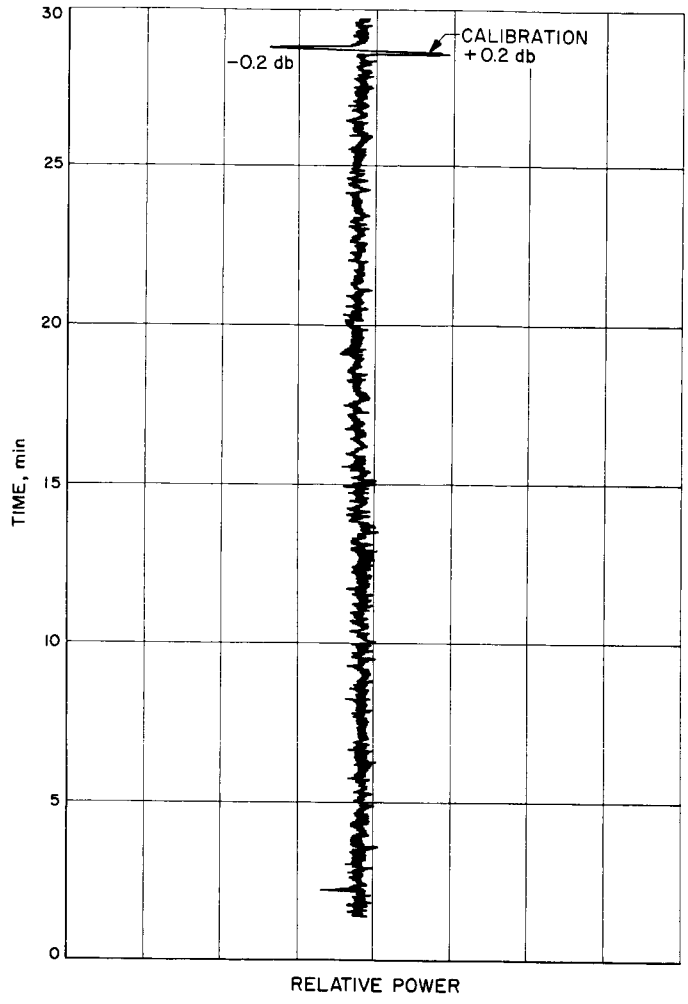

Fig. 21. Received signal level, 16 Gc, 20:00 PDT

both 8.5 and 16.3 Gc on various occasions. Qualitative attempts to correlate this behavior with weather conditions are completely inconclusive; however, no real attempt to instrument meteorological data has yet been made.

d. Gain measurement. Early in the use of the Venus-Mount Tiefort path the decision was made to abandon the usual substitution-type gain measurement, wherein a relatively broad-beamed (10 to 20 deg) standard gain (20 to 25 db) horn reference is used at the receiver site. As Fig. 19 shows, a broad-beamed horn at the Venus Station would suffer extreme sensitivity to multipath. The method decided on (absolute space loss method) requires accurate knowledge of the physical separation, about 12.7 miles. This was conveniently and accurately obtained by a ranging Tellurometer measurement; thus, the gain measurement is to be considered dependent on the absolute space loss, −142.82 db, referred to isotropic collectors. An additional atmospheric dissipative loss factor of −0.68 db was calculated using work based on Van Vleck (Ref. 1) and represents nearly equal contributions due to the oxygen and water vapor molecular absorptions. Standard atmospheric conditions were assumed; i.e., a water vapor content of 7.5 g/m^3. Relative humidity-temperature data for the period indicates a range of 2.0 to 7.0 g/m^3, the higher water content occurring during the gain measurement period.

Also, early in the test program the desirability of using a relatively high received power level, approximately 0.1 mw, was decided on. The advantage obtained allows the use of an insensitive thermistor-type power sensor as a transfer standard between transmitter and receiver sites. The transmitter output, when decoupled, can be determined using the same instrument, thus eliminating the requirement for absolute microwave power measurement accuracy. Linearity is required instead, in this case about

20 db. This method is available at the expense of a high-power source or a high-gain illuminator in order to provide the required effective radiated power (ERP).

A relatively high-gain (45 db) illuminator was selected on the basis of 1 w of available source power. The illuminator selected is a high-quality machined aluminum paraboloidal casting, 48-in. D, providing 1.0 deg half-power beamwidth. Special attention was given to mechanical stability of the feed and mounting brackets; the final configuration is a Cassegrain feed providing a conveniently located feeding port. A carefully calibrated (Ref. 2) low sidelobe dual mode reference horn is bracketed and collimated with the high-gain antenna allowing on-site gain calibration of the high-gain unit by gain differencing the two. This method was considered essential, since the rigors of helicopter transport were considered to induce distrust of the previous 48-in. paraboloid gain calibration.

Fig. 22 shows a block diagram of the transmitter equipment. Power output to each illuminator antenna was determined, using a variable attenuator having high precision but unknown accuracy as a transfer standard. The use of this method with the highly linear thermistor units available[2] has been described in *SPS 37-33*, Vol. III, pp. 69–81. The attenuator used for power output determinations was also used during the illuminator gain difference tests. Using the predicted ($\approx$20 db) gain difference between illuminators inserted in the attenuator which is in the high-gain arm, the receiver at the 30-ft reflector is monitored. The attenuator is adjusted for equal received signals from each illuminator; at this time producing approximately 1 μw received level. At equal received signals the ERP of the gain standard is equal to the ERP of the high-gain illuminator, and the high-gain antenna gain value is obtained.

During the course of the gain difference determination, with the 1-μw received signals, the behavior of the thermistor sensor became the limiting factor. Baseline or zero drift slope did not remain constant during one observing period. One observing period consists of (1) observe reference signal, (2) observe attenuated

[2]Hewlett Packard Co., Model 431B Meter and Model 8402A Meter Calibrator.

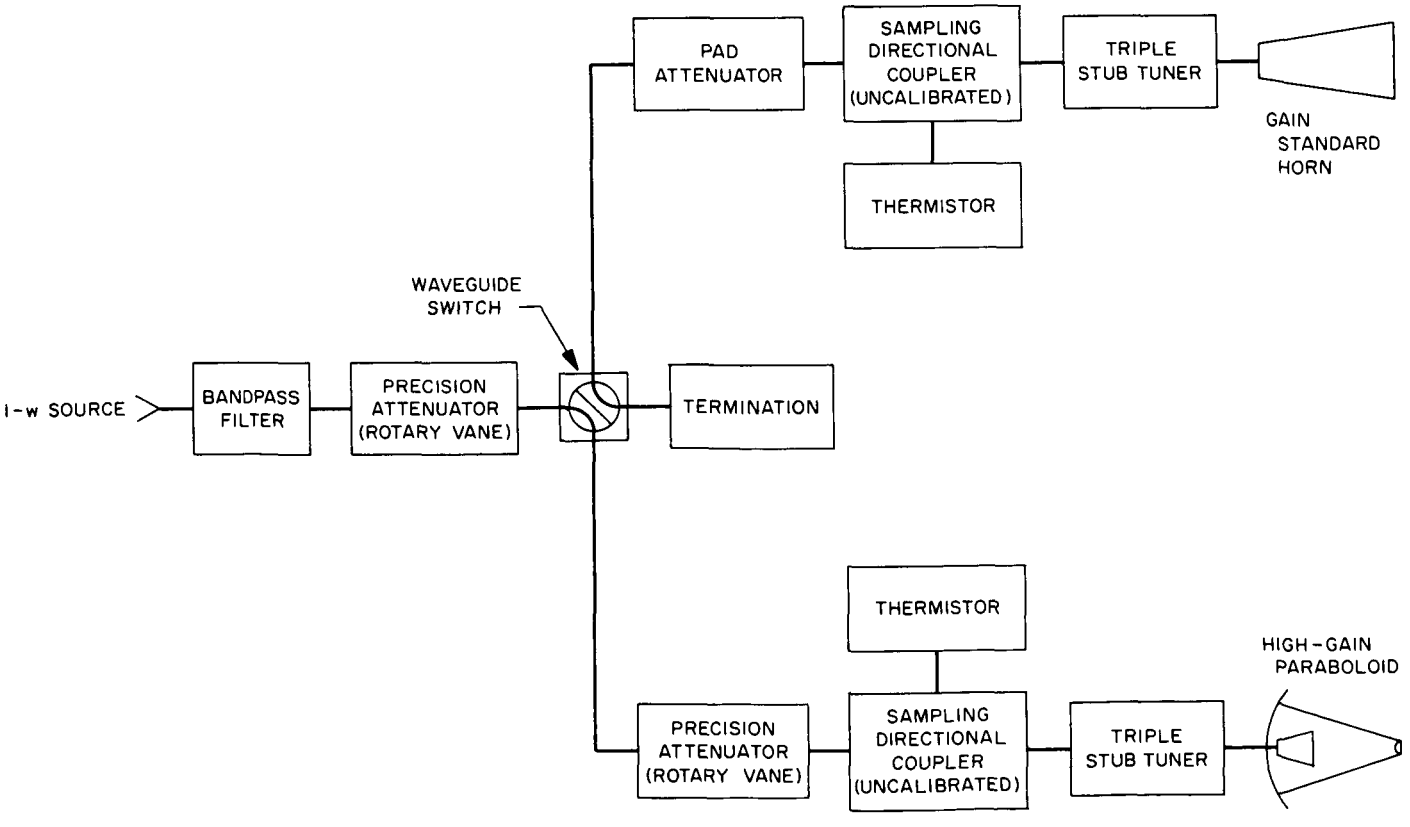

Fig. 22. Transmitter equipment

high-gain signal at Level 1, (3) observe attenuated high-gain signal at Level 2 for calibration purposes and, (4) reobserve reference signal. In order to avoid the drift problem, it was necessary to square-wave modulate the source in order to allow AC-coupled video amplification to be used at the receiver, employing a bolometer sensor. Fig. 23 shows the resulting recording of one observing period. It is clear in Fig. 23 that propagation conditions during this test were relatively poor; peak-to-peak scintillation is in excess of 1.0 db.

The mode of operation was returned to CW using the now-calibrated high-gain illuminator and the thermistor receiver at the 0.1 mw received signal. Fig. 24 represents a 30-min recording of received signal. Again, propagation conditions were poor. Extreme recorded levels

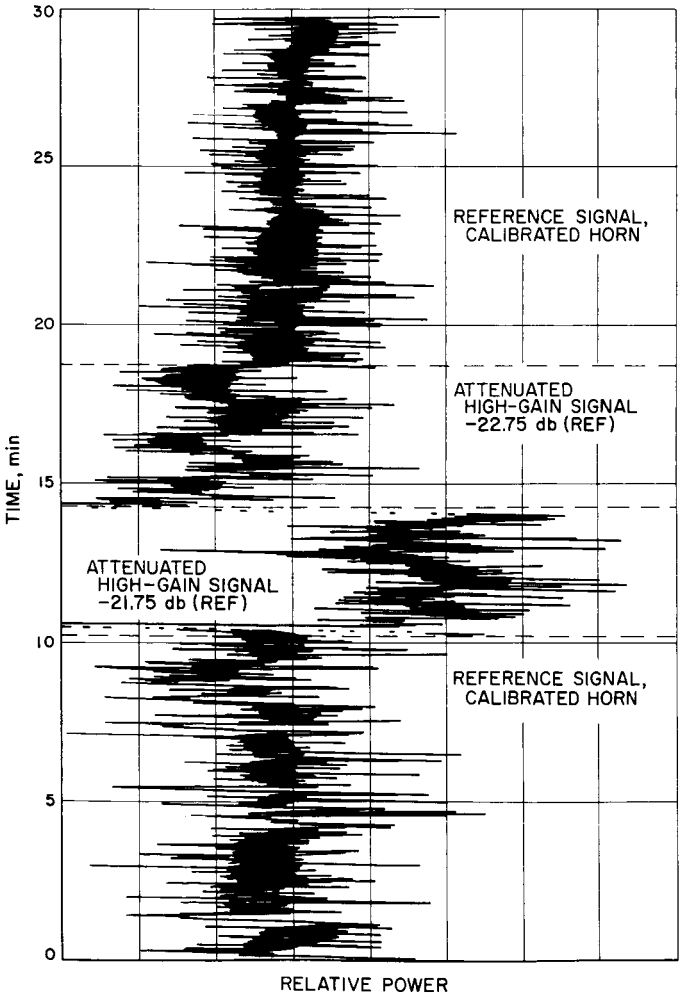

Fig. 23. Received signal levels during gain differencing test

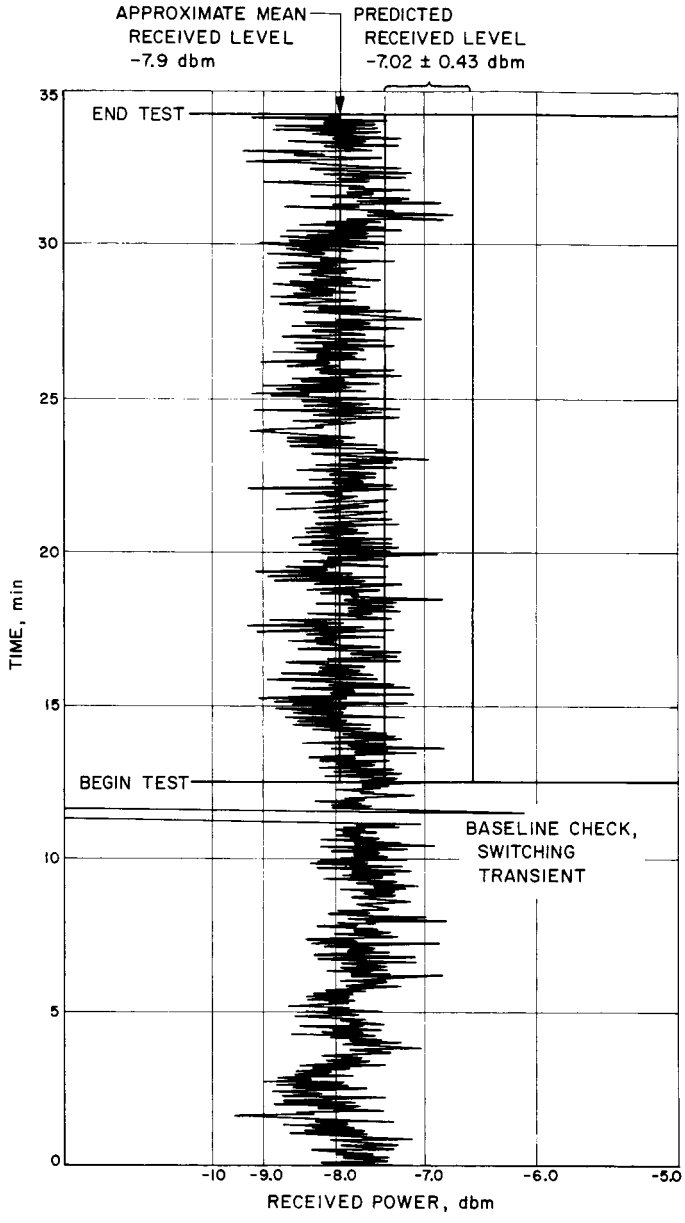

Fig. 24. Received signal level during absolute gain measurement

are a maximum of −6.69 dbm and a minimum of −9.58 dbm, a 2.9-db spread. No statistical reduction has been attempted; a simple visual mean is taken as −7.9 dbm. This value, as shown in Fig. 24, clearly includes a probable error estimated to be in the order of a few tenths of a decibel.

Table 1 shows factors considered for the received signal level and aperture efficiency predictions.

Table 1. Efficiency factors

Transmitter		
Power output, Mount Tiefort	+29.87 dbm	(measured)
Reference antenna gain	+22.02 db	(measured and calculated)
High-gain antenna gain difference	+23.03 db	(measured)
High-gain antenna dissipative loss	− 0.05 db	(estimated)
Path attenuation	−142.82 db	(calculated)
Path absorption (7.5 g/m^3 water vapor)	− 0.68 db	(calculated)
Receiver		
100%η 16-sided polygon aperture	+63.78 db	(calculated)
Feed illumination loss	− 1.26 db	(calculated)
Reflector surface loss	− 0.40 ± 0.18 db	(calculated and estimated)
Quadripod blockage loss	− 0.43 ± 0.25 db	(calculated and estimated)
Receiver dissipative loss	− 0.08 db	(estimated)
Net		
Predicted received level	− 7.02 ± 0.43 dbm	
Predicted 30-ft reflector aperture efficiency	0.62 ± 0.06	

A predicted model efficiency remains accuracy limited by two factors: the 30-ft reflector individual panel manufacturing accuracy, believed to range 0.010 to 0.019 in. RMS as described in *SPS 37-33*, Vol. III, pp. 14–18; and the quadripod opacity. Using the geometrical outline quadripod shadow area, about 7%, the loss ranges −0.18 to −0.68 db for an expected 30 to 100% opacity. Feed amplitude and phase illumination loss, including apex blocking has been calculated as −1.26 db. Reflector surface loss has been bounded by assuming the above-mentioned panel manufacturing accuracy range with the incoherent sums of panel deadload deflection, 0.007 in., and optical measurement uncertainty, 0.005 in. Ideal conditions for thermals and windloads are assumed. The resulting statistical reflector accuracy loss ranges from −0.22 to −0.58 db.

As shown in Fig. 24, an over-all predicted received signal level of −7.02 ±0.43 dbm compares well with the peak signals received during the gain measurement; however, the approximate mean received level remains 0.9 db below the prediction. Pending a deeper understanding of the propagation instability witnessed in these data, it is not clear how the mean value of −7.9 dbm relates to the value which would have been observed under more favorable meteorological conditions. One might assume that favorable conditions such as shown in Fig. 21 would yield a received level 0.9 db higher, thus implying an atmospheric loss. Alternately, one might define a mean aperture efficiency, in the presence of the experienced unfavorable meteorological conditions, to be 50%, down 0.9 db from the expected 62%.

The recordings obtained indicate the primary scintillation component period to be in the order of 5 sec, and based on scintillation tests purposely performed off boresight axis, has a physical scale small compared to the 30-ft aperture. Measured half-power beamwidths are 0.131 and 0.138 deg, for the azimuth and elevation planes, respectively. These values, obtained under more favorable conditions, e.g., Fig. 20, were repeatable within ±0.002 deg and are considered accurate within ±0.004 deg.

b. Summary. During the May 1965 Phase II AAS model tests at 16 Gc, a variety of propagation conditions were encountered. Periods of quiescent atmosphere were used to boresight and focus the system. During the latter test period an absolute gain measurement suffered propagation anomalies. An understanding of propagation vagaries is presently lacking.

While no statistical reduction of received signal level data has been made, it appears the mean received level during poor conditions is below the predicted value by nearly 1 db. Further data evaluation and planning for possible further 16-Gc gain testing is in progress.

C. Madrid 85-ft Antenna Erection

Construction work was recently completed on the 85-ft polar-mounted antenna at Madrid, Spain, bringing DSIF-61 closer to operational status. The four-month task was

completed on schedule, despite extremely inclement weather. The new antenna at the Madrid Station incorporates such new DSIF features as an enclosed two-level electronics house, a truss quadripod, modified counterweight cages, air conditioning, an optical acquisition aid assembly, and a modified Cassegrain cone and hyperbola assembly.

The Madrid Station antenna also has the new high-performance S-Band surface panels, increased hour-angle coverage, a four-legged pedestal and beefed-up structure for improved surface tolerance and over-all stiffness, and modified hour-angle and declination drive skids for improved adjustability and stiffness. Figs. 25–28 show the Madrid Station antenna at various stages of completion.

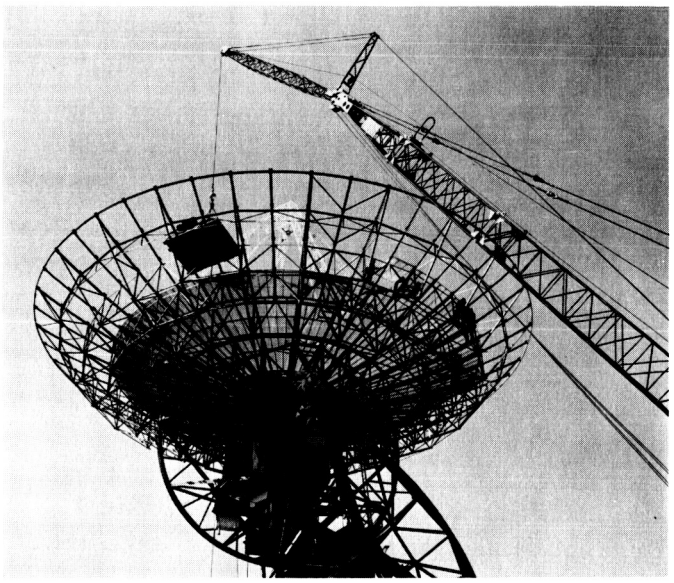

Fig. 26. Installation of dish panels

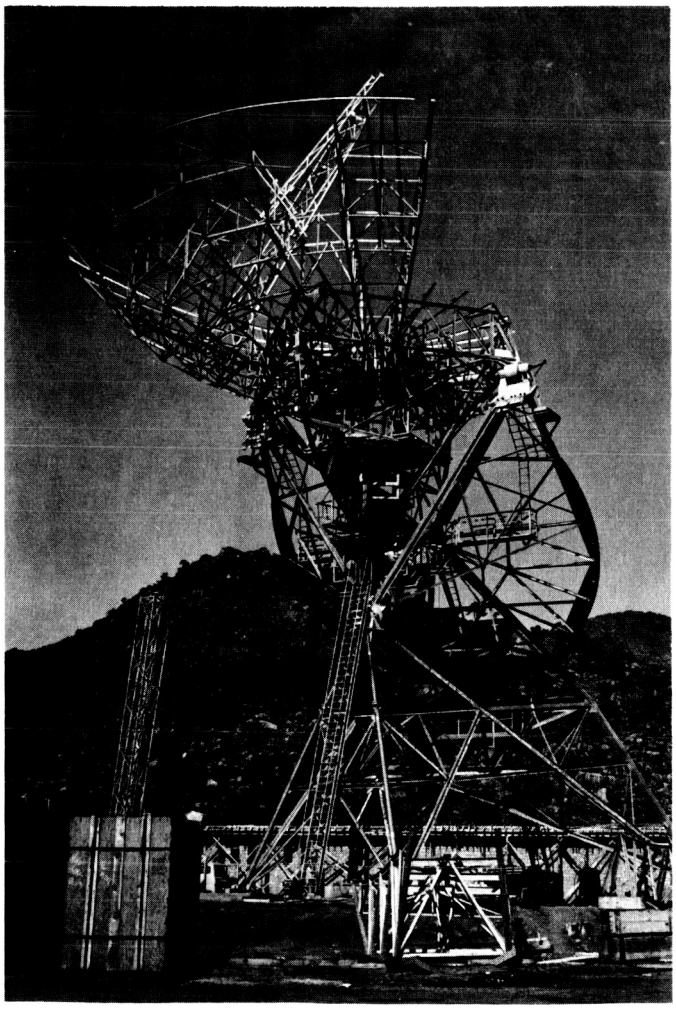

Fig. 25. Completion of pedestal and wheels and start of dish and electronics house construction

Fig. 27. Completion of air conditioning and electronics house installation

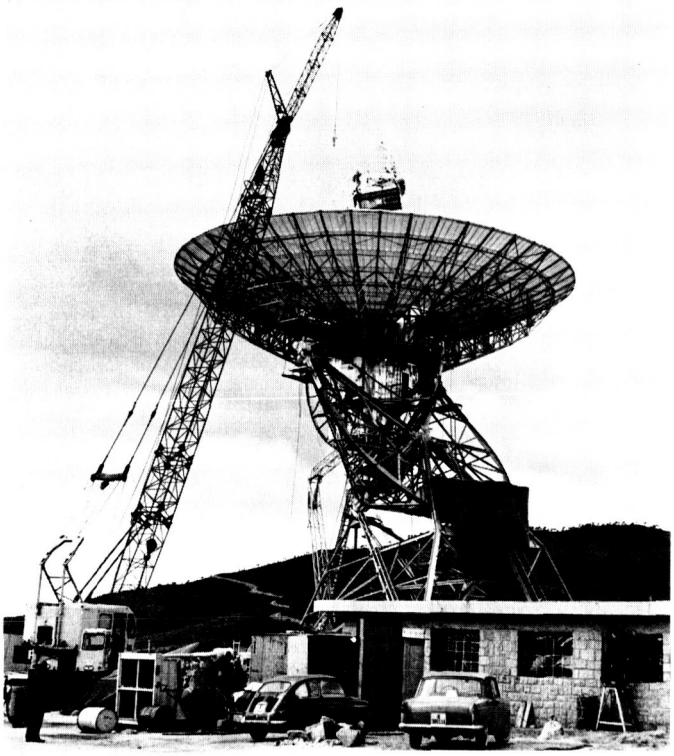

Fig. 28. Installation of Cassegrain cone and hyperbola assembly

D. Modifications to 30-ft Az-El Antenna

1. Introduction

In a continuing effort to increase the operational capabilities of the 30-ft Az-El antenna at the Venus Station, modifications to the basic design have been incorporated. The major portion of these modifications were implemented to provide a true operational scale model of the 210-ft advanced antenna system (AAS). They are:

(1) Replacement of the feed support (quadripod) with a true 1/7-scale model of the 210-ft AAS quadripod.

(2) Provision of a precision 1/7-scale model AAS subreflector.

(3) Provision of a precision hyperbola adjusting mechanism.

(4) Replacement of the cable windup assembly with an upgraded design.

2. Requirements

a. 1/7-Scale AAS quadripod. The technique of utilizing scale models for engineering evaluation is common in shipbuilding, in aircraft manufacture, and in other areas where the items to be constructed are exceedingly large. This technique works well in utilizing the 30-ft antenna as a scale model of the 210-ft AAS.

Simulation of AAS performance, using the existing 30-ft reflector, simply requires an appropriate reduction in the wavelength of operation, provided all aspects of the mechanical structure are scaled. The existing equipment provided a 1/7-scale model (30/210) with one important exception; the feed support or quadripod. The original design characteristics of the 30-ft antenna quadripod included solid construction of round members, four of which formed the quadripod legs, which were orthogonal and in the planes of the antenna axis. The original design therefore provided an imperfect model. (*SPS 37-21*, Vol. III).

b. Subreflector and positioner. To provide a true 1/7-scale model of the AAS subreflector, a requirement was placed on the manufacturing accuracy with respect to the hyperbolic contour. The allowable mean error as a departure from the theoretical hyperboloid was 2×10^{-3} in. with a peak allowable error of 4×10^{-3} in.

The design of the hyperboloid positioner did not require a true scale representation of the AAS, as the area directly behind the hyperboloid is within the shadow of the hyperboloid. However, the design required a capability for adjusting the hyperboloid smoothly through ± 3.0 in. axially with a resolution of 0.005 in., and a tilt adjustment of 0.01 deg over a ± 1.0-deg range in the X-X/Y-Y planes.

c. Cable windup assembly. During the design of the 30-ft antenna, various cable windup concepts were studied. The design most adaptable to the limited confines of the shelf-type pedestal was the dual-drum configuration. This design suffered in the method of cable support. To handle the numerous electrical cables and coolant lines without inducing damaging tensions, kinks, and bends in the process of operation, a new cable-handling harness had to be provided. The new design had to function through ± 300 deg in azimuth and had to be adapted to the basic concept.

Table 2 lists the cabling and coolant lines required to run through the cable windup assembly. The wrapup cables originate at the exit port of the alidade, go through

Table 2. Cable and coolant lines

Cable No.	Quantity	OD, in.	Description
18	7	Miscel-laneous	Conduction to data box
17			2 of RG-9, 3 of RG-214
16	5	0.420	RG-9
15		0.09	No. 12 wires (miscellaneous)
14	1	1 1/4	Power, 400 cps
13	1	1 1/4	Power, 60 cps
12	1	1 1/4	Transmitter
11	1	1 1/4	Transmitter (8 TSP3, No. 16 wire)
10	1	1 1/4	Transmitter (56 conductors, No. 16 wire)
9	1	1 1/8	Microwave group
8	1	1 1/4	Receiver (S-band requirements only)
7	1	1 1/4	Maser (56 conductor, No. 16 wire)
6	1	1 1/8	Microwave group
5	1	1 1/4	Intercom, JPL Dwg. 1-73070
4	1	1 1/4	Servo, JPL Dwg. 106895
3	1	1 1/4	Servo, JPL Dwg. 106895
2	1	1 1/4	Datex
1	1	1 1/4	TV, JPL Dwg. D9153432
C	4	1 1/4	Coolant lines

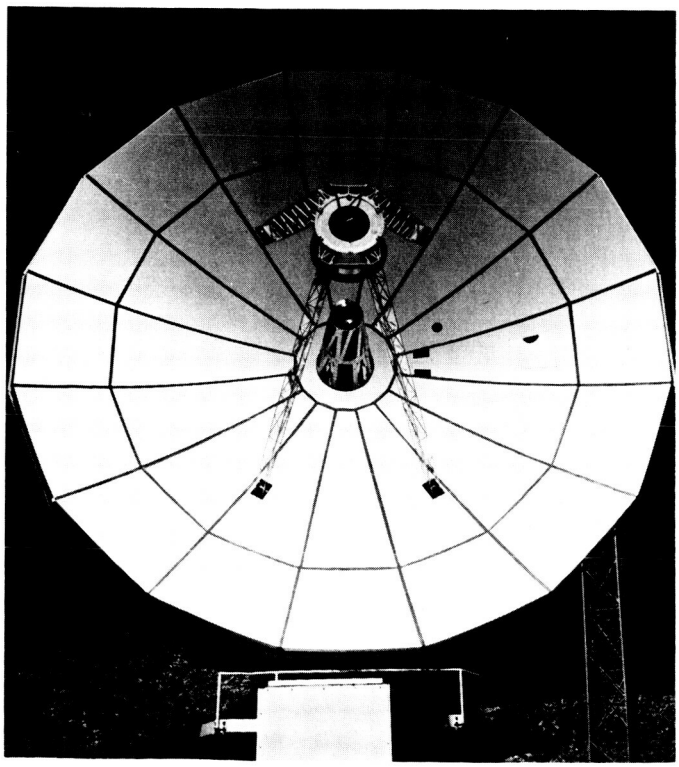

Fig. 29. 30-ft diameter dish, front view

the kingpost into the primary drum, extend through the cable harness, go around the secondary takeup drum, and terminate at the antenna pedestal.

3. Systems Installation

a. 1/7-Scale AAS quadripod. Figs. 29 and 30 show the completed installation, quadripod, apex, and subreflector. The modification required a new support structure (Figs. 31 and 32) at 45-deg rotation to the original design within the reflector backup structure.

The interface plane of the support structure and quadripod was installed within 0.010 in. and parallel to the reflector boresight axis reference plane. This was accomplished by use of a precision sweep gage and theodolite (Fig. 33).

The quadripod deflections, measured at the focal point, are as follows:

(1) Deadload deflection. Zenith to horizon with an apex load of approximately 500 lb = 0.099 in. (Rotation about the X-X plane Y-Y plane.)

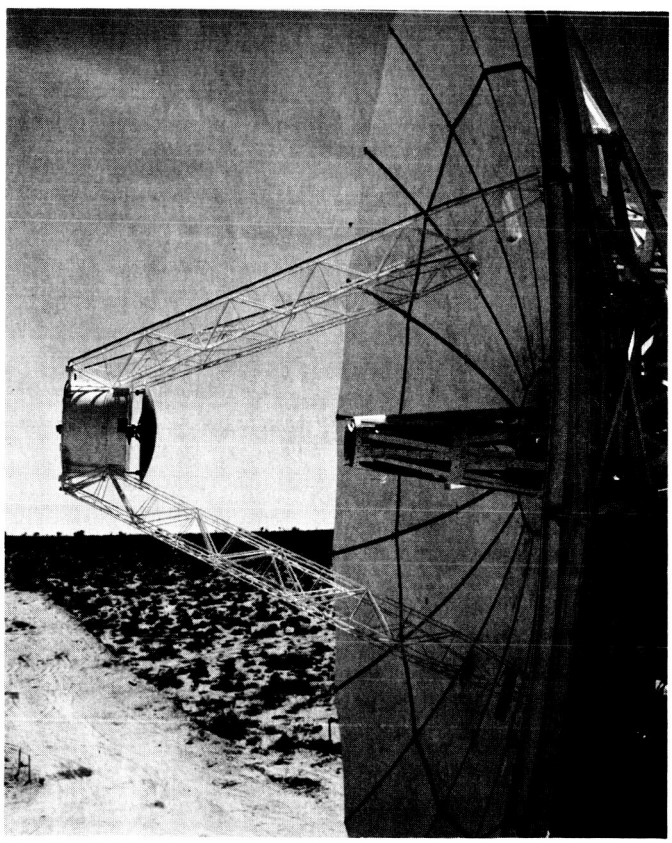

Fig. 30. Quadripod, apex, and subreflector

(2) Translation. Zenith to horizon (with same load condition) = 0.008 in. (Rotation about the Y-Y plane.)

Further studies are planned in the immediate future to determine the effects of the quadripod deflections under static and dynamic conditions to the true mechanical boresight of the primary reflector.

For the 1/7-scale AAS RF studies (*SPS 37-33*, Vol. III, pp. 14–18), the quadripod, primary, and secondary reflectors were required to be mechanically aligned along a common axis at 0.0 deg elevation (horizon look). For this immediate study, the tests were considered generally under static conditions (structural and mechanical characteristics not affected by dynamic and gravity loading). These alignments are discussed later in this report.

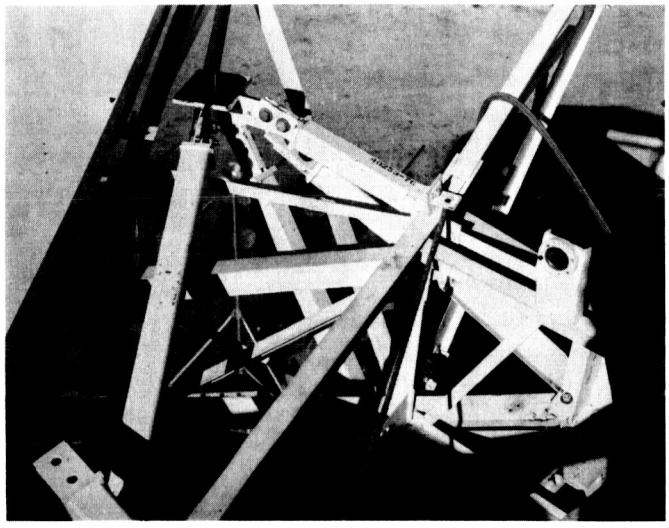

Fig. 31. Support structure, detail

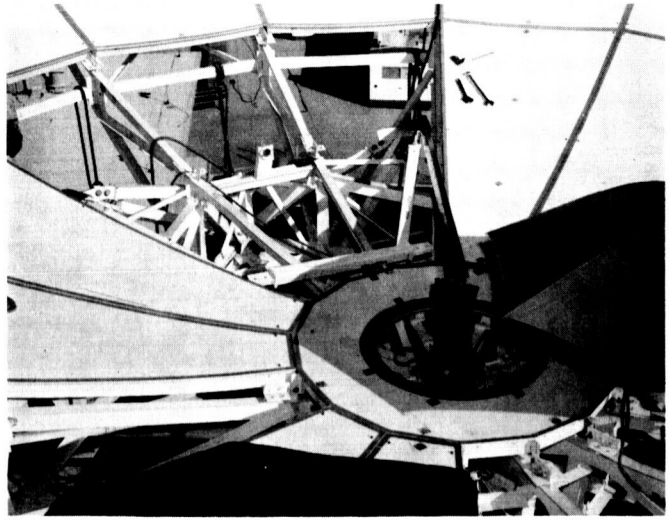

Fig. 32. Support structure behind reflector panels

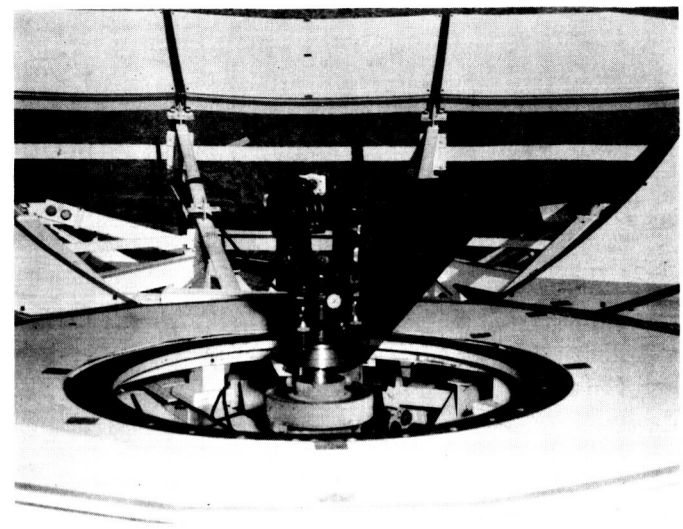

Fig. 33. Precision sweep gage and theodolite

b. Subreflector and positioner. To manufacture a precision hyperbolic reflector to a surface accuracy of 4×10^{-3} in. peak, it was necessary to investigate materials best suited for this application. The reflector structure and interface area (Fig. 34) (hyperbola positioner) were manufactured from a solid piece of material. The material selected to provide thermal and dimensional stability was Pioneer 921-T DC Aluminum Tooling Plate Alloy, which is produced to obtain the high stability required in the tooling industry. With this desirable characteristic, dimensional stability and close tolerances were achieved. The surface accuracy fell within the specified tolerance. The surface finish was 30μ in., approaching 25.

Fig. 35 shows the complete hyperbola and positioner on a support ring. The positioner assembly, Fig. 36, provides the axial and tilt adjustments as shown in the block diagram of Fig. 37. The completed installation with its weather protective cover can be seen in Fig. 30.

At the central point or vertex of the hyperbola, where the support ring attaches (Fig. 35), and precisely on axis, internal threads and shoulder are provided for installing an optical flat and target assembly, to facilitate the subreflector alignment to the boresight of the primary reflector. This alignment is accomplished by optical instrumentation located at the vertex of the primary reflector. After all alignments are completed, the optical flat and target assembly are replaced by a plug, machined to the reflector contour.

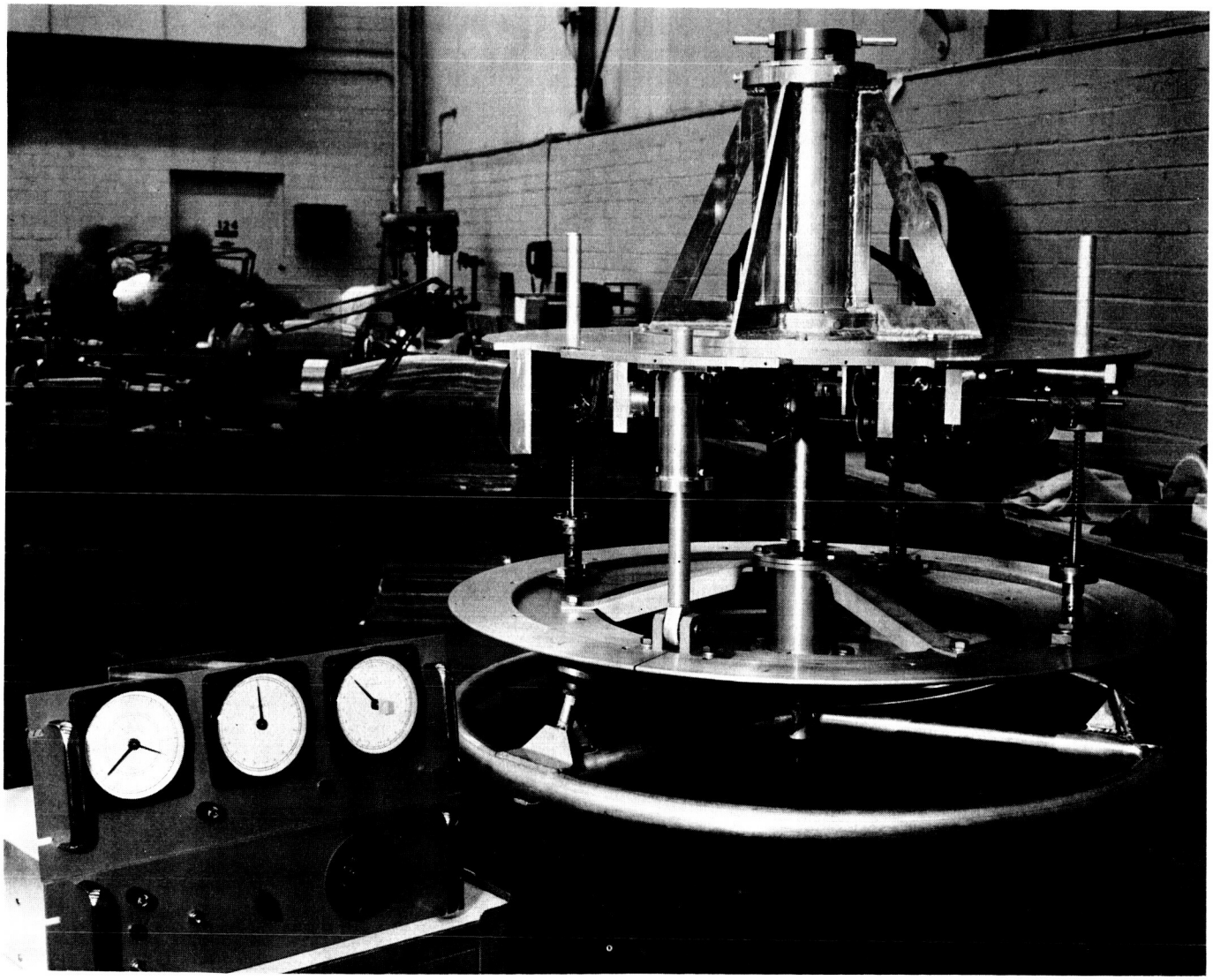

Fig. 34. Hyperbola and positioner interface

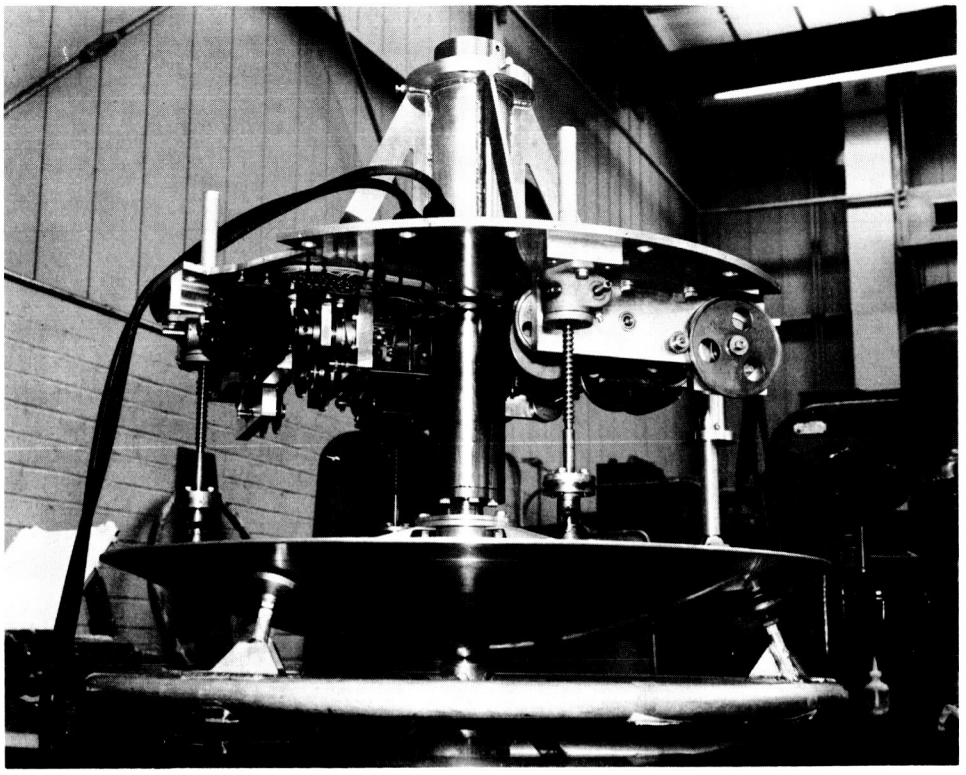

Fig. 35. Hyperbola and positioner on support ring

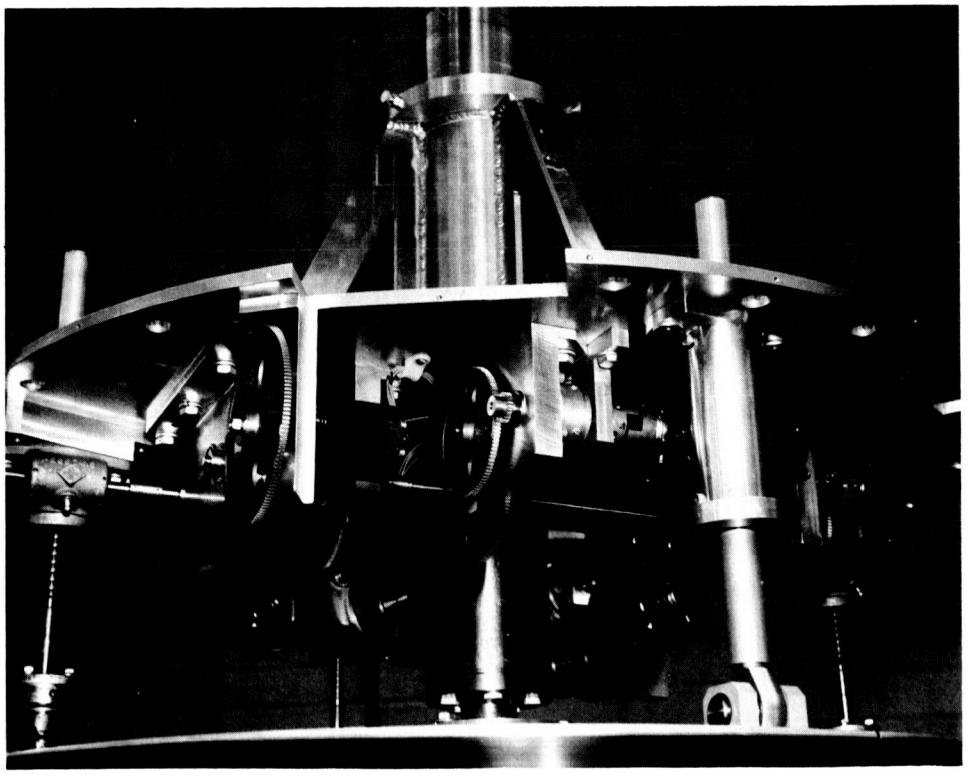

Fig. 36. Axial and tilt adjustments on positioner

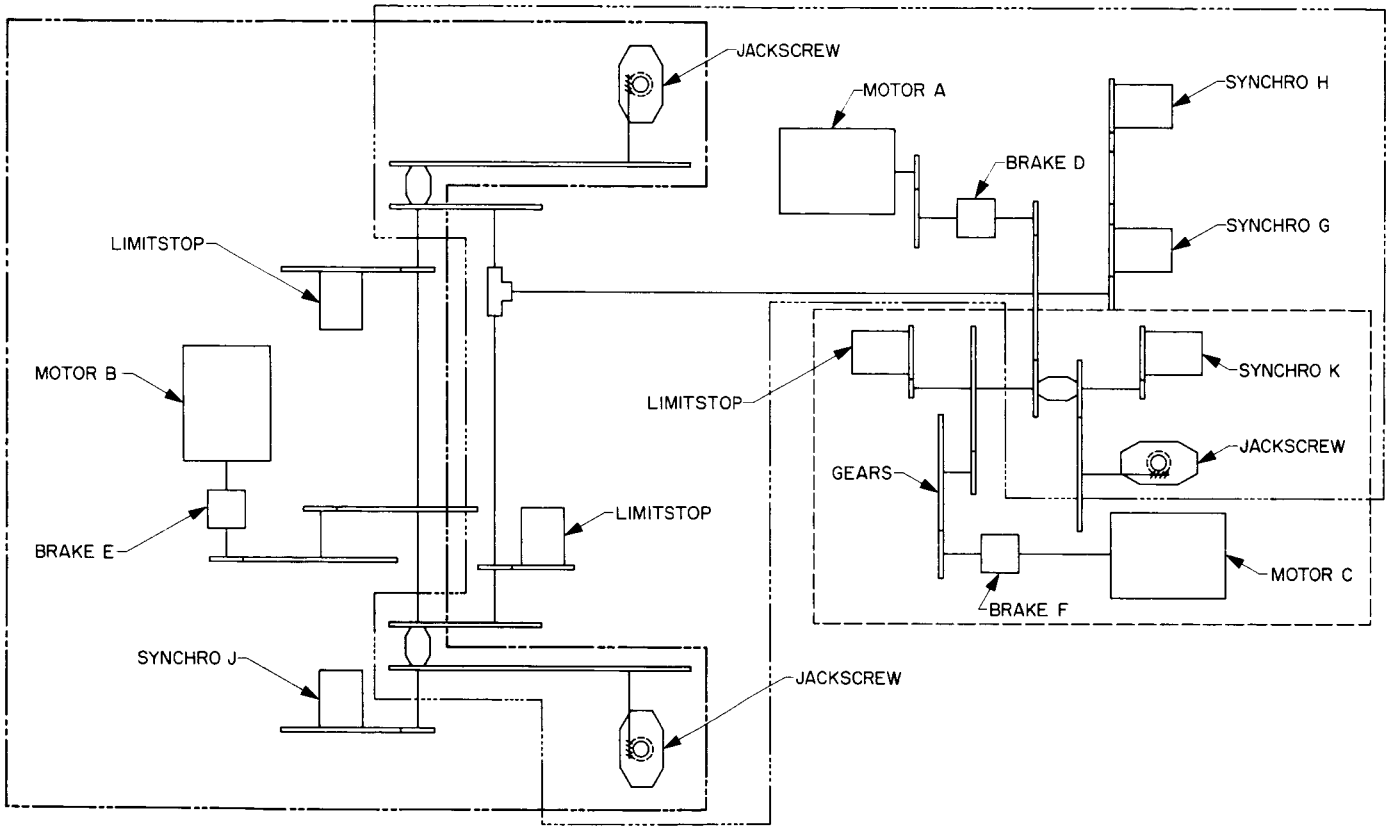

FOCUS	TILT	
AXIAL	EAST-WEST	NORTH-SOUTH
MOTOR A	MOTOR B	MOTOR C
BRAKE D	BRAKE E	BRAKE F
LIMITSTOP	LIMITSTOP	LIMITSTOP
SYNCHRO G, SYNCHRO H	SYNCHRO J	SYNCHRO K
POWER ON: MOTOR A, BRAKES E AND F	POWER ON: MOTOR B, BRAKES D AND F	POWER ON: MOTOR C, BRAKES D AND E
POWER OFF: MOTORS B AND C, BRAKE D	POWER OFF: MOTORS A AND C, BRAKE E	POWER OFF: MOTORS A AND B, BRAKE F

Fig. 37. Hyperbola adjustment mechanism

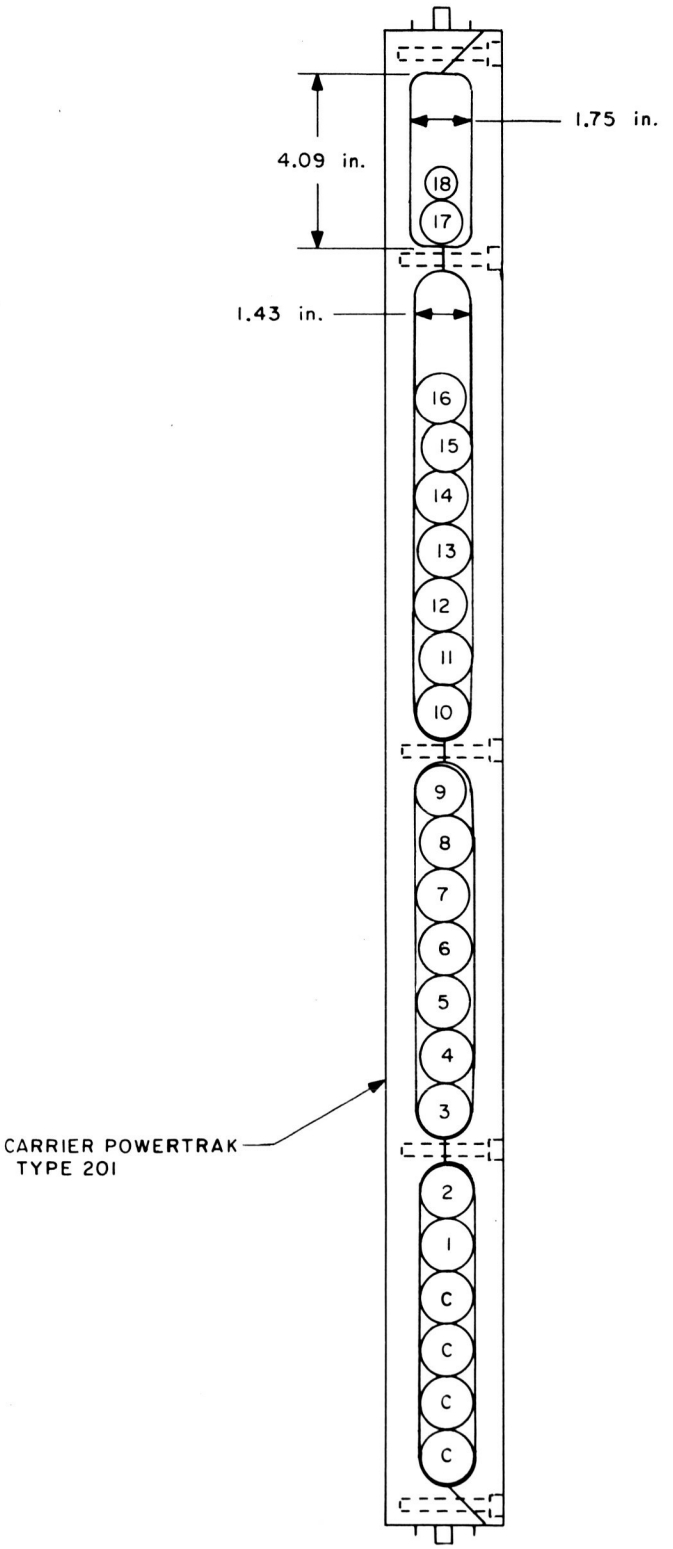

Fig. 38. Powertrak cable carrier

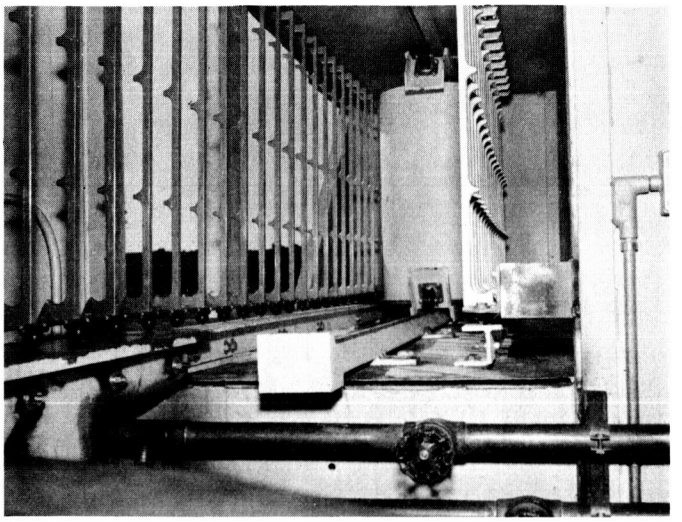

Fig. 39. Powertrak installed in cable windup enclosure

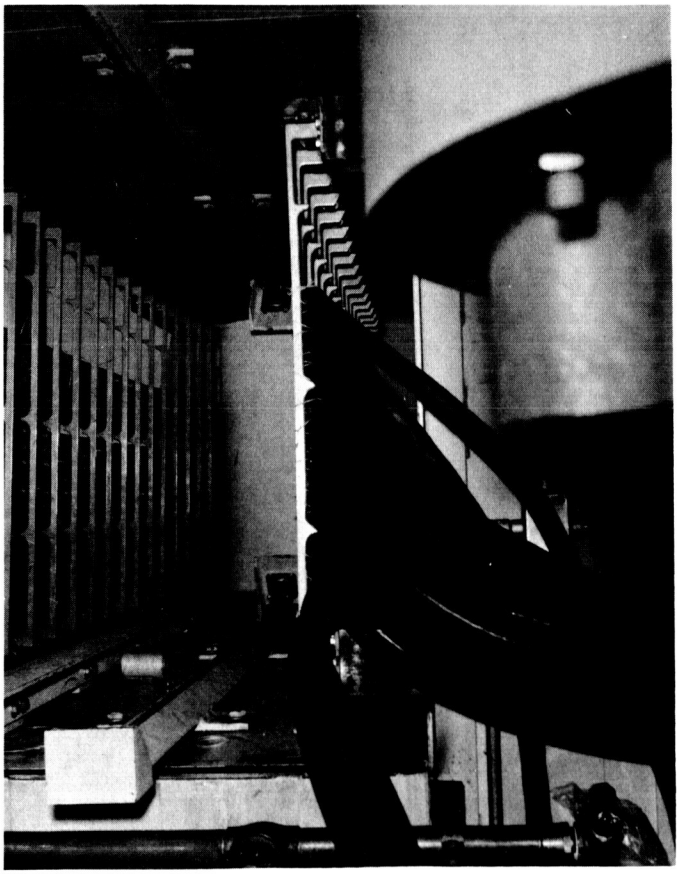

Fig. 40. Cable and coolant lines installation

c. Cable windup assembly. The cable windup assembly incorporates a cable harness with the trade name "Powertrak", which is manufactured by Gleason Reel Corporation of Mayville, Wisconsin. The size and cable capacity of the harness is fabricated to customer requirements. The cables listed in Table 2 have been installed in the order shown (Fig. 38).

Fig. 39 shows the Powertrak unit installed in the cable windup enclosure, which extends approximately 12 ft to the south of the antenna pedestal center. The unit is drawn along rails by a counterweighted drum. The design provides a continuous travel of 600 deg in azimuth. The limits are set for a ±300-deg travel from the nominal 180-deg azimuth attitude.

Fig. 40 shows the cables and coolant lines as they are being installed. The modified system operates in much the same manner as the original; however, the cables and coolant lines ride freely with no extraneous loads applied.

Table 3. Error distribution for parabolic reflector; precision operation (0 mph wind), 0-deg elevation

	For 0.019-in. manufacturing accuracy panels[b]		For 0.010-in. manufacturing accuracy panels[b]	
	Error, in. × 10^{-3}	(Error)^2, in.^{2} × 10^{-6}	Error, in. × 10^{-3}	(Error)^2, in.^{2} × 10^{-6}
Reflector panels				
Manufacturing	19	361	10	100
Deadload	7	49	7	49
Windload	0	0	0	0
Field installation				
Setting accuracy	4[a]	16	4[a]	16
Instrument error	2	4	2	4
Thermals				
Transient	2	4	2	4
Steady	2	4	2	4
Reflector structure				
Deadload	0	0	0	0
Windload	0	0	0	0
Thermals				
Transient	7	49	7	49
Steady	7	49	7	49
	Σ (error)^2 = 526		Σ (error)^2 = 275	
	σ^c = 23		σ^c = 17	

[a] Deviation from best-fit paraboloid based on best-fit RMS computer program (run April 25, 1965).
[b] Error values apply only at 0-deg elevation.
[c] $\sigma = \sqrt{\Sigma (\text{error})^2}$.

4. Alignments

The alignments for the 1/7-scale RF performance studies consisted of the following:

(1) Align the subreflector (hyperboloid) perpendicular and symmetrical to the primary reflector datum plane at 0.0 deg elevation.

(2) Align the primary reflector surface to a true paraboloid at 0.0 deg elevation.

In the alignment of the primary reflector surface, the following must be noted. Previous estimates based on RF experience with the 30-ft reflector, *SPS 37-33*, Vol. III, pp. 14–18, 69–81) include a discussion of the manufacturer's stated panel accuracy of 0.019 in. RMS. The stated accuracy is a conservative figure, well within the original manufacturing specifications. It has been estimated in the above referenced reportings to be 0.010 to 0.019 in. RMS. In addition, some mention is made to superior performance during the latest test period. Therefore, two tabulations are made (Table 3).

E. Study of Amplifier Drift Effect on Tracking Accuracy

In order to establish the complete reliability of the present vacuum tube configuration in the precision servo drive of the 30-ft Az-El antenna at Goldstone, an experimental study was recently conducted to determine the relationship of amplifier drift to system tracking accuracy.

In recent years, substantial progress in the state-of-the-art has been made in regard to both vacuum tube and solid-state components. However, when the current servo-drive design was developed, JPL's antenna experience was limited to vacuum tube applications, and since experience was regarded as the only true measure of reliability, a vacuum tube design was selected. For additional improvement in reliability and stability, chopper stabilized amplifiers were used wherever applicable. Fig. 41 shows the amplifier chain used for both azimuth and elevation drives.

To determine the relationship of amplifier drift to system tracking accuracy, the amplifier chain was carefully

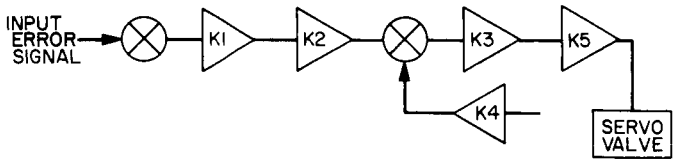

AMPLIFIER		DC GAIN
NUMBER	NAME	
K1	ISOLATION	10^{-1}
K2	INTEGRATION	10^{8}
K3	RATE SUMMING OUTPUT	10^{2}
K4	RATE SUMMING INPUT	10
K5	VALVE DRIVER	2.7 ma/v

Fig. 41. Amplifier chain

balanced, and drift data was obtained at the middle and at the end of the 10-wk test period. The results are shown in Table 4.

An evaluation of the drift data was then made in a series of additional tests which utilized the entire control system. Position-tracking commands were introduced through the on-site computer, with the tracking rate set at 0.004 deg/sec. Each amplifier in the chain was unbalanced, one at a time, until the tracking error was greater than 0.010 deg, or the limit of the balance control was reached. The results of these tests are shown in Table 5.

It can be seen that the only amplifiers which have an effect on the tracking performance are the isolation amplifier and the integration amplifier. This was as expected, inasmuch as the position loop is closed around the remaining amplifiers in the chain, and the balance of the system gains are insignificant compared to the high DC gain of the integrator. However, drift and stability are, of course, a factor over a wider range than was experienced in these tests, because of their adverse effect upon system gain and stability.

Table 4. Amplifier drift

Amplifier	Balance voltage, mv		
	Start	5 wk	10 wk
Azimuth isolation	>1.0	4.2	7.8
Azimuth integration	>1.0	1.2	1.0
Azimuth rate summing output	>1.0	27	56
Azimuth rate summing input	>1.0	13	14
Azimuth valve drive, side 1	540	540	540
Azimuth valve drive, side 2	540	540	540
Elevation isolation	>1.0	68	60
Elevation integration	>1.0	7.0	8.0
Elevation rate summing output	>1.0	7.0	1.0
Elevation rate summing input	>1.0	16	16
Elevation valve drive, side 1	600	600	600
Elevation valve drive, side 2	600	600	600

Table 5. Amplifier drift effect on tracking accuracy

Amplifier	Balance voltage, mv	Tracking error, deg	Amplifier bias voltage, mv
Azimuth isolation	2.5	0.010±0.002	1750
Azimuth integration	1.0	0.010±0.002	160
Azimuth rate summing output	1.0	±0.002	1300
Azimuth rate summing input	1.0	±0.002	4000
Azimuth valve drive, side 1	460	±0.002	160
Azimuth valve drive, side 2	460	±0.002	1050
Elevation isolation	1.0	0.010±0.002	1400
Elevation integration	2.0	0.010±0.002	160
Elevation rate summing output	1.0	±0.002	1250
Elevation rate summing input	1.0	±0.002	4000
Elevation valve drive, side 1	600	±0.002	200
Elevation valve drive, side 2	600	±0.002	1150

"S" curve from computer, 40 mv = 0.001 deg.

On the basis of these tests, which proved the high reliability of the vacuum tube design, the requirement for amplifier balancing was changed from a daily function to a monthly function. This reduces the daily checkout procedure time of the servo from a half-hour to just a few minutes.

The 30-ft Az-El antenna control system is a Type II position tracker. The over-all system is discussed in *SPS 37-26*, Vol. III, pp. 23 and 24.

F. Gear Box Lubricant Experiment

Testing of the newly installed precision drive system for the 30-ft Az-El antenna at Goldstone was conducted during the summer months of 1964 with satisfactory results. However, early in 1965 the maximum slewing

velocity appeared to be greatly reduced in the late evening and early morning hours. The trouble symptoms indicated that the sluggishness was caused by a change in viscosity of the gear box lubricant.

The lubricant originally used, Tellus 69, was the one recommended by the gear box manufacturer for the expected temperature range and operating conditions. In order to find a more suitable alternate, several petroleum manufacturers were contacted. The alternate chosen was Rotella T, 10W-30, a high-pressure oil of varying weight that could provide lubrication over the wide temperature range of 0 to 135°F, while undergoing only a small change in viscosity.

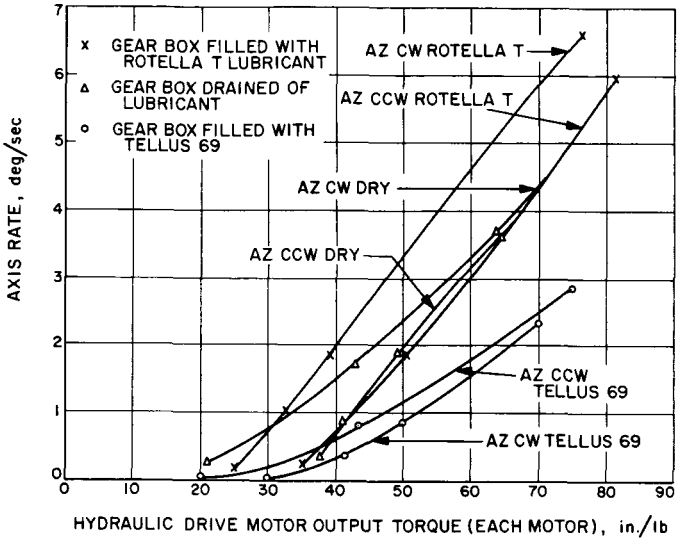

Fig. 42. Drive torque versus rotation rate, azimuth axis

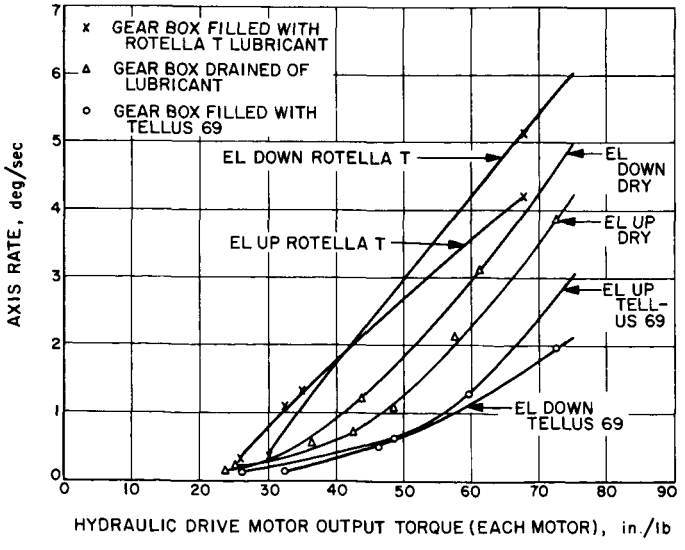

Fig. 43. Drive torque versus rotation rate, elevation axis

To confirm these properties, a series of tests were conducted on the 30-ft antenna under wind velocity conditions of less than 5 mph. Data obtained from the tests are given in Table 6. Plots of the hydraulic drive motor output torque versus antenna axis-rotation rate are shown in Figs. 42 and 43.

Test results indicated that the original oil, Tellus 69, presented a greater amount of resistance or damping than the Rotella T. It should be noted that in the dry or "lubrication drained" condition during the tests, the gear boxes were not flushed; and, therefore, a small amount of oil remained in the bearings and on the gear teeth. The slope of the curve at high rotation rates for Tellus 69 is nearly the same as for Rotella T.

Subsequent tests, conducted since the lubricant was changed, supplied data which closely approximate the slope of the Rotella T curves.

G. Digital Instrumentation Subsystem

The initial configuration of the digital instrumentation subsystem (DIS) previously reported in *SPS 37-16, -20, -21*, Vol. III, has recently been revised and broadened with the completion of the latest phase of expansion.

The basic digital instrumentation subsystem is composed of an SDS 910 computer, SDS 920 computer, and associated peripheral and data-gathering equipment. The computers and peripheral equipment form two completely independent subsystems, designated Alpha and Beta. In the event of a failure in any portion of either subsystem, the alternate subsystem may assume the responsibility for performing assigned tasks on a priority basis.

1. Subsystem Update

The configuration of the DIS was expanded to include the following functional units:

(1) Perforated paper tape punch and coupler–Alpha

(2) Paper tape spooler–Alpha

Table 6. Gear box lubricant effects in high-speed modes

Run	Axis	Primary gear reducer lubrication condition	Rotation	Axis rate deg/sec from Datex printout	System pressure, psi	Return pressure, psi	Replenishing pressure, psi	Hydraulic Motor 1				Hydraulic Motor 2				Mean ΔP of two motors, psi[a, b]	Mean output torque at mean ΔP for each motor (75 % efficiency), in.-lb	Mean lubricant temperature of two primary gear reducers, °F	Viscosity of lubricant at mean temperature, SSU[c]
								P_1, psi	P_2, psi	ΔP, psi	Counter-balance, psi	P_3, psi	P_4, psi	ΔP, psi	Counter-balance, psi				
1	Az	Tellus 69	CW	0.028	1800	10	130	450	1300	850		900	500	400	450	625	30.3	50	7500
2	↓	↓	CCW	0.054	↓	↓	↓	1000	600	400	100	600	1100	500		450	21.8	50	↓
3			CCW	0.500				1225	500	725	150	500	1375	875		800	38.8	50	
4			CW	0.408				350	1450	1100		1025	425	600	500	850	41.2	51	
5			CW	0.88				225	1500	1275		1100	300	800	475	1038	50.3	51	
6			CCW	0.88				1250	400	850	100	400	1350	950		900	43.7	51	
7			CW	2.4				0	1750	1750		1250	100	1150	600	1450	70.3	51	
8		↓	CCW	2.6	↓	↓	↓	1650	150	1500	75	75	1650	1575		1538	74.6	51	↓
9	↓	Lubricant drained	CW	0.28	1800	10	130	450	1550	1100		950	550	400	700	750	36.4	59	Dry case
10			CCW	0.28				1050	650	400	100	650	1150	500		450	21.8	59	
11			CCW	0.90				400	500	100	750	450	1300	850		475	23.0	59	
12			CW	0.90				300	1400	1100		1000	400	600	500	850	41.2	60	
13			CW	1.8				250	1500	1250		1100	300	800	450	1025	49.7	60	
14			CCW	1.7				1250	400	850	100	400	1350	950		900	43.7	60	
15			CCW	3.7				1450	200	1250	150	200	1600	1400		1325	64.3	60	
16			CW	3.6	↓			50	1650	1600		1200	150	1050	550	1325	64.3	60	
17			CCW	4.2	2500			1750	500	1250	150	500	1900	1400		1325	64.3	61	
18			CW	4.2	↓			400	1950	1550		1800	450	1350	200	950	46.1	61	
19			CCW	0.87				1400	800	600	150	750	1500	750		675	32.7	61	
20			CW	1.0	↓	↓	↓	700	1600	900		1600	800	800	100	850	41.2	61	
21			CW	>5.2	2700	10	130	350	2150	1800		2000	400	1600	200	1700	82.5	66	
22		↓	CCW	>5.2	2700	10	130	1950	500	1450	200	450	2100	1650		1550	75.2	66	↓
23	↓	Rotella T 10W-30	CW	0.25	2700	10	130	800	1650	850		1500	900	600	250	725	35.2	65	670
24			CCW	0.18				1350	900	450	150	900	1500	600		525	25.5	65	
25			CCW	1.0				1550	950	600	150	900	1650	750		675	32.7	65	
26			CW	1.8				700	1850	1150		1700	800	900	250	1025	49.7	65	
27			CW	0.8				850	1750	900		1550	900	650	250	775	37.6	65	
28			CCW	1.1				1500	950	550	200	900	1650	750		650	31.5	65	
29			CCW	1.8				1600	850	750	100	850	1700	850		800	38.8	65	

30			CW	6.0				350	2150	1800		1950	400	1550	250	1675	81.2	65		
31			CCW	6.6				1950	450	1500	150	450	2100	1650		1575	76.4	65		
32	EL	Tellus 69	Up	0.13	1800	10	0	350	850	500	100	950	350	600		550	26.7	53	7000	
33			Down	0.18				1200	500	700		650	1300	650	50	675	32.7	54		
34			Down	0.57				1250	250	1000		450	1350	900	100	950	46.1	54		
35			Up	0.62				250	1300	1050		1200	250	950	100	1000	48.5	54		
36			Up	1.3				200	1500	1300		1350	200	1150	150	1225	59.4	54		
37			Down	1.9				1500	0	1500		200	1700	1500	0	1500	72.8	54		
38		Lubricant drained	Down	0.2	1800	10	0	1050	500	550		650	1150	500	50	525	25.5	56	Dry case	
39			Up	0.13				350	800	450	100	900	350	550		500	24.3	56		
40			Up	0.64				350	1150	800		1050	350	700	100	750	36.4	56		
41			Down	0.67				1200	300	900		450	1300	850	50	875	42.4	56		
42			Down	1.2				1200	350	850	100	400	1350	950		900	43.7	56		
43			Up	1.14				250	1300	1050		1200	250	950	100	1000	48.5	56		
44			Up	2.1				200	1400	1200		1250	200	1050	150	1125	54.6	56		
45			Down	3.1				1350	50	1300		200	1450	1250	50	1275	61.8	56		
46			Up	3.8	2650	10	0	350	2000	1650		1900	450	1350	250	1500	72.8	56		
47			Down	5.1				1850				600	1950	1350				56		
48		Rotella T 10W-30	Up	0.29				700	1300	600		1250	750	500	100	550	26.7	61	750	
49			Up	1.14				800	1600	800		1400	850	550	250	675	32.7	61		
50			Down	0.38				1600	1050	550	100	1050	1700	650		600	29.1	61		
51			Down	1.3				1600	900	700	50	950	1700	750		725	35.2	61		
52			Up	4.2				450	1950	1500		1800	500	1300	200	1400	67.9	61		
53			Down	5.1				1850	550	1300	50	600	1950	1350		1325	64.3	61		
54	Az		CW	3.4	1800															
55	Az		CCW	3.8				System normal operating pressure												
56	El		Down	3.65																
57	El		Up	2.8																

[a] Theoretical output torque per 100 psi ΔP for one motor = 6.46 in.-lb.

[b] Output torque per 100 psi at 75% efficiency = 4.85 in.-lb.

[c] SSU = Saybolt Seconds Universal.

(3) Signal coupler chassis–Alpha and Beta

(4) Expanded subsystem control panel

(5) Revised analog-to-digital converters, digital-to-analog converters, and multiplexers

(6) Modified negative true digital input assemblies

(7) Updated SDS 910 and 920 computers

(8) Alpha and Beta magnetic tape units equipped with reflective spot sensing at the beginning and end of the tape

The DIS, as upgraded, now provides identical peripheral equipment for the Alpha (SDS 910) and Beta (SDS 920) portions, the data-gathering equipment being common to, and addressable by, both units.

To contain the additional elements, the subsystem has been increased from the previous seven rack cabinets to eight rack cabinets. The subsystem format has been modified accordingly, to group Alpha and Beta equipment with their respective computers. Access to the subsystem control panel, the two computer control panels, and the input/output equipment was arranged for operator convenience. The eight cabinets, together with two communications buffer cabinets on the left side, are shown in Fig. 44.

2. Subsystem Extension

The second phase of expansion for the DIS provides for additional computer-oriented equipment and a communications capability. The following are new elements which function with the computer sections of the subsystem:

(1) Input/output character buffer (Y)–Alpha and Beta

(2) Four additional levels of priority interrupt–Alpha and Beta

(3) Interrupt arming chassis–Alpha and Beta

(4) Memory expansion of SDS 910 Computer from 2048 to 8192 words of magnetic core memory–Alpha

(5) Memory expansion of SDS 920 Computer from 4096 to 8192 words of magnetic core memory–Beta

a. Input/output character buffer. The Y-buffer provides a second character buffer for connecting to and addressing peripheral input/output equipment. The Y-buffer operates at a rate of up to 50,000 characters per second, in the same manner as the W-buffer.

b. Priority interrupt. The four additional levels of priority interrupt increase the interrupt capacity available for external system use to a total of 16 channels each (for Alpha and Beta). The computer retains for its own use additional interrupts of higher priority for *power fail-safe* (2), Y-buffer (2), and W-buffer (2). Interrupts are generated by the application of a +8-v pulse of 12 ± 4 μsec in width. An interrupt signal will cause the computer to interrupt its normal program and honor the interrupt in the sequence established by the priority assignments.

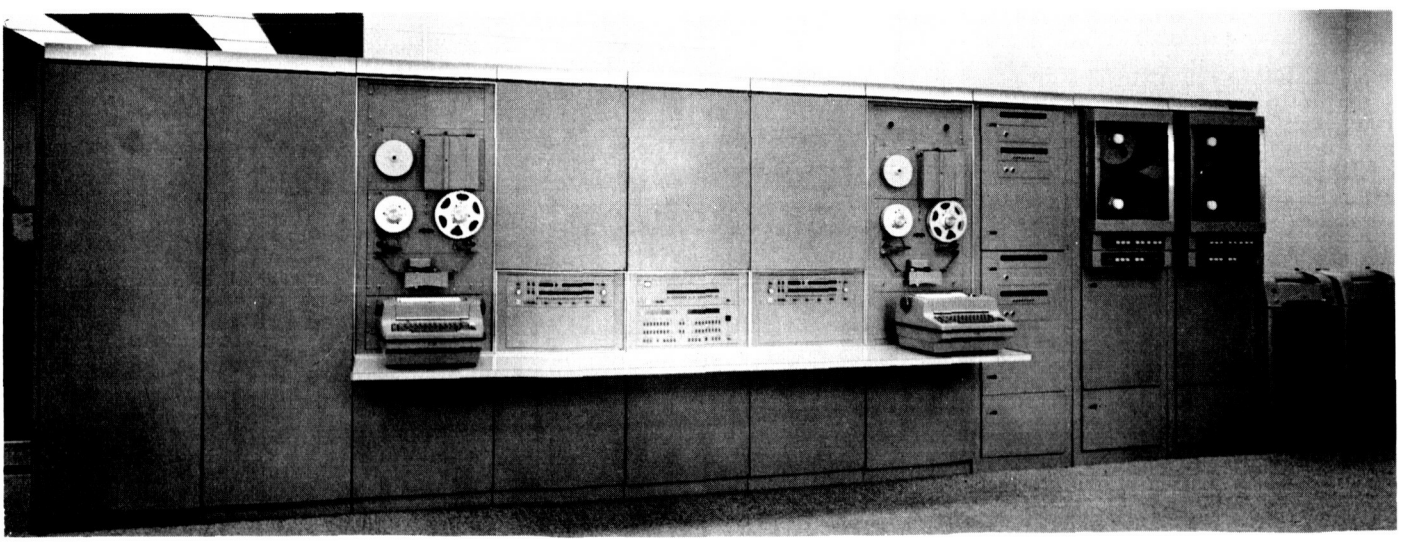

Fig. 44. Digital instrumentation subsystem

c. Interrupt arming chassis. The interrupt arming chassis permits interrupts to be selectively armed and disarmed under program control. The interrupt arming chassis is addressed with an energize output mode/parallel output (EOM/POT) sequence with the bit configuration of the POT word establishing the arming and disarming pattern as illustrated in Fig. 45.

d. Magnetic core memory. Capacity of both Alpha and Beta computers is increased to 8192 words (24 bits plus parity). All 8192 words are directly addressable. Memory access time is 8 μsec. The memory is nonvolatile and retains stored data in the event of a power failure.

3. Communications Buffers

The communications buffers (Fig. 46) provide the DIS with a capability for transmitting and receiving via full duplex teletype units, and with a send-only mode for transmitting by way of a high-speed data line. The communications buffers are constructed as two completely independent units for operation with the respective Alpha and Beta subsystems. Communications equipment is contained within two additional rack cabinets attached to the eight existing cabinets of the subsystem (Fig. 47).

The communications buffers are composed of the following functional elements:

(1) Three full duplex teletype units–Alpha and Beta

(2) Teletype patch panel–Alpha and Beta

(3) High-speed data line register–Alpha and Beta

(4) Time/display register–Alpha and Beta

(5) Interface buffer–Alpha and Beta

(6) Interface connector panel

(7) Interrupt patch panel

(8) Parallel input/parallel output junction chassis

a. Teletype communications equipment. Three full duplex teletype communications channels for Alpha and for Beta, each capable of simultaneously transmitting and receiving, interface directly with common carrier transmission lines. Standard five-level Baudot code characters are transmitted and received at either 60 or 66.7 words per minute (wpm), as determined by the interfacing communications equipment in use at each station. This requirement exists as a result of the disparity between U. S. and overseas teletype rates. The overseas rate of 66.7 wpm is reduced to an equivalent 60 wpm rate through generation of an extended stop pulse (refer to "Overseas modified Mode 3" in Table 7). Separate clocking circuitry in the send and receive units allows data to be transmitted at a different rate than it is received. The teletype receiving equipment will synchronize on incoming signals with bias distortion as great as 20% without degradation.

b. Teletype send logic. The teletype send equipment is made up of a send-logic chassis, send-channel chassis, and three send-channel positions. The send-logic chassis

Table 7. Nominal telemetry signal characteristics

Telemetry signal	U. S. Standard Mode 1	Overseas standard Mode 2	Overseas modified Mode 3
Character Baudot Code sequence, units	7.42	7.5	7.5
Stop pulse length, units	1.42	1.5	2.16
Modified code sequence length, units	7.42	7.5	8.16
Transmission rate, Baud	45	50	50
Transmission rate, wpm	60	66.7	60
Receive rate, Baud	45	50	50
Receive rate, wpm	60	66.7	66.7
Unit interval, msec	22	20	20
Character length, msec	163	150	163

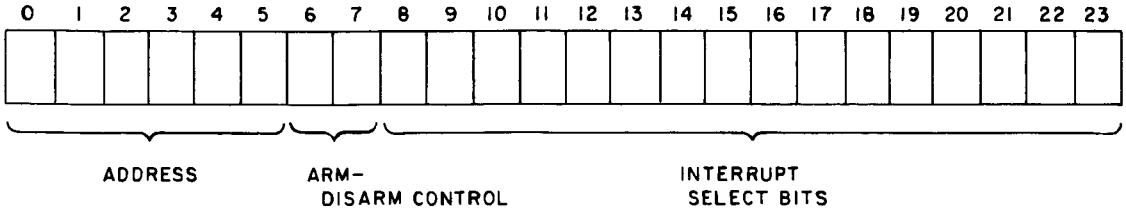

Fig. 45. Interrupt arm-disarm parallel output word format

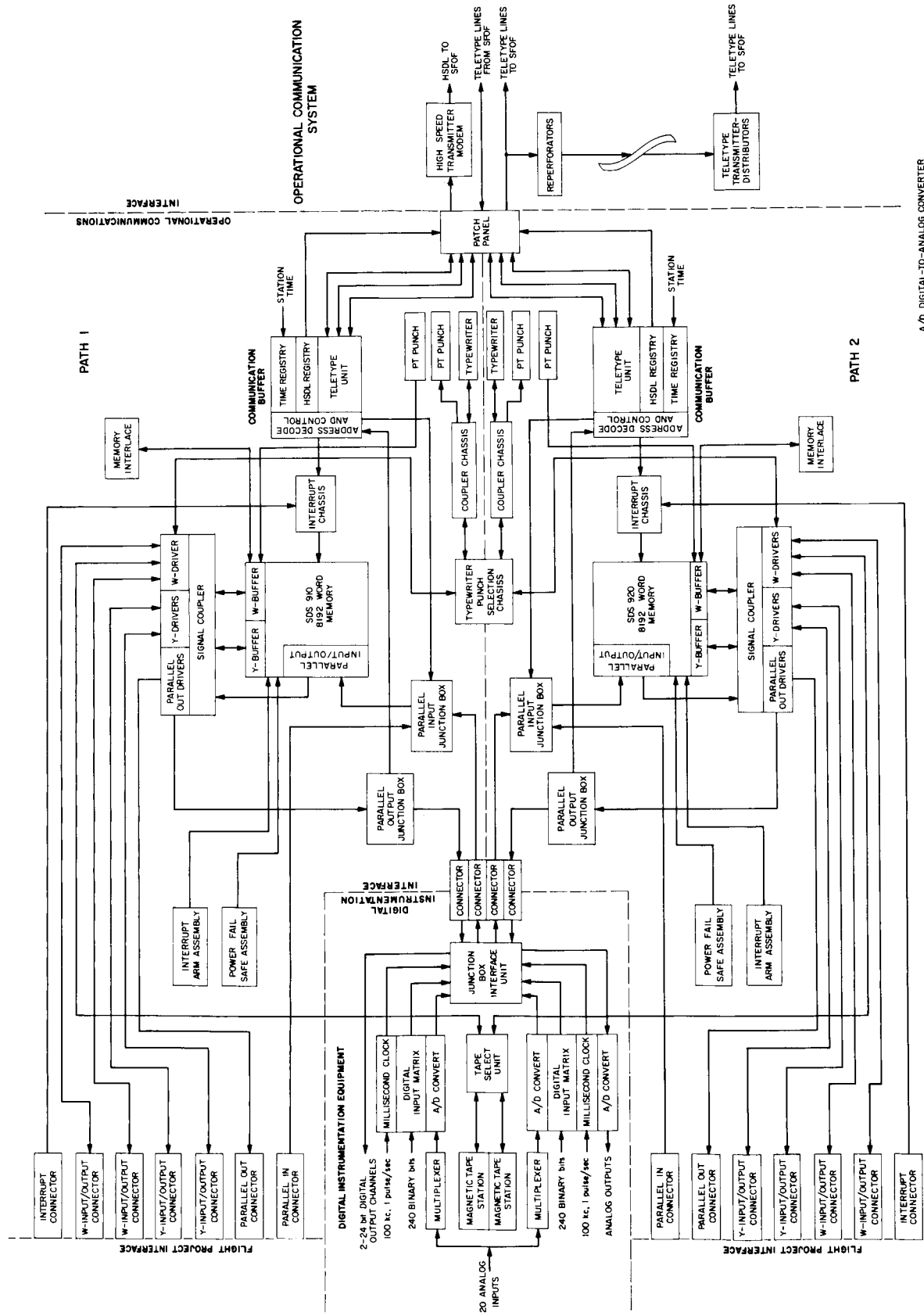

Fig. 46. Digital instrumentation subsystem, block diagram

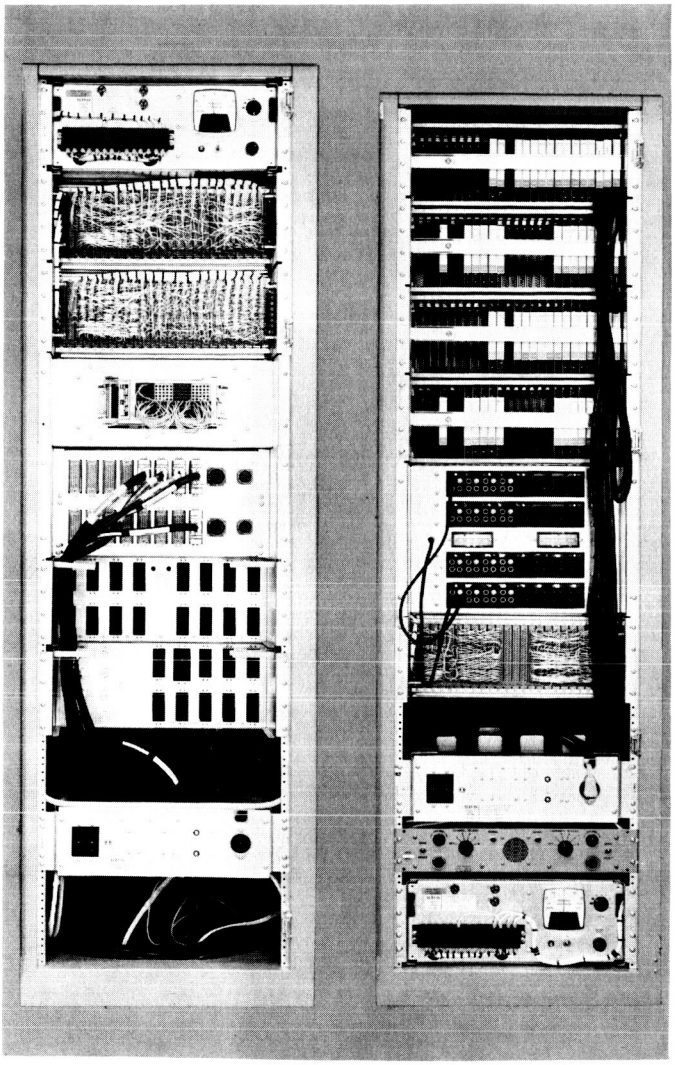

Fig. 47. Communications buffers, doors removed

establishes the transmission rate from a tuning fork oscillator frequency of 400 or 720 cps, the output of which is divided down to 50 or 45 Baud, respectively, to derive the rate for the particular station. Start (space) and stop (mark) bits are added to the five data bits to define the character.

The send-channel chassis accepts the character bit-parallel and stores and presents it to the send-channel position shift register flip-flops for conversion to a serial bit stream. The character, including data and control bits, is shifted out in serial to the line-driving relay for output to the transmission line in a neutral or polar loop current configuration.

The teletype send equipment operates under interrupt control. The program performs an SKS (skip if signal not set) to determine if the send channel is ready for loading. When available, the computer outputs a character to the send channel with an EOM/POT sequence, the POT word containing the address of the output channel and the data to be transmitted (Fig. 48(a)). The POT word then deselects the loaded channel. When all send channels have been loaded, the program issues a *send EOM* instruction which initiates transmission at the clock rate of the unit. The empty send registers generate an interrupt to the computer and the cycle repeats until disconnected.

c. Teletype receive logic. The teletype receive equipment is composed of a *receive logic* chassis, *receive channel* chassis, and three *receive channel* positions. The output of a 720 or 800 cps tuning fork oscillator in the *receive logic* chassis is divided down to the selected receiving rate of 45 or 50 Baud, respectively. A 200-kc oscillator provides the clocking signal for the channel scanner, which inspects each of 128 possible receive channels for a loaded condition. The *receive channel* positions contained in the *receive channel* chassis accept the serial input from the line-isolating relay.

A three-stage bit-sampling counter clocks the serial bits into the shift register flip-flops at the time when bias distortion is minimized. Data bits are converted to a five-bit character for parallel presentation, along with the channel address, to the computer. An *end of message* recognition circuit inspects incoming data for a *figures, Z, letters* sequence and initiates a disconnect for the selected channel when detected.

The teletype receive equipment operates in an interrupt mode in a manner similar to the send equipment. An SKS inspects the receive channels to determine if they are loaded. When the scanner detects a full channel, an interrupt to the computer will be generated. The data, along with the channel address, is entered into the computer with an EOM/PIN (parallel input) sequence (Fig. 48(b)). The PIN operation then deselects the channel, and the scanner is released to search for another full channel. Should a new word be received by a channel before the computer has accepted the current word, the old word would be obliterated and the new word would be entered into the computer along with the error indication bit.

Upon detection of a *figures, Z, letters* sequence, an *end of message* interrupt will be produced, and the channel will be disconnected. A channel is also disconnected with an EOM/POT sequence, the POT word containing a

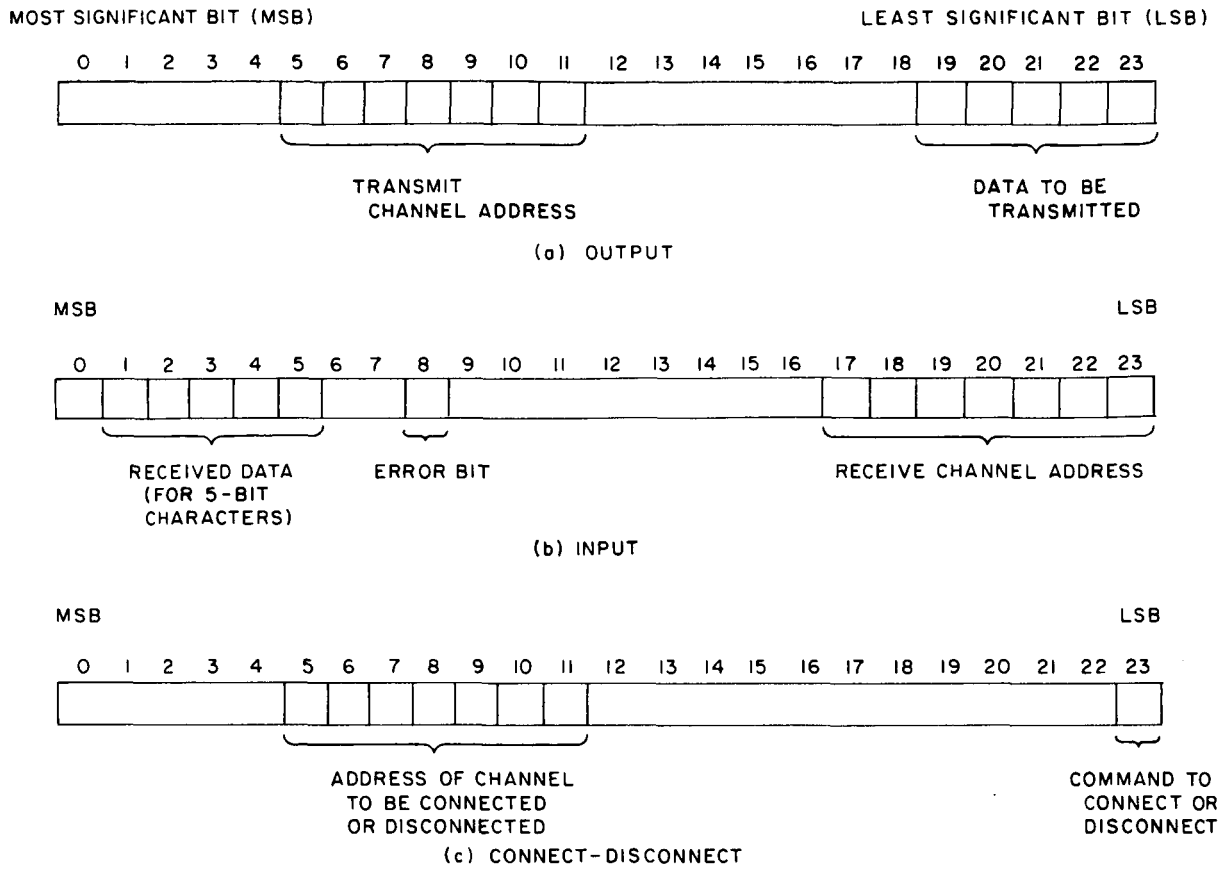

Fig. 48. Telemetry word format

disconnect bit together with the address of the channel to be disconnected [Fig. 48(c)].

d. Teletype patch panel. The teletype patch panels for Alpha and Beta allow send and receive channels to be connected to selected teletype lines. One set jack and two loop jacks for each channel provide for disconnecting or reconnecting any channel to alternate positions. An indicator lamp presents a visual display of the condition of each line. A panel-mounted line current meter is patched into the current loop for measuring and adjusting line current.

e. High-speed data line. The high-speed data line registers for Alpha and Beta communications buffers accept data from the computer parallel output lines for conversion to a serial bit stream. The serial output is presented to a high-speed data line modem for transmission at the clock rate determined by the modem (typically 600 or 1200 bps, to a maximum of 4400 bps). The high-speed data line register operates in an interrupt mode with the computer. Data from the parallel output is stored in the register and the computer is released. A complete word is the serial output from the register and an interrupt generated to signal the computer to present the succeeding word.

The high-speed data line register consists of 26 shift register flip-flops, 24 of which accept the parallel output word. The clock signal from the modem is gated to shift out the contents of the register. A flag bit is set into the register after the last data bit to indicate when the register is empty (Fig. 49). This flag bit is generally inserted in the register as part of the data word. For the 24-bit data word, the flag bit is inserted in an extra register position with a pair of thumbwheel switches set to the word length. A gate detects the empty register and flag bit and turns off the clock pulse from the modem to halt the shifting. The interrupt to the computer is then initiated and the cycle repeated.

An EOM/POT sequence selects the high-speed data line register and presents the data word on the parallel output lines. The contents of the word-length thumbwheel switches are entered with an EOM/PIN sequence if required for verification of the switch setting.

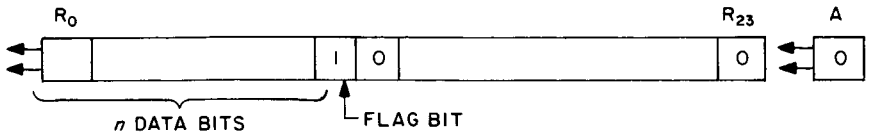

(1) THE (n) SIGNIFICANT BITS CONTAIN DATA
(2) THE ($n+1$) MOST SIGNIFICANT BIT CONTAINS A *ONE*
(3) ALL REMAINING BITS INCLUDING "A" ARE *ZERO*

Fig. 49. High-speed data line parallel output word

f. Time/display register. A time register accepts station time as an input for Alpha and Beta. Time information is entered as two words on the parallel input lines. The first word contains 24 bits of binary coded decimal data representing hours, minutes, and seconds. The second word contains 14 bits of binary coded decimal data representing the day of the year. Each word is entered with an EOM/PIN sequence. The time register logic levels are gated in as negative true signals, level shifted to the positive true logic of the computer and transformer coupler to the parallel input lines. The time input word formats are shown in Fig. 50.

The display register presents subsystem data to two remote in-line decimal displays (*SPS 37-30*, Vol. III). The output consists of 13 bits of binary coded decimal data (for a maximum decimal count of 1999) together with two data condition bits. The parallel output is level-shifted from the computer positive true to the negative true logic levels required by the external display registers. An EOM/POT sequence for each of two words will gate the output to the selected external display storage register (Fig. 51).

g. Interface buffer. The communications buffers are equipped with cable drivers for the W-buffer, Y-buffer, and parallel output of each computer. A terminated output with an impedance of 33 Ω in both states is provided for driving cables which have a 33-Ω characteristic impedance.

h. Interface connector panel. All interfacing with Alpha and Beta subsystems is performed at the interface connector panel. Connectors for output to the W-buffer, Y-buffer, parallel output, telemetry display, and high-speed data line, and for input from the parallel input,

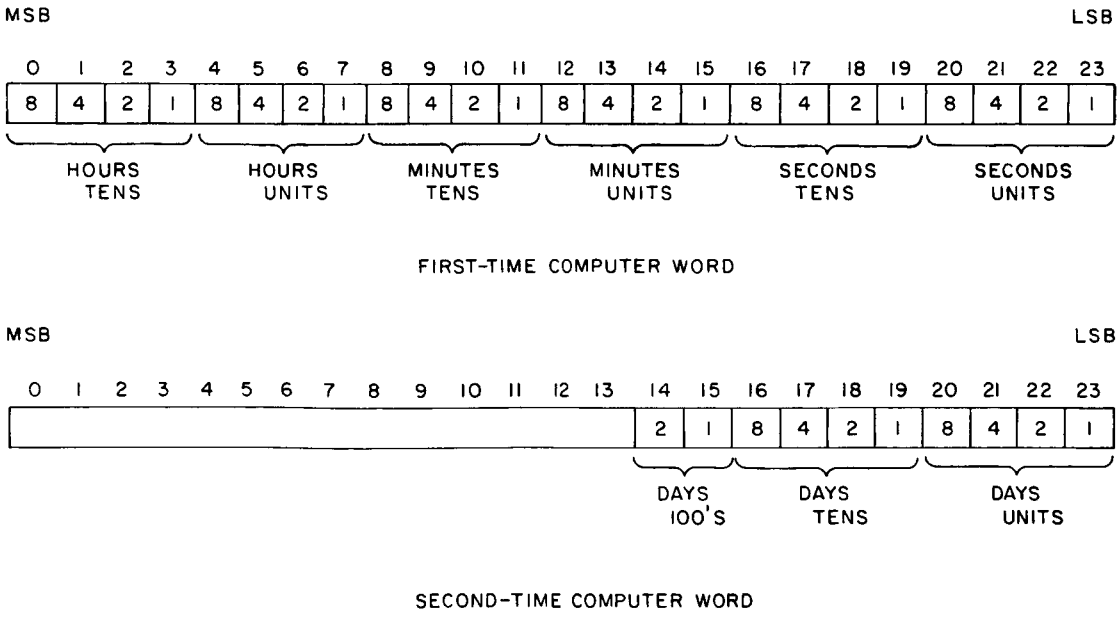

Fig. 50. Time register input word format

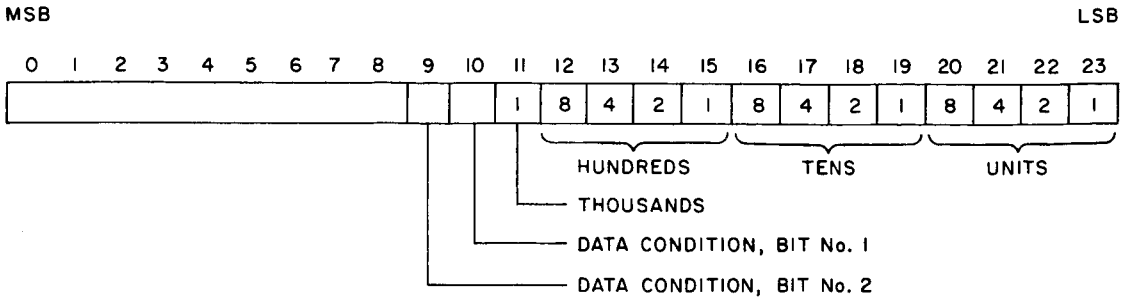

BIT CONFIGURATION		CONDITION	
No. 2	No. 1		
1	0	NOT ALLOWED	(NO LIGHT)
1	1	GOOD	(GREEN)
0	0	BAD	(RED)
0	1	QUESTIONABLE	(AMBER)

Fig. 51. External data display word format

priority interrupts, and station time are located on this panel.

i. Interrupt patch panel. All 16 external system priority interrupts for Alpha and Beta subsystems are routed through a 10 × 20 patch panel. Priority interrupt inputs from external mission-dependent equipment and interrupt inputs from the data gathering equipment of the DIS are brought out to the patch panel. These interrupts are patched from either source to the Alpha or Beta computer priority interrupt chassis. Priority levels are established by appropriate patch panel jumper connections. Unused interrupts are returned to ground through a portion of the patch panel allotted for this function. Rapid interchange of interrupt assignments or priorities is accomplished with removable plug boards, which may be prewired. Panel areas assigned for various functions are identified by different colors.

j. Parallel input/parallel output junction chassis. Parallel input and parallel output lines from both computers are routed through a junction chassis. Signals which otherwise would experience a loading effect are isolated in this unit through transformer coupling.

References

1. Straiton, A. W., and Tolbert, C. W., "Anomalies in the Absorption of Radio Waves by Atmospheric Gases," *Proceedings of the IRE*, May 1960, pp. 898–903.

2. Potter, P. D., "A New Horn Antenna With Suppressed Sidelobes and Equal Beamwidths," *The Microwave Journal*, Vol. VI, No. 6, June 1963, p. 71.

III. Communications Engineering Development

A. S-Band Implementation for the DSIF

1. Traveling Wave Maser for the DSIF

All systems are operating very satisfactorily and failure rates have been reduced. Weekly reporting of the daily log on pertinent pressures and temperatures in the closed cycle refrigerator (CCR) to JPL has helped considerably in enhancing the confidence factor.

A significant contribution to improve system reliability has recently been made by the manufacturer of the CCR, A. D. Little, Inc., Cambridge, Massachusetts (ADL) by developing a gas sampling device with extremely high sensitivity. This device consists of a capillary tube immersed in liquid nitrogen with provisions for connecting the high pressure supply line of helium gas with an intermediate pressure return line. A pressure gauge is appropriately tapped into the return side so that one can monitor the rate at which contaminants accumulate (freeze out) in the cold capillary tube. A poor compressor will plug the tester in a few minutes whereas a good one will operate for many hours. A quantitative measure of the kind of purity desired was demonstrated by using the tester on a bottle of gas labeled "special high-purity helium." The capillary clogged in exactly 3 min.

With the aid of the tester, ADL appears to have found the cure for the oil carry-over problem in the compressor. One of the oil separators consists of a glass fibre pack wet with oil; as the helium gas flows through this pack molecules of oil come into contact with other molecules and tend to form large drops of oil which are readily removed. ADL found recently that by doubling the amount of glass fibre in the separator its effectiveness increases significantly. Tests performed at JPL have confirmed their findings. All stations will be instructed to repack their filters as soon as practicable; in the interim, satisfactory operation will be ensured by keeping the compressor in a cool (50 to 75°F) environment.

2. Acquisition Aid for the Ascension Island Station (DSIF-72)

The design for the DSIF-72 acquisition aid antenna system (*SPS 37-33*, Vol. III, p. 26) has been completed and final fabrication is in progress.

The acquisition aid system consists of two antennas (1) a low gain horn monopulse tracking antenna (Fig. 1) to be located at the 30-ft antenna apex, and (2) a low gain 10-kw transmitter horn (Fig. 2) to be located on the 30-ft antenna surface.

Two low gain monopulse tracking antennas have been completely fabricated except for the polarizer section and hybrid assembly. The final design requires two complete hybrid bridges to reduce the overall antenna length, as the difference channel modes and sum channel mode

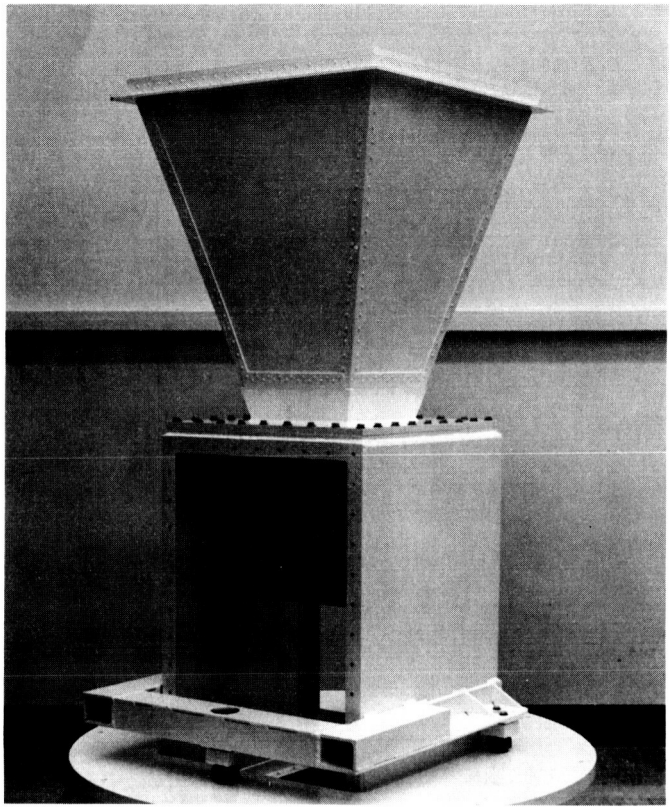

Fig. 1. Monopulse tracking antenna

required a rather long (≈27 in.) phasing section to yield right handed circular polarization (RCP) from the same bridge ports. As a result, the phasing section has been shortened (≈9.0 in.), and both the RCP and left handed circular polarization (LCP) error and sum functions will be available (sum channels and error channels are of the opposite sense on the same bridge). Only the RCP outputs will be used in the initial acquisition aid system. Space will be available in the RF enclosure box at the 30-ft antenna apex to add polarization diversity switching if required at a later time, (three RF switches and control circuitry).

The monopulse tracking antenna equipment will be delivered to the Goldstone Pioneer Station 30-ft antenna mock up in early July for mechanical assembly. RF testing (patterns and gain) will continue on the second unit at the JPL Mesa antenna range thru August.

The transmitter horn antenna assembly is complete and antenna measurements are in progress. A complete and tested transmitter horn antenna will be delivered and installed on the mechanical mock up in early July.

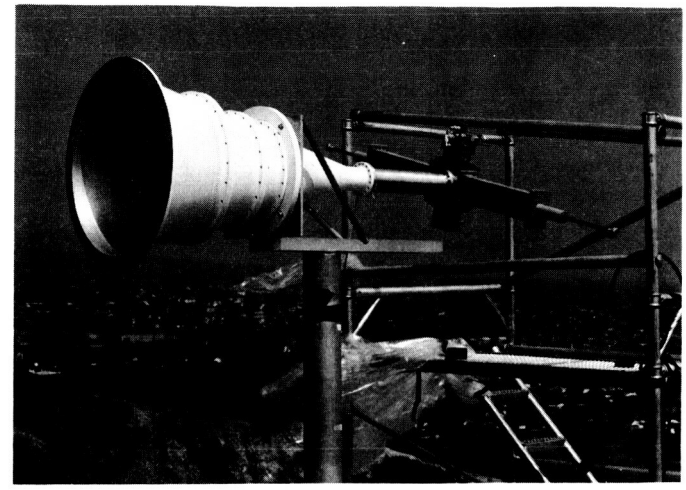

Fig. 2. Transmitter antenna

The RF filters, coax, and waveguide are 90% complete and final delivery of all components will be made in late July. Installation of these items will be made with the monopulse and transmitter acquisition aid horns.

3. Upgrade of the Pioneer Station (DSIF-11) Acquisition System

a. Summary. The DSIF-11 acquisition aid system (SAA) to support *Apollo* back-up requirements is being upgraded. During this reporting period the DSIF-11 waveguide associated with the SAA was broadbanded and calibrated.

b. Present Status of System. DSIF-11 waveguide sections made of copper, which were temporarily installed originally were replaced by aluminum sections, identical to those in use at DSIF-51 (Johannesburg) and DSIF-41 (Woomera).

An effort was made to tune the sum reference channel electrically for the *Apollo* DSIF receiver band (2270 to 2300 Mc) for both the RCP and LCP operation. Waveguide spacers were used to phase out discontinuities in the line. The results listed below were obtained without the use of tuning screws; since tuning screw use proved ineffective to improving the results, the following appears to be optimized:

Frequency, Mc

		2265	2270	2275	2280	2285	2290	2295	2300	2305
VSWR	RCP	1.13	1.05	1.25	1.14	1.18	1.06	1.25	1.06	1.27
	LCP	1.14	1.21	1.28	1.19	1.11	1.04	1.19	1.03	1.20

The test point used was the paramp bypass switch, a point at which no maximum VSWR is specified. However, the paramp input VSWR is 1.5 (maximum); and, pending tests with the paramp, it is believed that the above results will not exceed compliance with the specification when the remainder of the sum channel is added to complete the connection to the paramp.

Other test results were obtained of the transmit line from the electronics interface outside the Room to the point of entry into the diplexer: VSWR = 1.09 at 2105 Mc.

c. Work to be Completed. A complete electrical evaluation of the DSIF-11 acquisition system is necessary to insure its satisfactory performance for *Apollo*; but it will not be practical to make the evaluation until after the *Mariner IV* encounter because of a schedule conflict on the 85-ft antenna. This evaluation will entail, for the most part, appropriate readjustment of tuning devices already a part of the system. Some feed modification on the collimation tower horn is envisioned, since its performance is presently optimized for a midband frequency of 2295 Mc, rather than the 2285 Mc midband frequency of the *Apollo* DSIF. A new polarizer probe and shorts are indicated by this new frequency requirement. Changes made at DSIF-11 and the final test results will serve as guidelines for a subsequent upgrade of the overseas installations.

B. Ground Instrumentation for *Mariner* C Occultation Experiment

1. Summary

The *Mariner IV* occultation measurements will differ from those ordinarily made by the DSIF in that the duration of the phenomena involved will be short. The integration techniques normally used to obtain precise data cannot be applied in this experiment. To measure the occultation phenomena, two separate implementations will be employed. The first is the normal S-band configuration on receiver channel No. 1. From this configuration the received power as a function of time will be determined from the static and dynamic automatic gain control (AGC) voltages. The doppler frequency will be obtained from the doppler extractor. To increase the resolution and decrease the quantization error, the normal doppler output will be multiplied by eight and will have its constant frequency bias removed.

The second channel will operate as an open loop triple conversion superheterodyne. All three local oscillator signals will be derived from the rubidium standard and synthesized to the required frequency. The output of the second channel will then be a frequency translated, amplified version of the S-band received signal, which will be in the 1 to 3 kc range at the output so that it can be predetection recorded on magnetic tape.

2. Simulation of Expected Amplitude Modulation

The *Mariner IV* occultation modifications have been made at the Goldstone Pioneer and Echo Stations. To test these receivers, an amplitude simulation of the anticipated Fresnel modulation has been made. To adequately simulate the diffraction phenomena an IBM 1620 program was written for the voltage function necessary to drive an RF modulator to produce the expected Fresnel effect. The punched card output of this program was then used on the digital PDP4 computer to obtain a digital to analog conversion. The analog function was recorded on magnetic tape, which was then used on the FR 1400 tape recorder, along with the appropriate amplification and biasing equipment, to drive the HP 8714A modulator. The modulator was placed between the test transmitter and the receiver input.

Fig. 3 shows the simulation of the amplitude fluctuations for a free space signal level of −120 dbm. The top trace is the modulator drive; the second trace is the dynamic AGC of receiver No. 1 in the manual gain control (MGC) position. A 50 cps low pass filter was used. The third trace is derived from the open loop receiver where the signal has been put through a 10 cps band pass filter prior to detection.

In Fig. 4 the configuration is the same as in Fig. 3, except that receiver No. 1 is in AGC. Fig. 5 has an input power level of −158 dbm and receiver No. 1 is in MGC. Fig. 6 also has an −158 dbm input and receiver No. 1 is in AGC.

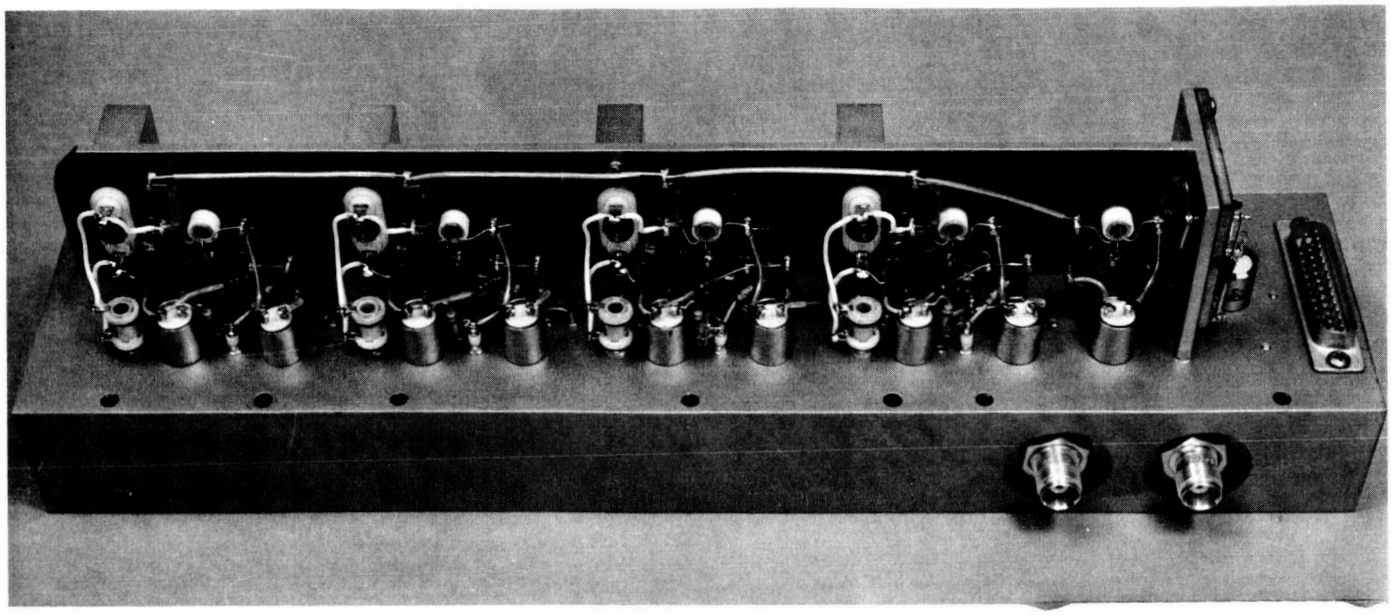

Fig. 16. Multiple VCO

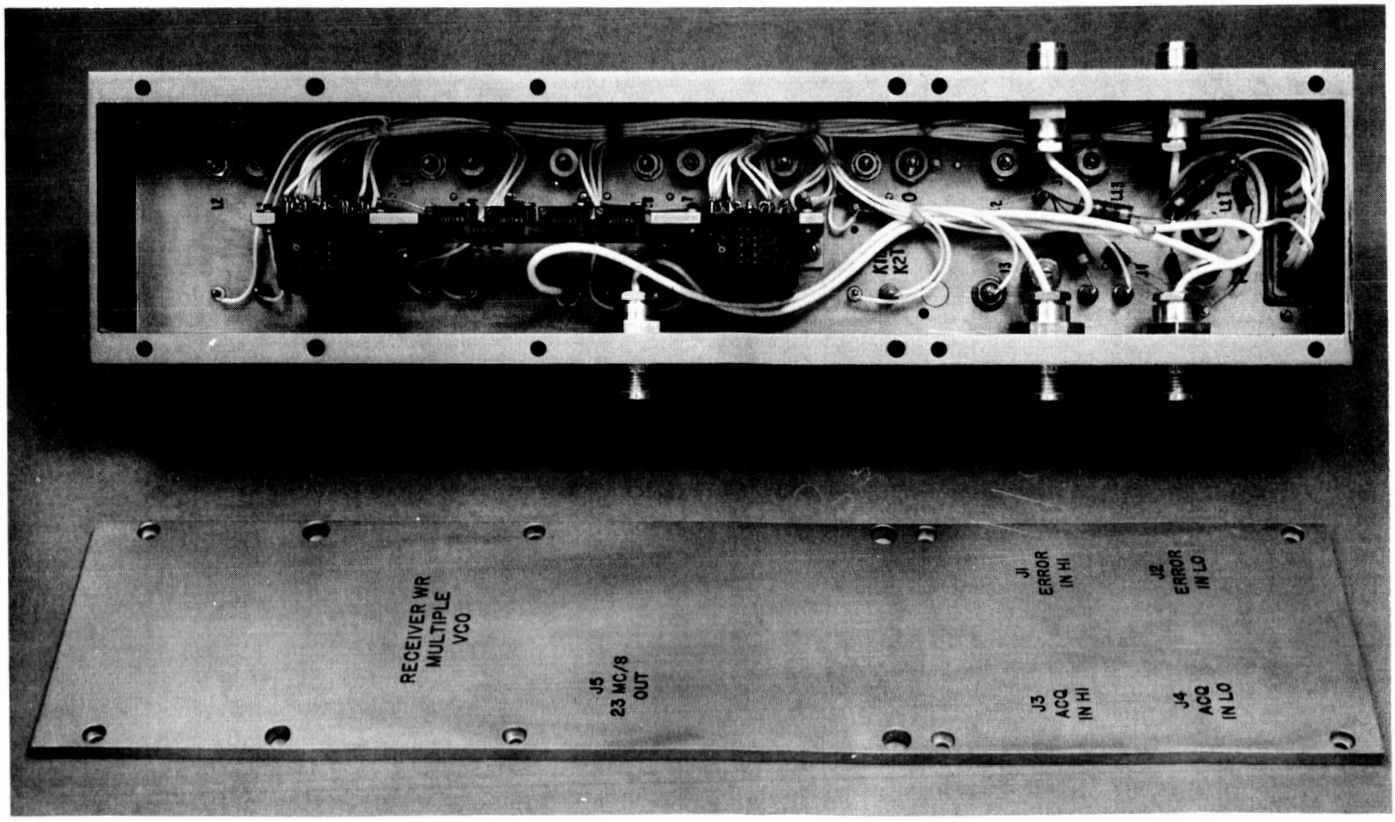

Fig. 17. Multiple VCO

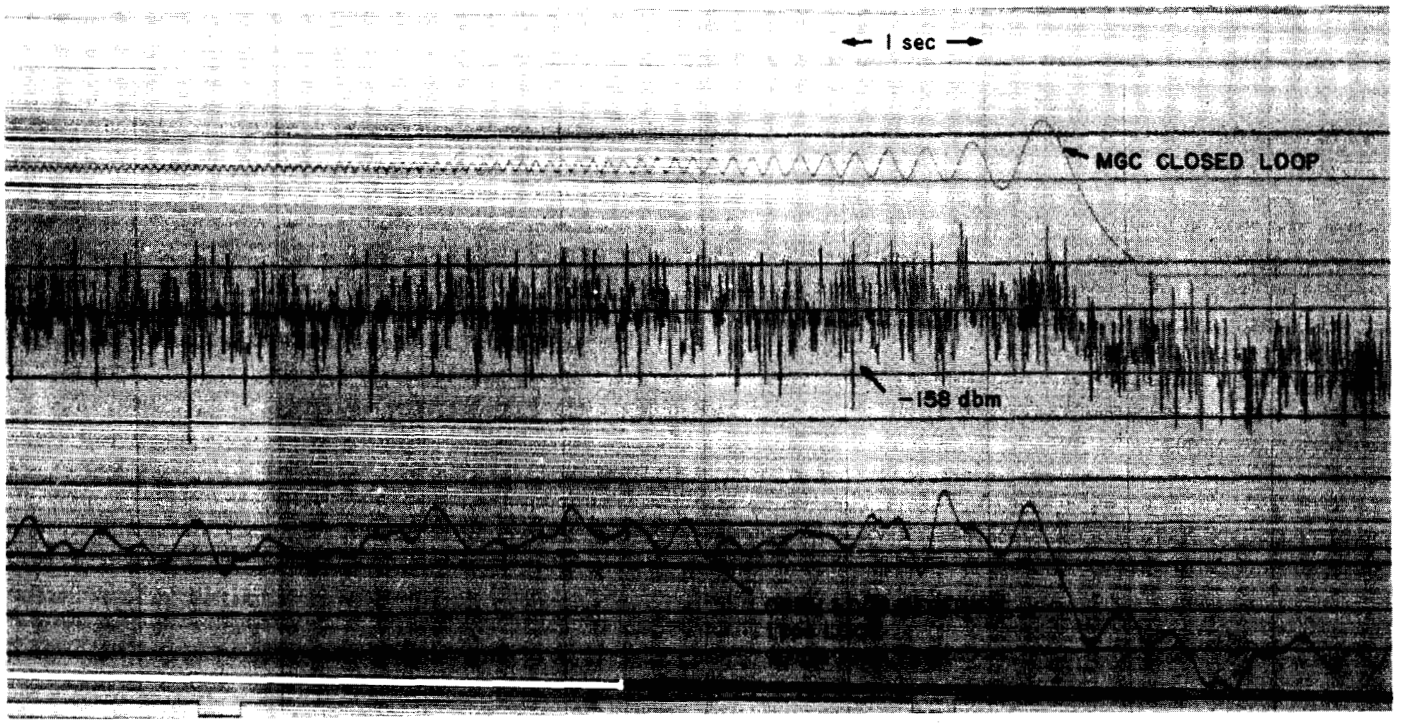

Fig. 5. Occultation simulation, input power −158 dbm, receiver No. 1 in manual gain control

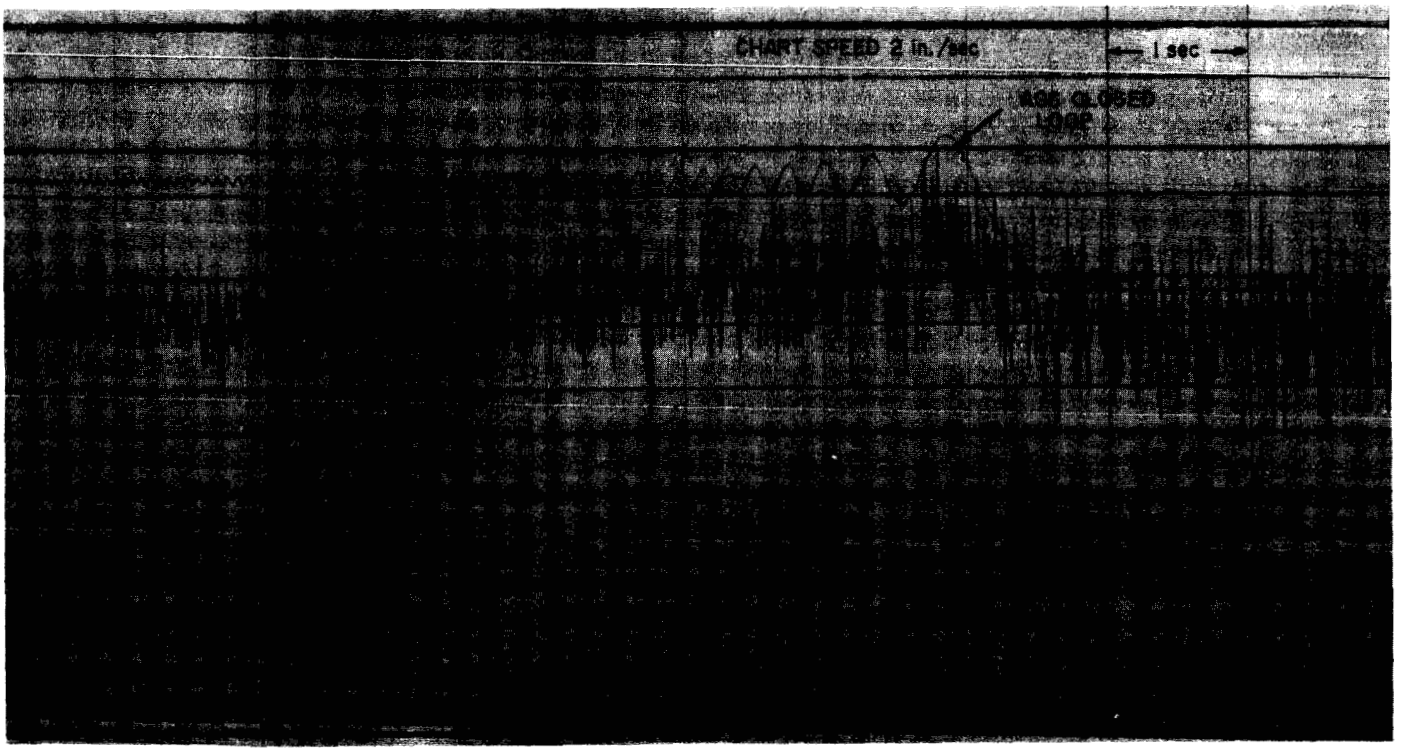

Fig. 6. Occultation simulation, input power −158 dbm, receiver No. 1 in automatic gain control

3. Doppler Accuracy as a Function of Signal Level

In *SPS 37-33*, Vol. III, p. 32, the standard deviation of the doppler count as a function of input signal level was discussed. Preliminary measurements and the experimental set-up were also discussed. The data have now been reduced and Fig. 7 shows the relationship of the standard deviation of 1 sec cumulative doppler count as a function of the input signal level in dbm. The upper curve was made without using RF multiplication and the lower curve was made using a times eight multiplier.

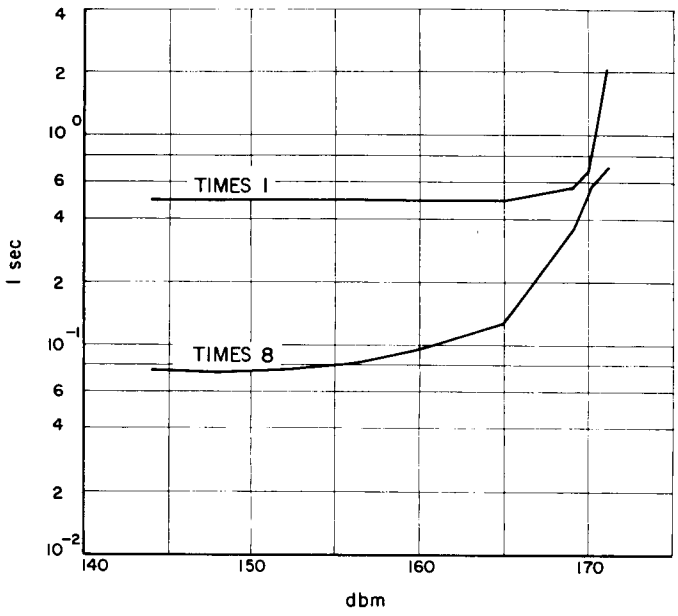

Fig. 7. Cumulative doppler standard deviation

C. S-Band Cassegrain Monopulse Cone Assemblies

1. Summary

Detailed noise temperature data are presented for a typical S-band Cassegrain monopulse (SCM) cone assembly mounted on a DSIF antenna. Results of a special high power diplexing test on the Echo Station, SCM cone assembly are discussed. Development and fabrication of the SCM cone assemblies and SCM feeds were reported in *SPS 37-33*, Vol. III, p. 43, and earlier summaries.

2. System Temperature

Prior to installation within an SCM cone assembly, the characteristics of components and subassemblies affecting system noise temperature are carefully measured and recorded. After delivery to Goldstone, each complete SCM cone assembly is fully ground tested to verify that its overall noise temperature is within a few degrees of the predicted value, and that the major subassemblies are performing as anticipated. The noise temperature determinations are repeated when the SCM cone is mounted on its 85-ft antenna and mated with the Goldstone duplicate standard receiver and transmitter. During tracking missions, the system temperature is monitored continuously by chart recorder; and occasional checks are made to verify that the relative contributions of the traveling wave maser (TWM), receiver, and antenna (including component insertion losses) are nominal.

From all of these measurements, as well as supporting experiments in the area of Cassegrain antennas, feeds, aperture blockage and scattering, and atmospheric/extra-atmospheric effects, a fairly precise breakdown of the factors contributing to the total system temperature can be made.

Table 1 itemizes the contributions to system temperature for a typical DSIF S-band antenna system using any one of the five SCM cone assemblies now in operation. Variations measured throughout the DSIF network in the zenith system temperature of 42°K shown in

Table 1. S-Band system temperature breakdown

Source of noise temperature	Contribution, °K	
(1) Atmosphere and extra-terrestrial background	3.0	
(2) Quadripod scatter	5.0	
(3) Paraboloid spillover	1.0	
(4) Paraboloid surface leakage	1.0	
(5) SCM feed insertion loss, including coupling to other ports	5.0	
Antenna temperature		15.0
(6) Diplexer insertion loss	5.5	
(7) Waveguide switch insertion loss, two switches, total	4.6	
(8) Waveguide insertion loss, 12 ft at 0.0035 db/ft	3.9	
Insertion loss subtotal		14.0
(9) TWM, referred to coupler input	10.0	
(10) Receiver follow-up	3.0	
Receiver temperature		13.0
System temperature, antenna at zenith		42.0

Table 1 are less than ±4°K and are primarily due to differences in TWM gain and measurement tolerances.

The ten separate contributions shown in Table 1 have been grouped into three subtotals according to the accepted definitions of antenna temperature (measured at the antenna feed output), receiver temperature (preamplifier input temperature plus receiver effective temperture reduced by the preamplifier gain), and component and transmission line insertion losses between the antenna feed and preamplifier.

System temperature as a function of antenna elevation angle is shown in Fig. 8. Very little increase is evident at elevation angles down to 45 deg. From 45 to 10 deg, the rise is uniformly gradual except for a detectable perturbation in the vicinity of 20 deg, apparently due to direct feed spillover past the hyperboloid reaching ground level. Below 10 deg elevation the rise is very rapid as the atmospheric absorption path becomes very long and the secondary antenna pattern sidelobes reach ground level.

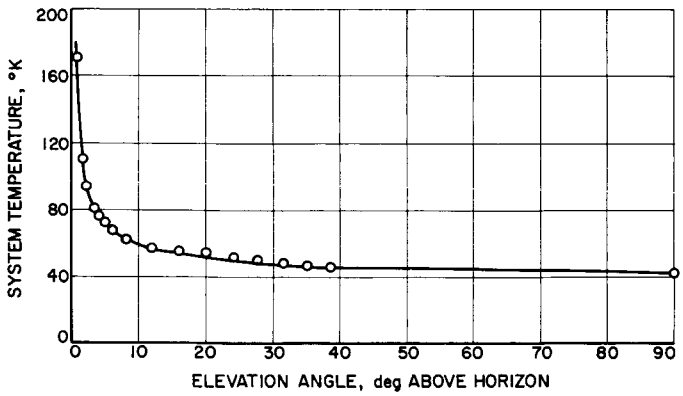

Fig. 8. System temperature as a function of antenna elevation angle

A useful rule of thumb for low noise Cassegrain antennas is that at 10 deg elevation the antenna temperature is twice that at zenith. For the SCM cone assembly, this is equivalent to about 50% increase in total system temperature.

3. High Power Diplexing Test

During normal operations of the DSIF, the SCM cone assembly is diplexed at a transmitter power level of 10 kw. Although each SCM cone was thoroughly ground tested at power levels slightly higher than this with satisfactory results, several stations have reported occasional noise bursts during testing and operations. Generally, these noise bursts are infrequent and of very short duration, with amplitudes up to several hundred deg K when recorded with a 1 sec time constant.

It is felt that these noise bursts are primarily the result of contaminants within the waveguide system, especially water vapor. In order to verify that there exists no flaw in the basic design or fabrication techniques of the SCM cone assembly, however, a special high power diplexing test was conducted on April 30, 1965 at Goldstone, using the serial number 6 SCM cone.

This cone had completed normal ground tests and was awaiting installation on the Echo antenna. Using a new klystron now available with the test transmitter at the Goldstone Test Station, the SCM cone was diplexed on both right handed circular and left handed circular sum channels at power levels up to 22 kw, the limit of the klystron.

The system temperature for this test, using the Echo TWM with a monitor receiver, was 33°K (for a ground test of an SCM cone assembly, contributions 2 thru 4 in Table 1 are not present). Although the resolution available for noise burst detection was approximately 0.5°K, no noise bursts were observed at any time during the test. In addition, no detectable increase in background noise temperature during diplexing, as compared to the quiescent system temperature, could be observed. For this measurement, the resolution available was less than 0.4°K.

It appears, therefore, that the SCM cone assembly design is adequate for present DSIF transmitter power levels and that more care in maintaining dry nitrogen pressure within the waveguides should eliminate the occasional noise bursts.

D. 50-Mc IF Amplifier (FM Telemetry)

1. Introduction

Frequency modulation (FM) will be one of the methods used for transmitting information on the down-link signal for the Manned Space Flight Network (MSFN). The

information to be sent by FM will be television or analog data, voice, and telemetry.

To accommodate the reception of the FM signals, a 50-Mc IF amplifier was developed for the ground receiver to increase the FM signals to the power level required by the demodulator. The amplifier was designed for a minimum half-power bandwidth of 10 Mc and a maximum gain of 40 db. Within the amplifier module a self-detection automatic gain control (AGC) system is incorporated (Fig. 9). The AGC system maintains the amplifier output signal level within 5 db of the nominal −20 dbm over a 40 db dynamic range.

2. Performance

A series of tests were conducted on the receiver FM channel of the laboratory research and development (R&D) system (Fig. 10) to evaluate the performance of the 50-Mc IF amplifier, using FM spectra of different modulating frequencies and indices over the range of receiver input signal levels. The primary purpose of the tests was to evaluate the AGC system in the FM channel.

The first set of measurements was made using an unmodulated carrier to determine the effects of threshold noise. The threshold of the FM channel is assumed to

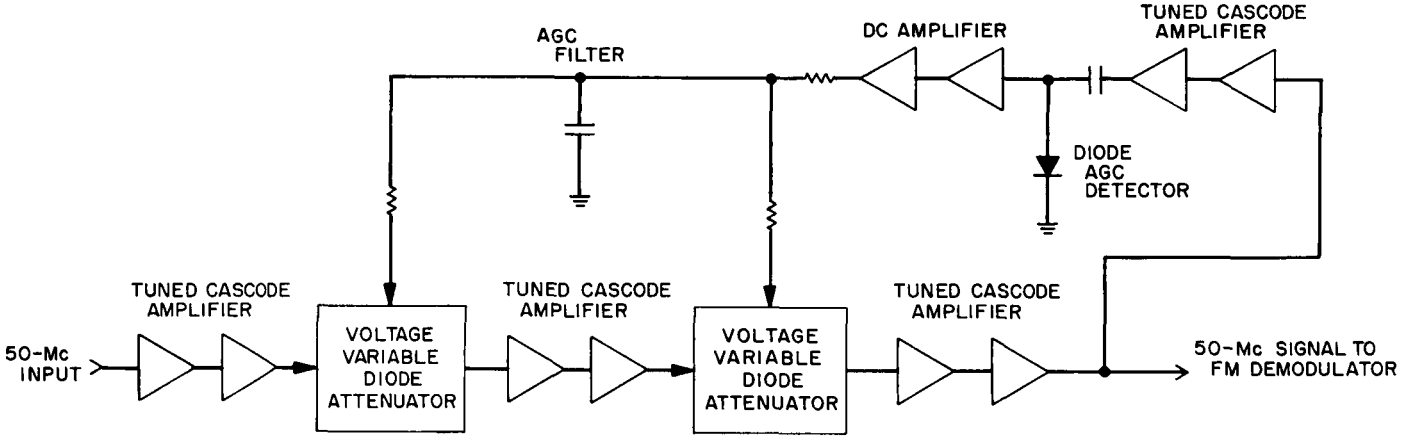

Fig. 9. Block diagram — 50 Mc IF amplifier

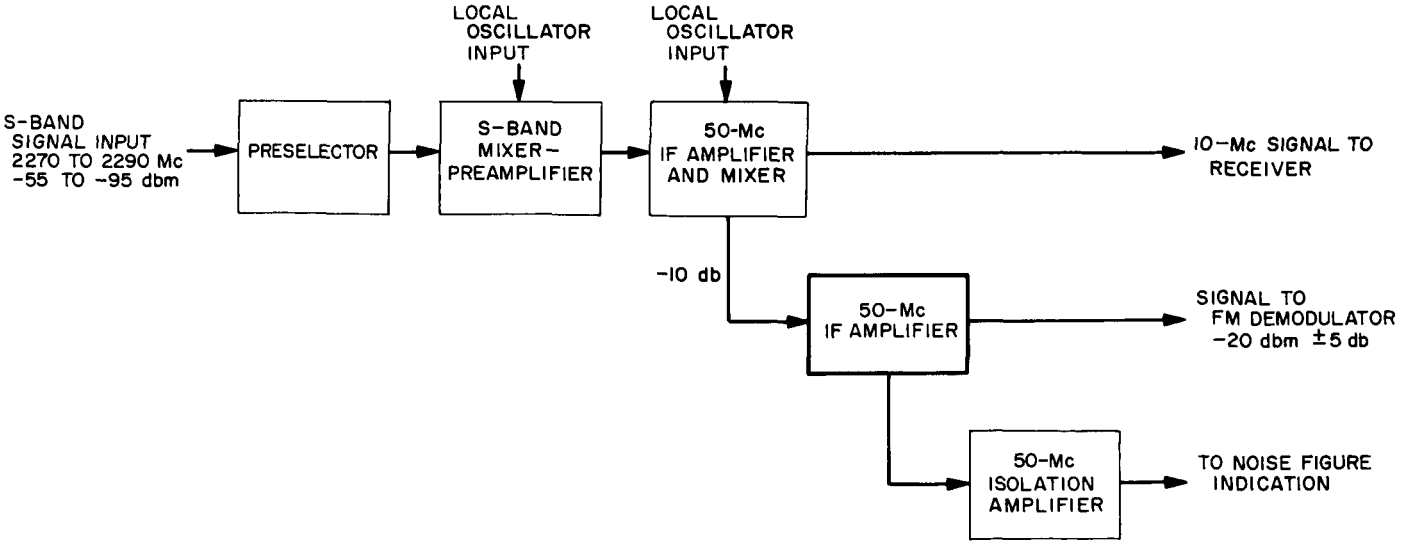

Fig. 10. Receiver FM channel

occur at a signal-to-noise ratio (S/N) of 6 db, with a possibility of recovering useful information at a level 6 db below this. To determine the threshold signal level, it was first necessary to calculate the noise bandwidth of the FM channel from the receiver response. The receiver response at the 50-Mc FM output (Fig. 11), measured with a fixed gain control of 0 v, indicates a half-power bandwidth of 9.1 Mc. The noise bandwidth as calculated from this response curve is 10.8 Mc. With a measured receiver noise figure of 10.5 db at the preselector input, and a noise bandwidth of 10.8 Mc, a S/N of 0 db occurs at −93.2 dbm. Measurements were, therefore, made over the dynamic range of −55 to −95 dbm.

Receiver noise in the FM channel causes the AGC voltage to deviate from the noise-free condition at a S/N of 6 db (Fig. 12). As the signal is reduced below this level, the AGC becomes controlled more and more by receiver noise until the AGC is clamped by the fixed noise level at a S/N of approximately −10 db. The effect of this AGC action is also shown in Fig. 13. When the S/N is less than 6 db, the signal no longer fully controls the AGC and the output falls below the nominal value of −20 dbm.

The effect of the wide bandwidth of the noise can also be seen in Fig. 13. As the input is reduced from −55 to −75 dbm, the amplifier output level drops normally. However, as the input level is reduced more, the total power output of signal and noise is increased. This increase in output power level is a result of the frequency response of the AGC predetection bandwidth and is demonstrated by the fact that when a constant signal level input to the 50-Mc IF amplifier is swept across the half-power bandwidth of the amplifier, the output increases approximately 1 db at the band edges (Fig. 11). This means the response of the tuned amplifier in the AGC loop is down 1 db at these frequencies, and the AGC loop compensates for this response. When the spectrum in the 50-Mc IF amplifier changes from a carrier signal with the power concentrated at the center of the band to a signal and noise with the power spread over the entire band, the response of the AGC system causes an increase in the amplifier output. The variation in the total power output due to noise at threshold is less than 1 db. This, however, offsets in part the decrease in the signal level at telemetry threshold due to noise saturation of the AGC system.

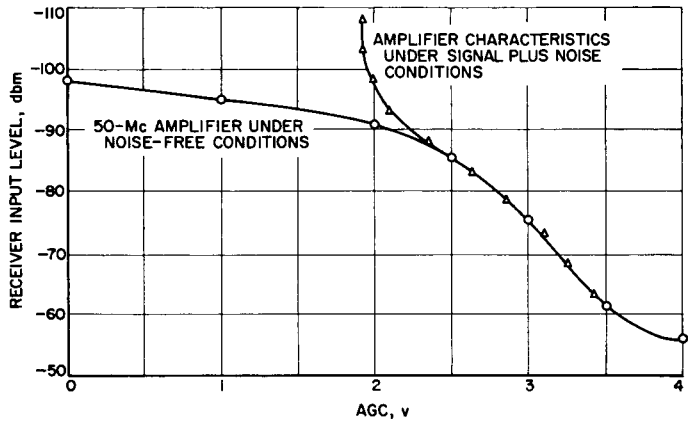

Fig. 12. Receiver FM channel AGC characteristics

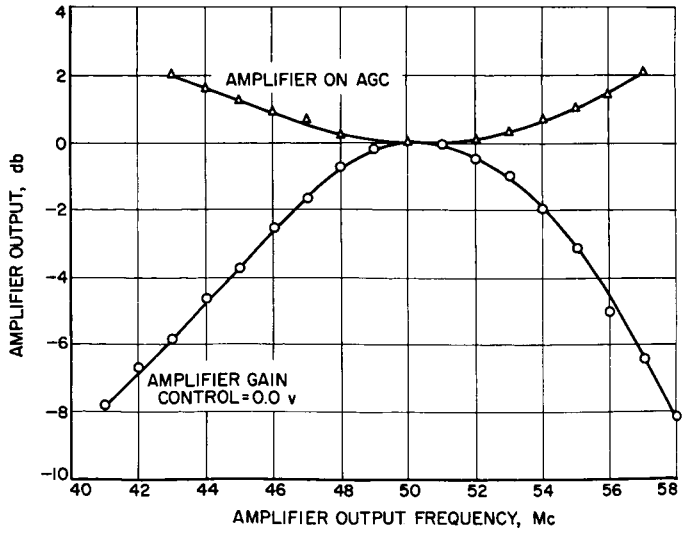

Fig. 11. Receiver FM channel frequency response

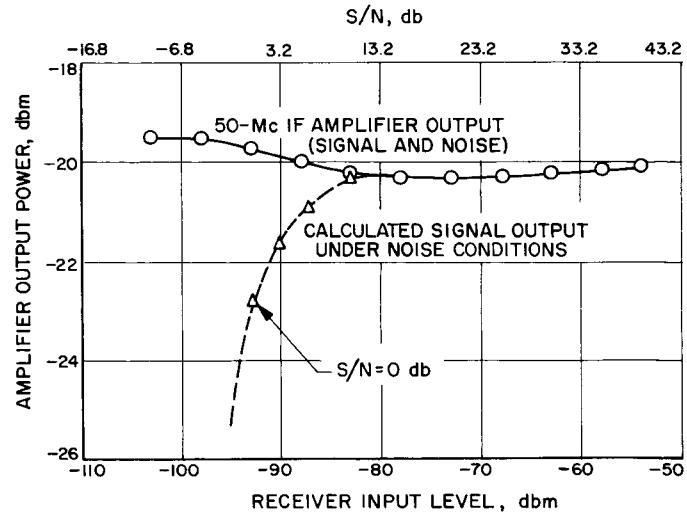

Fig. 13. Receiver FM channel AGC performance

The second set of measurements was made on strong signals with an FM signal to determine the effect of a wide band spectrum, composed of discreet frequencies. FM spectra obtained from single frequency modulating signals of 100 Kc, 500 Kc, and 1.25 Mc were used. As expected, the output level increases as the spectrum covers a wider bandwidth (Fig. 14). Again, the increase in output level above the nominal is not significant, less than 2 db.

In addition to the AGC action due to wide-band spectra of noise and modulation, the ability to track signal level variations is required. Frequency response measurements of the AGC system show a −3 db point greater than 150 cps. This indicates the AGC can follow any anticipated signal level variations due to spacecraft module orientation changes or transmission through antenna nulls.

3. Conclusion

After the AGC is adjusted for a nominal −20 dbm output level using an unmodulated carrier, variations in the output level resulting from a wide band FM spectrum or noise will be less than 3 db. This is within the design goal of 5 db.

E. RF Voltage Controlled Oscillator Development

1. Introduction

A block II receiver-exciter subsystem design was initiated to meet the requirements of the Manned Space Flight Network (MSFN). One of the major design changes has been the receiver and exciter voltage controlled oscillators (VCO's). High gain and wide frequency range, while retaining phase and frequency stability and design reproducibility, were the prime concern. These characteristics were dictated by the requirements of the acquisition scheme.

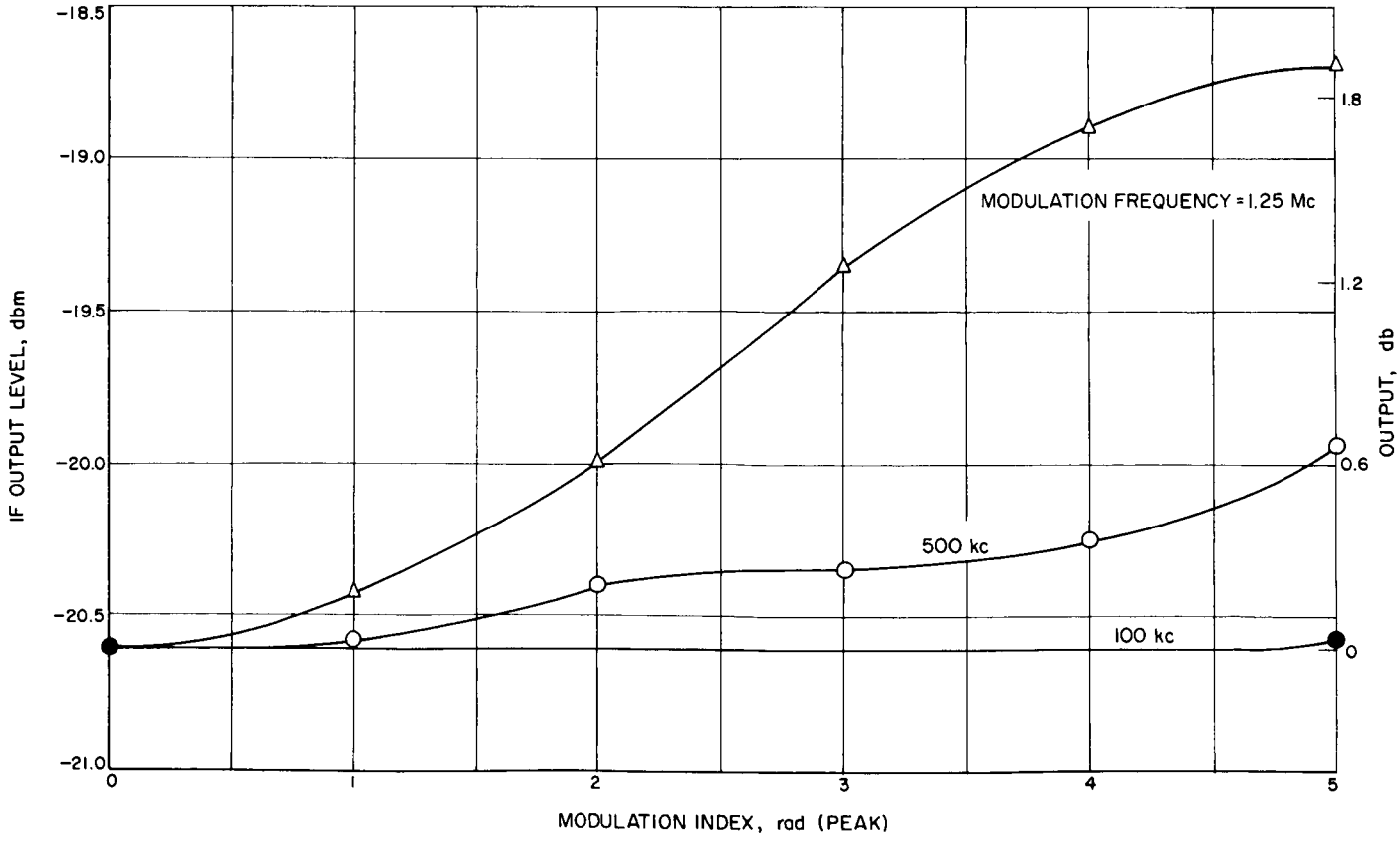

Fig. 14. Effect of wide band FM spectrum on AGC

Early developments of a 30-Mc phase-stable VCO have been reported (*SPS 37-15*, Vol. III, p. 34). This design was extended in subsequent developments to include such features as applying automatic level control (ALC) to the oscillator stage to maintain relatively constant crystal drive and consequently low phase jitter over the frequency range. However, these designs were concentrated on low gain narrow frequency range devices to obtain the most phase stable oscillators attainable.

This basic design was chosen as a starting point because of the repeatable performance obtained in the past. Modifications to the original circuit design were made in the following areas to accommodate the MSFN requirements.

(1) A 21 to 24 Mc frequency range was used in place of the original 30 Mc.

(2) A gain of 400 cps/v replaced the 70 cps/v of the original design.

(3) The frequency range was increased to ± 19 parts in 10^5 to meet the requirements of the acquisition scheme.

(4) The VCO had to remain in oscillation beyond the maximum range of acquisition voltage (± 6 v).

(5) The capability of immediate switching to any of the four assigned MSFN frequencies was required.

2. Circuit Description

The multiple VCO unit consists of four VCO stages, two series of amplifier stages, and an automatic level control circuit (Fig. 15).

The output of the oscillator stage is lightly coupled from the base, a low impedance point in the circuit. This light coupling plus the two buffer amplifiers provide adequate isolation of the oscillator from any loading effects at the output of the final amplifier. All voltages in the oscillator stage are zener regulated for additional stability. The base bias is variable and is adjusted during alignment to obtain optimum RF drive to minimize phase jitter generated by the crystal and to adjust the transistor bias for minimum noise output.

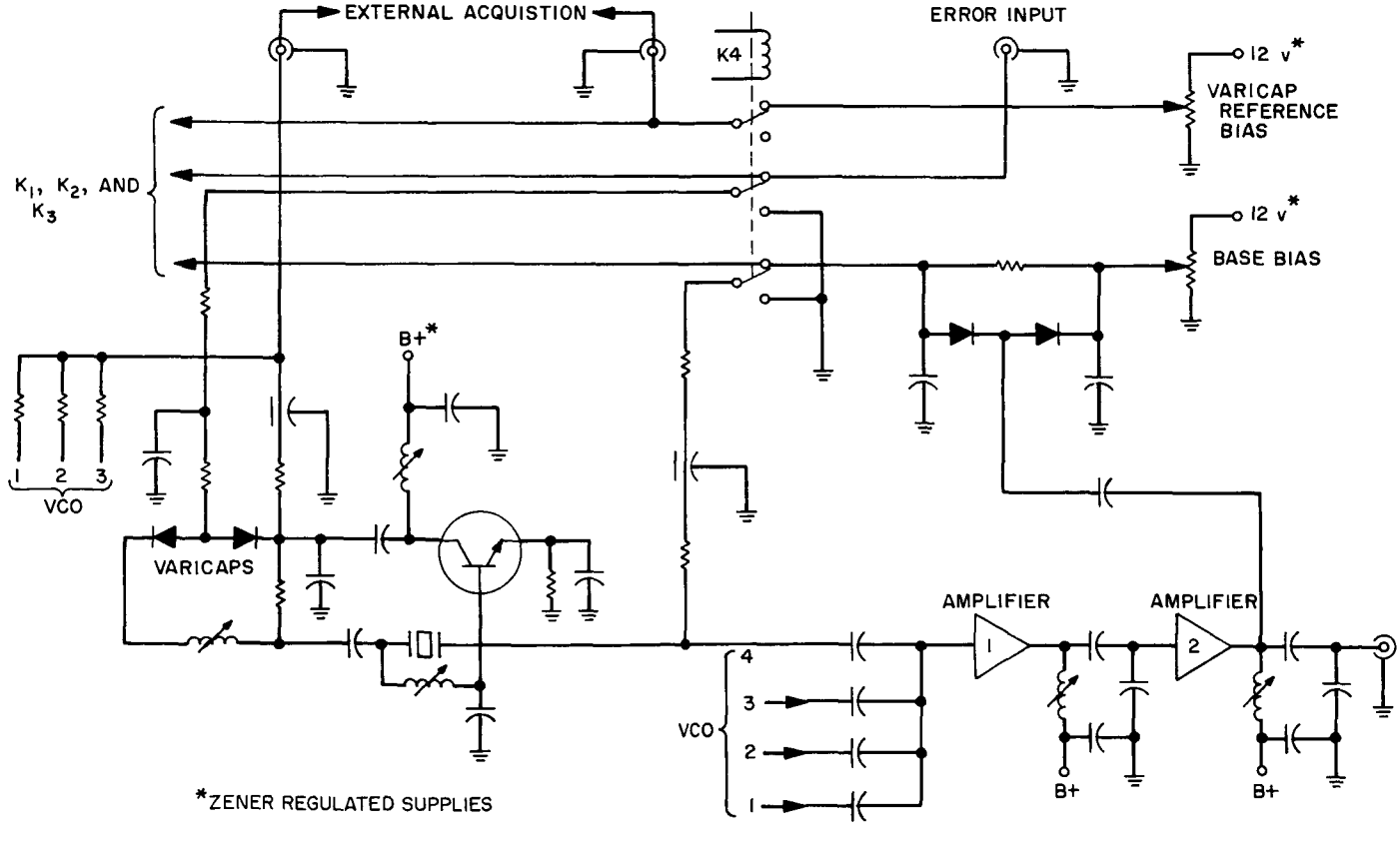

Fig. 15. Multiple VCO diagram

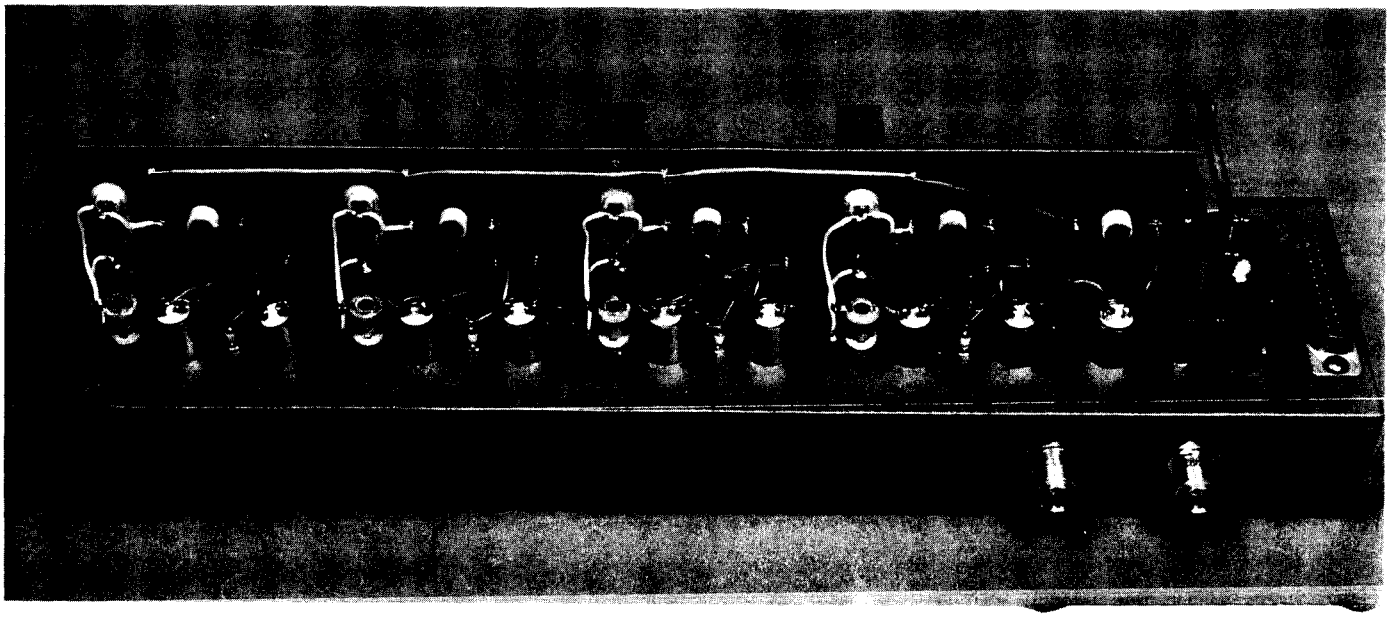

Fig. 16. Multiple VCO

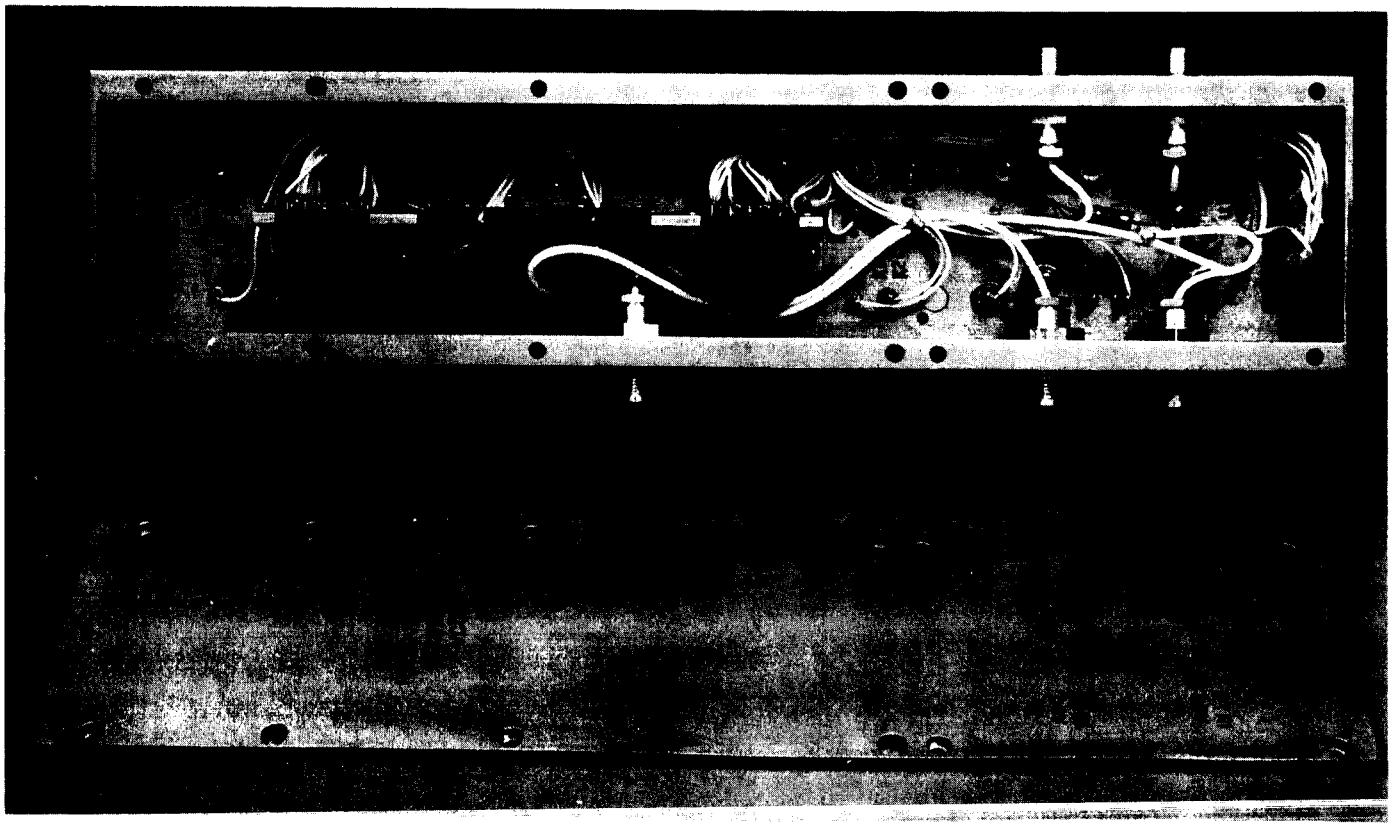

Fig. 17. Multiple VCO

The ALC circuit of the VCO adjusts the base bias to maintain a constant output level. The amount of adjustment required is sensed by a detector coupled to the output of the second amplifier. The following features are provided by this ALC circuit.

(1) A high positive bias is applied to the oscillator transistor base for a maximum gain when the oscillator is initially turned on, forcing the oscillator to start readily.

(2) The RF output is held constant over the desired frequency range.

(3) The level at the base of the oscillator transistor is held constant, maintaining an optimum RF current thru the crystal over the desired frequency range.

Any one of the four VCO stages may be switched into operation by a relay circuit which controls the following three separate inputs to the VCO stages.

(1) The error input voltage, which is applied to the active VCO stage, while the remaining stages are switched to ground potential.

(2) The varicap bias supplies, one for each stage, which allow individual VCO gain adjustment.

(3) The base bias supply which is combined with a level control voltage derived from the ALC circuit and is applied to the active VCO stage. The bases of the remaining three oscillator transistors are grounded, turning off these VCO stages.

3. Physical Design

Figs. 16 and 17 are views of the multiple VCO now being produced. In Fig. 16, the four separate oscillators and two amplifier stages are clearly visible. Fig. 17 reveals the relays and potentiometers which provide switching capability and individual stage biasing.

4. Crystal Design

The ratio of the crystal series capacitance to the variable capacitor of the external circuit is the determining factor in the ability of the crystal to be pulled from its resonant frequency. The larger this ratio, the greater the frequency range. The stray and fixed capacities of the circuit limit the minimum value of the variable circuit capacitor (varicap) that can be used. However, increasing the crystal series capacitor will increase this ratio and result in a greater frequency range. Since

$$Q = \frac{1}{\omega C_s R_s},$$

where

Q = quality factor

C_s = crystal series capacity

R_s = crystal series resistance

ω = radian frequency

increasing C_s reduces Q for a fixed R_s or reduces R_s for a fixed value of Q. Since C_s is a difficult parameter to measure, an attempt has been made to define the crystal characteristics by specifying the parameters Q and R_s. It is apparent that a large number of combinations of Q and R_s could satisfy the requirements for a particular value of C_s.

These various Q and R_s values are plotted in Fig. 18 to illustrate their effect upon 400 cps/v VCO performance. Satisfactory 400 cps/v VCO operation is defined as follows:

(1) K_v = 400 cps/v ±2% at center frequency
= 400 cps/v +25, −10% at ±9 parts in 10^5 frequency offset.

(2) Oscillation maintained out to ±6.1 v of control voltage.

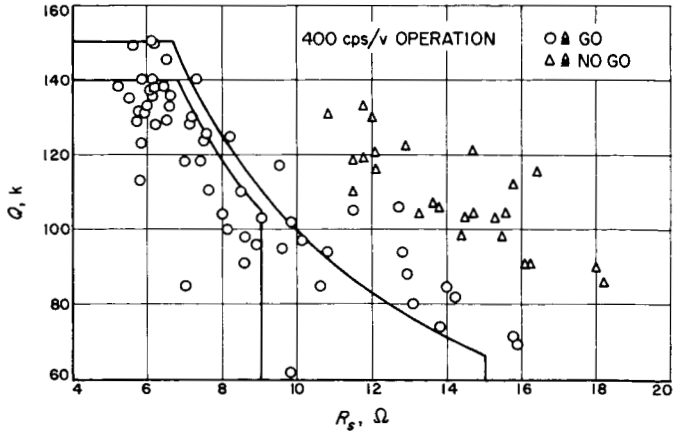

Fig. 18. Crystal characteristics

(3) No discontinuities in the gain curve over the frequency range of (1).

In Fig. 18, the line separating successful crystals from those that fail closely approximates the hyperbolic locus of constant $Q \times R_s$; i.e., constant C_s. The restrictions ensuring 100% crystal yield are that $Q \leq 50$ k, $R \leq 15$ Ω, and, in addition, that $Q \times R \leq 10^6$ Ω. This specification is superimposed on the scatter diagram.

Future requirements might demand a VCO with more gain and range. Consequently, a crystal specification is being formulated that will fulfill these requirements. Fig. 19 shows a scatter diagram with the VCO gain at 500 cps/v and with successful operation defined as above with the exception that

K_v = 500 cps/v ±2% at center frequency
= 500 cps/v +25, −10% at ±11.6 parts in 10^5 frequency offset.

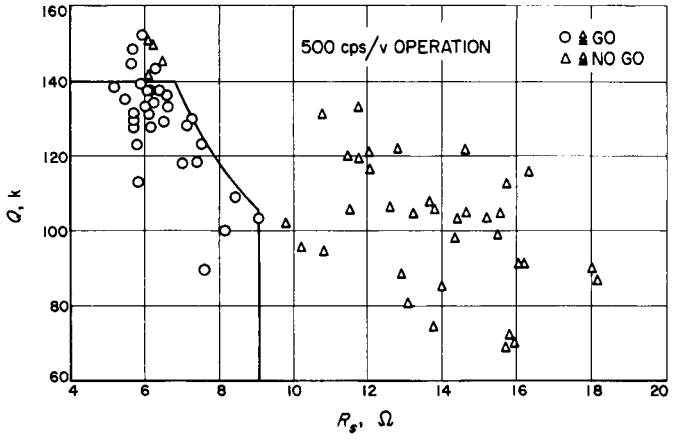

Fig. 19. Crystal characteristics

In this case, the restrictions allowing close to 100% crystal yield are that $Q \leq 140$ k, $R \leq 9$ Ω, and, that $Q \times R \leq 950$ k Ω.

The measuring scheme for Q and R_s is outlined in Fig. 20. A highly stable oscillator capable of fine frequency control drives a frequency counter and the test fixture. The 20-Ω resistor prevents the low impedance fixture from overloading the generator. Peak output voltage (V_2) is achieved by adjusting the generator frequency to the series-resonant frequency (f_o) of the crystal. V_1 and V_2 are measured with an RF voltmeter, and R_s is calculated as

$$R_s = 2\left(\frac{V_1 - V_2}{V_2}\right).$$

Q is then measured by recording the two frequencies at which V_2 is 0.707 of its peak value. The difference between these two −3 db frequencies is the bandwidth, and

$$Q \triangleq \frac{f_o}{BW}.$$

Fig. 21 graphs the deviation of these measurements which were taken by (A) the crystal vendor, (B) the VCO module vendor, and (C) JPL. All three sources used approximately the same measuring technique; (B) and (C) used the same test fixture. The plot indicates that, disallowing for the measurement biases existing between sources, random measurement error is quite tolerable for mass production acceptance.

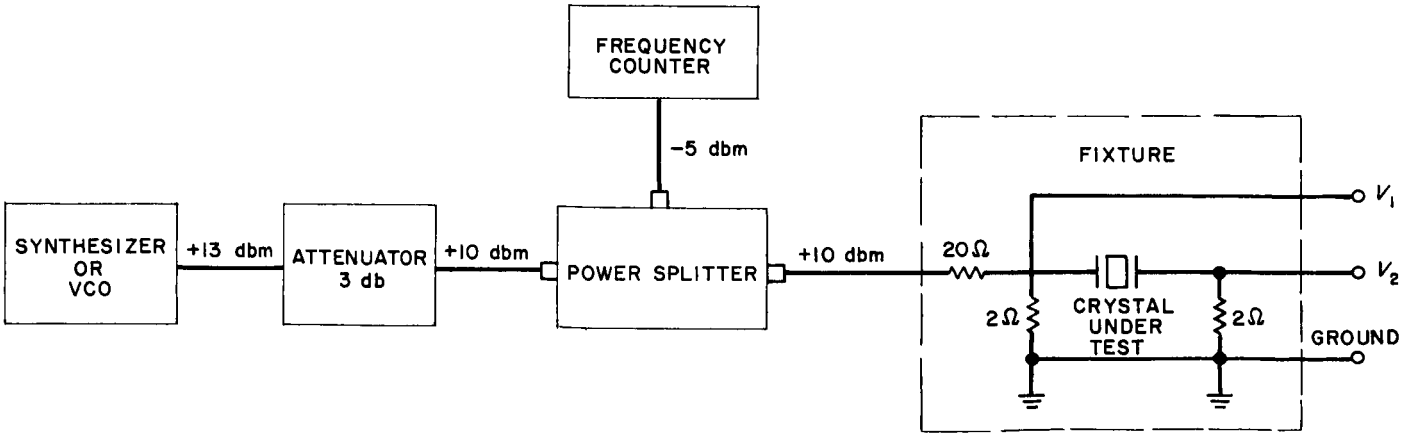

Fig. 20. Block diagram of crystal parameter tests

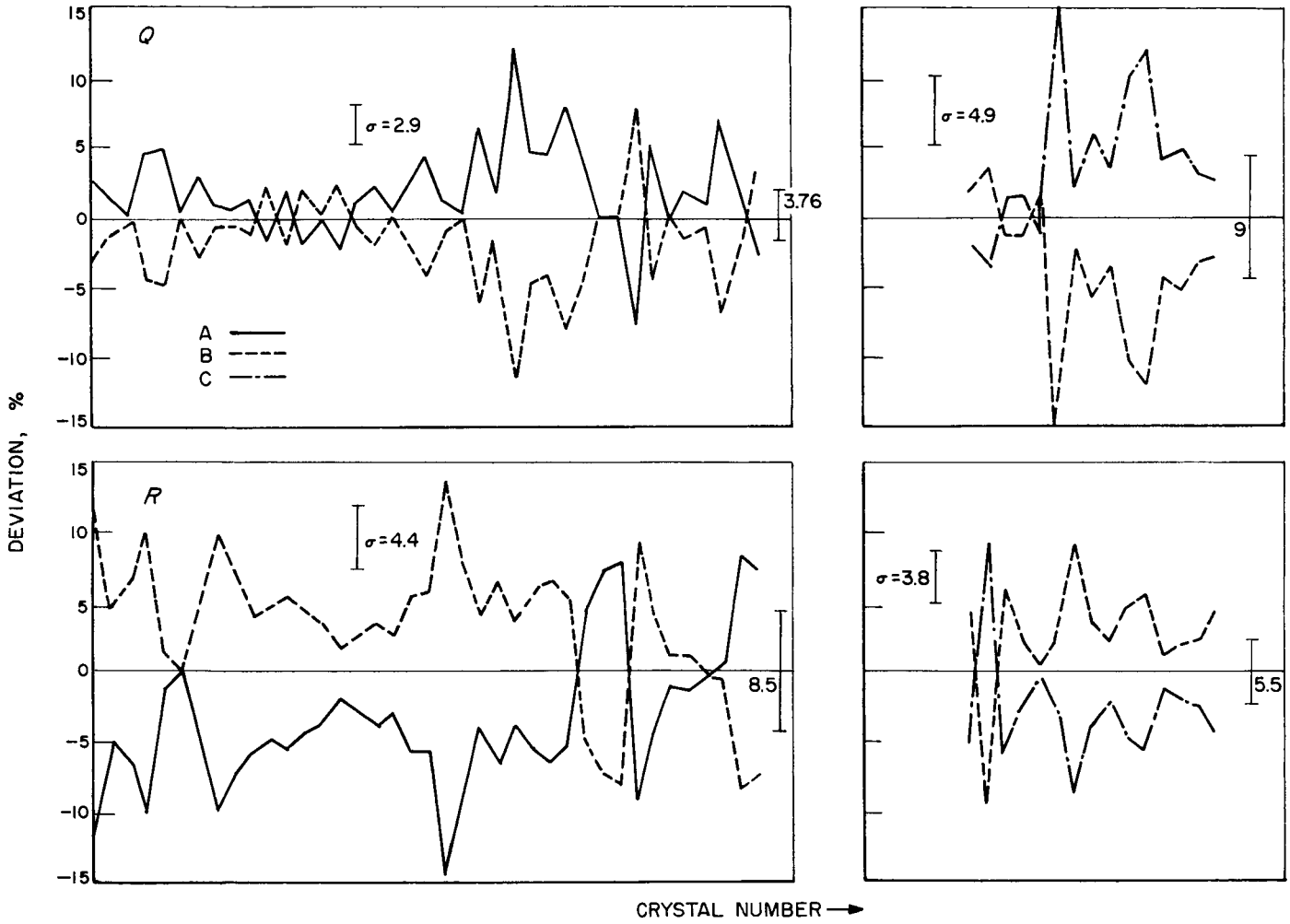

Fig. 21. Crystal measurement deviations

Early crystal designs were able to reduce C_s to the required value, but only at the expense of introducing unwanted spurious modes. These resonances were often of such strength and proximity to the main mode, that when the VCO was pulled from its center frequency it would lock to one or more of them. Consequently, an empirical study was run from which evolved a spurious specification (Fig. 22). Present crystals, including those plotted in Figs. 18 and 19, more than adequately meet this specification.

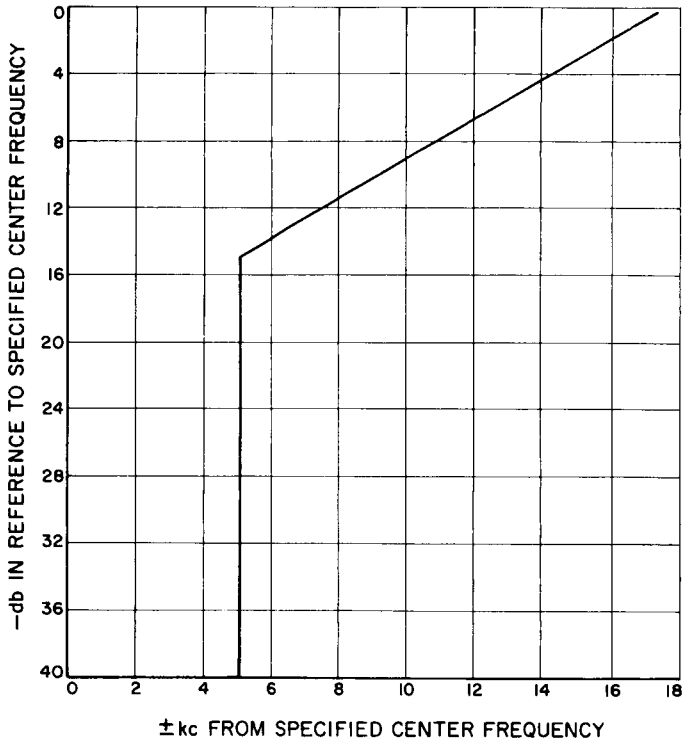

Fig. 22. Specification for crystal spurious output

5. Performance

The gain requirements at center frequency and over the frequency range indicate that a very linear characteristic is desired. With a crystal having the Q and R_s as specified, the VCO design is capable of meeting this characteristic. Typical VCO gain curves for 400 and 500 cps/v are plotted in Fig. 23.

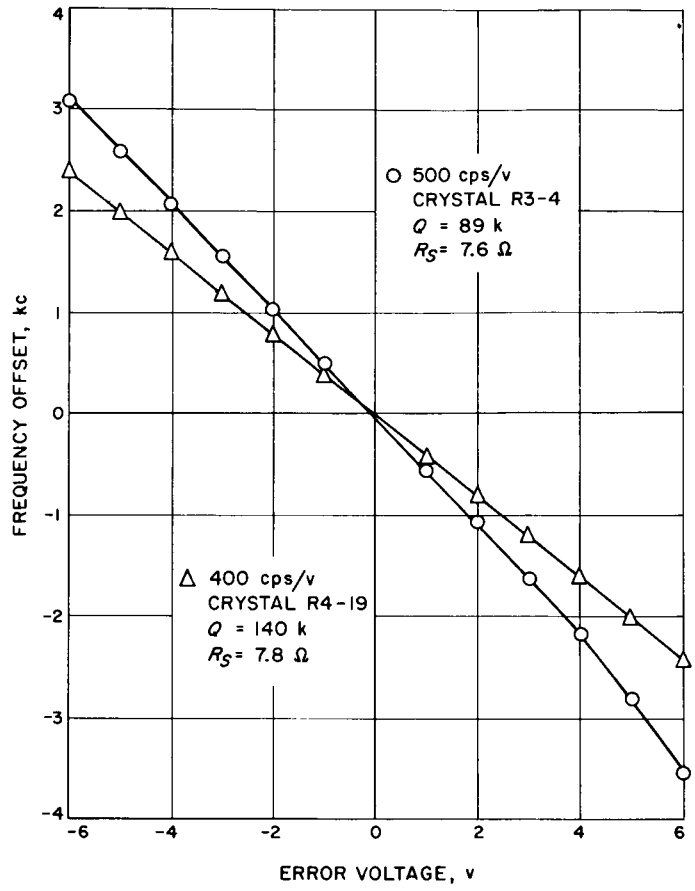

Fig. 23. VCO gain characteristics

Another critical parameter of the VCO is the phase stability over the frequency range. Phase stability has been measured with an MSFN receiver in the narrow bandwidth configuration ($2B_{L_0}$ = 50 cps) by introducing signal suppression in order to obtain the threshold bandwidth under strong signal conditions. At center frequency the combination of the receiver and exciter VCO's gives a phase error measurement on the receiver of 2 to 3 deg rms. This value increases to a factor of approximately two over the frequency extremes.

This VCO design fulfills all the requirements for the MSFN and is more than adequate for satisfactory system performance.

IV. Communications Research and Development

A. Experimental Closed Cycle Refrigerator (CCR) for Masers

Tests have been completed on the prototype CCR which has been equipped with a traveling wave maser (TWM) for 2295 Mc. Results indicate that a greatly improved machine has been developed.

The cool-down time of 6 hr was a significant improvement over the DSIF CCR's but an even faster rate was desired. Precooling tubes were installed so that the TWM assembly could be precooled with liquid nitrogen which has reduced the cool-down time to 3¼ hr. Operationally, this is significant since minor maintenance work could be scheduled between two successive tracking passes without loss of data.

Gain stability tests on the S-band maser were performed under various conditions and in all cases the results were equal to, or better than, the DSIF systems. Particularly encouraging was the stability with respect to mechanical orientation of the machine; with a gain of 36 db, the peak-to-peak variation was less than 0.1 db for angular excursions of ± 80 deg from the upright position. The stainless steel spokes used to support the DSIF maser structure in the vacuum chamber have been eliminated successfully. As a result, the refrigerator and TWM structure will be completely accessible simply by unbolting the top flange; whereas, the present DSIF units require a time-consuming disassembly operation because of the spokes.

Long- and short-term stability tests have also been conducted. As a continuous wave radiometer it has been demonstrated that the resolution is of the order of 0.001°K.

B. Experimental X-Band Lunar–Planetary Radar Project: Maser and Instrumentation

An 8448-Mc maser was purchased from Hughes Research Laboratories, Malibu, California. The maser is used in a low-noise radiometer–radar astronomy receiver for advanced communication, system, and components experiments on the 30-ft antenna at the Goldstone Venus Station. The maser has been modified, evaluated in the

laboratory for noise temperature performance, and reinstalled on the antenna.

1. Performance

The H-band Hughes maser has been at JPL and Hughes Aircraft Co., Fullerton, California, undergoing repair and testing since the last installation on the 30-ft antenna at the Venus Station (*SPS 37-31*, Vol. III, p. 40). The principal change was enlargement of the liquid helium fill opening to 7/16-in. inside diameter to accommodate standard 3/8-in. outside diameter fill tubes. Previously, a specially constructed fill tube was required (*SPS 37-23*, Vol. IV, p. 204). This fill tube was especially vulnerable to breakage when filling the maser on the antenna from the cherry picker.

Maser performance was evaluated at JPL before installation at Goldstone. The equivalent noise temperature of the maser defined at the input of the supporting structure was measured to be 18.3°K. This measurement was made with a liquid nitrogen load, Model SP 8023, Serial No. 013 (manufactured by Maury Microwave Corp.), and ambient WR-112 waveguide terminations in conjunction with a gas tube noise source (Fig. 1). This assembly will be retained as a lab standard for future evaluations. The equivalent noise temperature T_Y of the liquid nitrogen cooled termination defined at the maser input is

$$T_Y = 74.87 + 0.011\Delta P + 0.0322\ T_0$$

where

ΔP = atmospheric pressure above 760 mm Hg

T_0 = ambient temperature, °K

The maser temperature T_M is measured by firing the noise source first with the maser input connected to the nitrogen load and then connected to the ambient load. We have

$$T_M = \frac{T_0 (Y_0 - 1)\, T_N (Y_N - 1)}{Y_N - Y_0} \qquad (1)$$

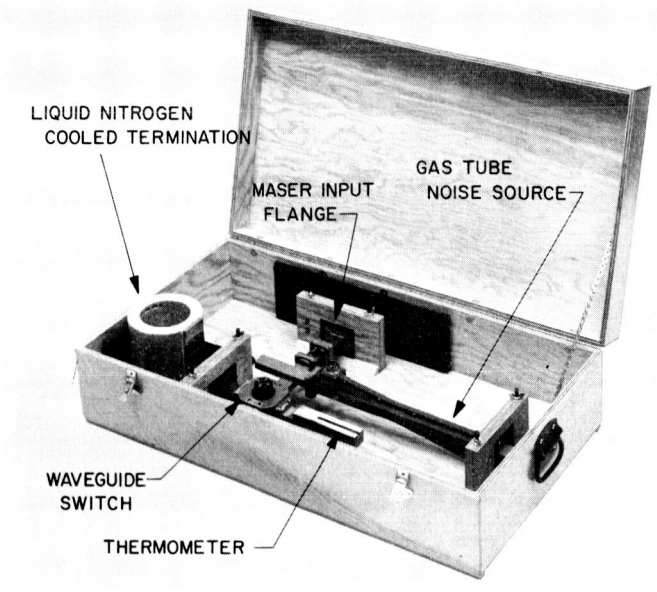

Fig. 1. WR-112 waveguide liquid nitrogen cooled and ambient termination test assembly

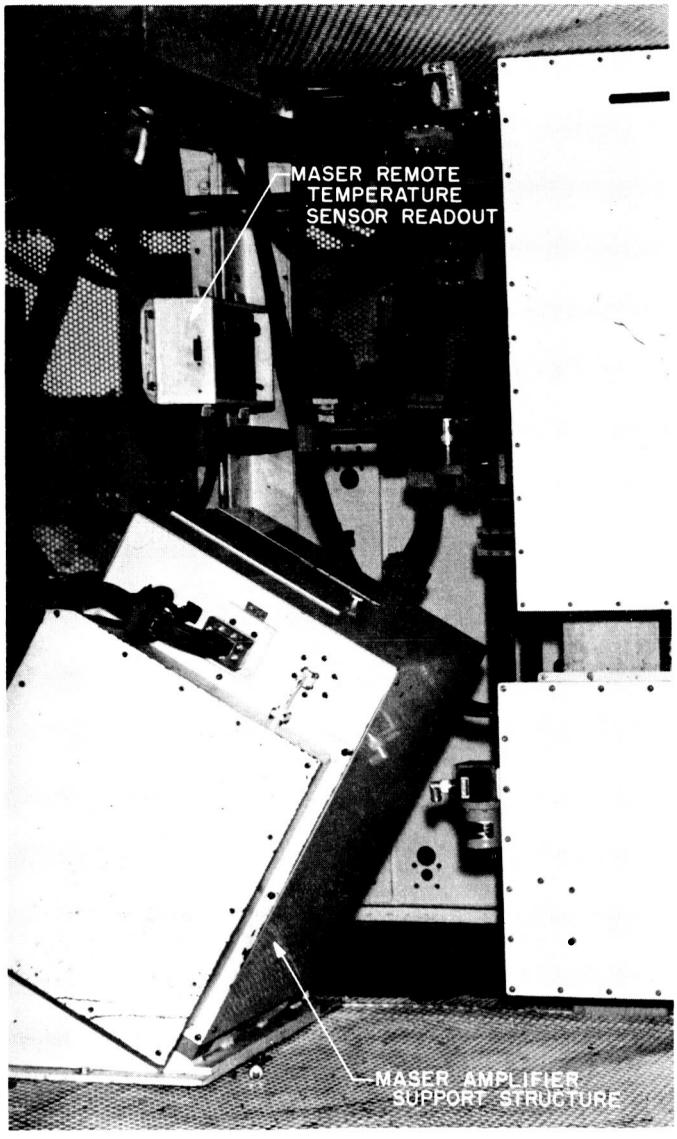

Fig. 2. 8448-Mc masers installed in electronics cage of Venus Station 30-ft antenna

where

T_0 = ambient temperatures, °K

Y_N = output power ratio due to turning the noise source on and off when the maser input is switched to the liquid nitrogen cooled termination

Y_0 = output power ratio due to turning the noise source on and off when the maser input is switched to the ambient terminations

This measurement technique has the advantage that the effect of maser gain changes during the measurement have practically no effect on accuracy. The input match of 1.0:2.5 was tuned out to less than 1.0:1.05 with a waveguide screw tuner mounted inside the maser support structure.

The experimental neon noise source previously built into this section (*SPS 37-29*, Vol. IV, p. 194) has been removed, thus eliminating approximately 0.8°K noise temperature contribution.

The maser has been installed in the electronics cage of the 30-ft antenna and has been operating since June 1, 1965 (Fig. 2).

C. X-Band Lunar Radar Transmitter

1. Introduction

The X-band 8.448-Gc high-power transmitter has been installed in the equipment cage of the 30-ft antenna at the Venus Station and is presently developing an output power of 9.5 kw for the X-band Lunar Radar Experiment.

The transmitter was originally used on the October–November, 1964 Lunar Radar Experiment. Primary improvement to the transmitter system has been replacement of the unreliable and unstable traveling wave tube (TWT) amplifier (*SPS 37-31*, Vol. IV, p. 46) with a new exciter driver amplifier (Fig. 3). A block diagram of the exciter amplifier, as used in the transmitter system, is shown in Fig. 4.

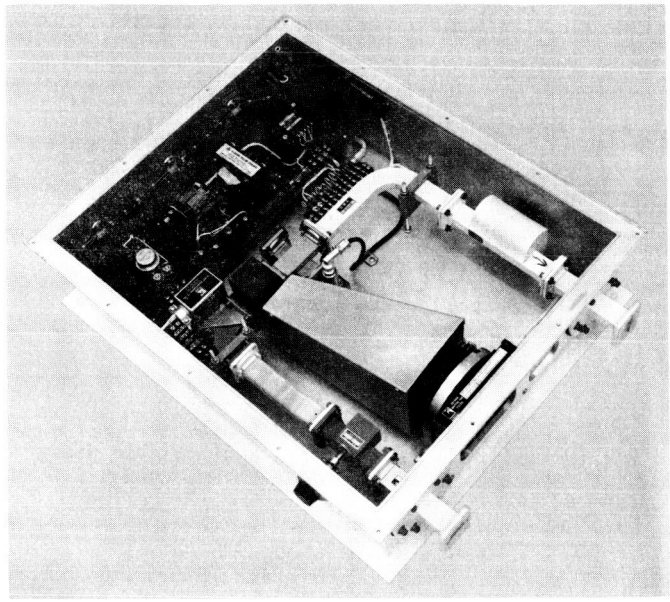

Fig. 3. Exciter driver amplifier

2. VA401 Klystron

The exciter amplifier uses an electrostatically focused, three-cavity, air cooled VA401 klystron. The electrical characteristics of the klystron, as measured by the manufacturer, are:

Frequency	8.448 Gc
Tuning range	±10 Mc
Power output	29.5 w
Gain	32.2 db
3-db bandwidth	15 Mc
Beam voltage (for maximum output)	1300 v
Beam current	160 ma
Maximum phase pushing	0.9 deg/v

3. Klystron Power Supply

An adjustable 1000- to 1500-v beam supply and filament supply are currently being fabricated by a vendor, according to JPL specifications. Both supplies will be packaged in a single watertight aluminum container. Until delivery of the unit, the exciter is being powered by a 1000-v rack-mounted power supply (Fig. 4) installed in the transmitter monitor cabinet. The exciter output is 10 w with 1000-v beam voltage and is marginally adequate for the present transmitter. Although the drive requirement for saturation of the high-power VA849

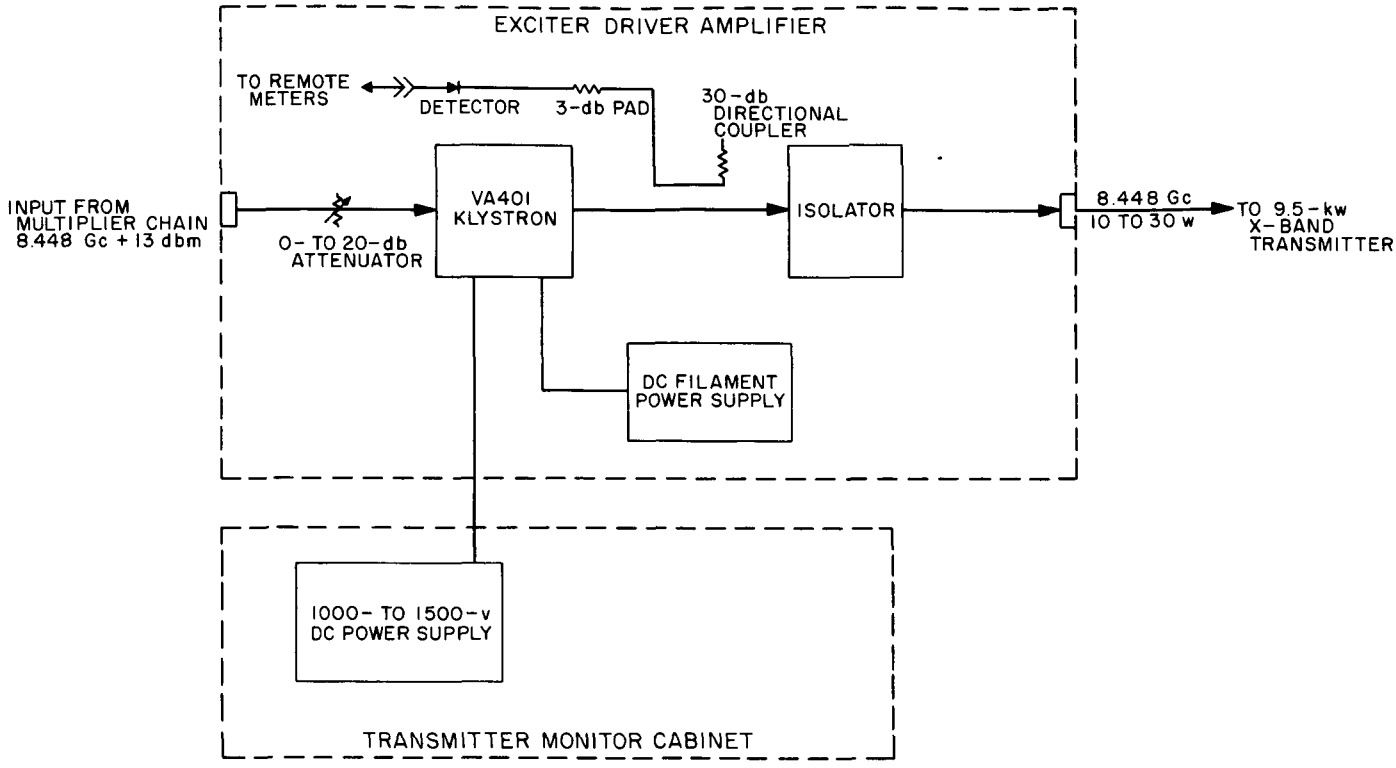

Fig. 4. X-band exciter driver amplifier block diagram

klystron amplifier is 1 w, the insertion losses of the interconnecting waveguide components (variable attenuator, crystal switches, isolators, etc.) increase the drive power requirement to nearly 10 w. The 1500-v beam supply will allow for aging of the VA401 klystron and for increased drive requirements of future more powerful transmitters.

The exciter driver amplifier contains a regulated DC filament power supply for the VA401 klystron and is temporarily being used until delivery and installation of the adjustable 1500-v beam supply and filament power supply.

4. Exciter Noise Reduction

In the previous X-band Lunar Radar Experiment, the noise from the TWT exciter amplifier (*SPS 37-31*, Vol. IV, p. 46) degraded the receiver system temperature from 63 to 193°K. The present exciter transmitter increases the receiver system temperature only 0.4°K as compared to 130°K on the former experiment.

5. Component Layout

Since stray magnetic fields can degrade the life and electrical performance of electrostatically focused klystrons, the primary concern in the layout design (Fig. 3) was to maximize the distance between the klystron and magnetic components (isolator, fan, and filament transformer).

6. Conclusion

The new exciter driver amplifier employs a klystron instead of the TWT amplifier used on the former Lunar Radar Experiment. A klystron permits better performance of the experiment by reducing the receiver noise temperature and should prove to be more reliable than a TWT amplifier.

D. X-Band Lunar Radar

1. Introduction

The S- to X-band conversion of the Mod IV receiver has been completed and is undergoing system tests. Developments during this reporting period have been directed mainly toward completion of the signal generator and modification of the X-band final ×4

multipliers in order to improve system reliability and performance.

The signal generator has been set to provide calibrated signals ranging between −90 and −190 dbm. As of this date, RF gasketing has not been completed, and RF leakage is above threshold, so that the signal generator has to be de-energized during the receive mode.

2. *Signal Generator*

Progress on the development of an X-band signal generator has been reported in *SPS 37-27*, Vol. III, p. 94–96; *37-28*, p. 77–79; and *37-29*, p. 86–87.

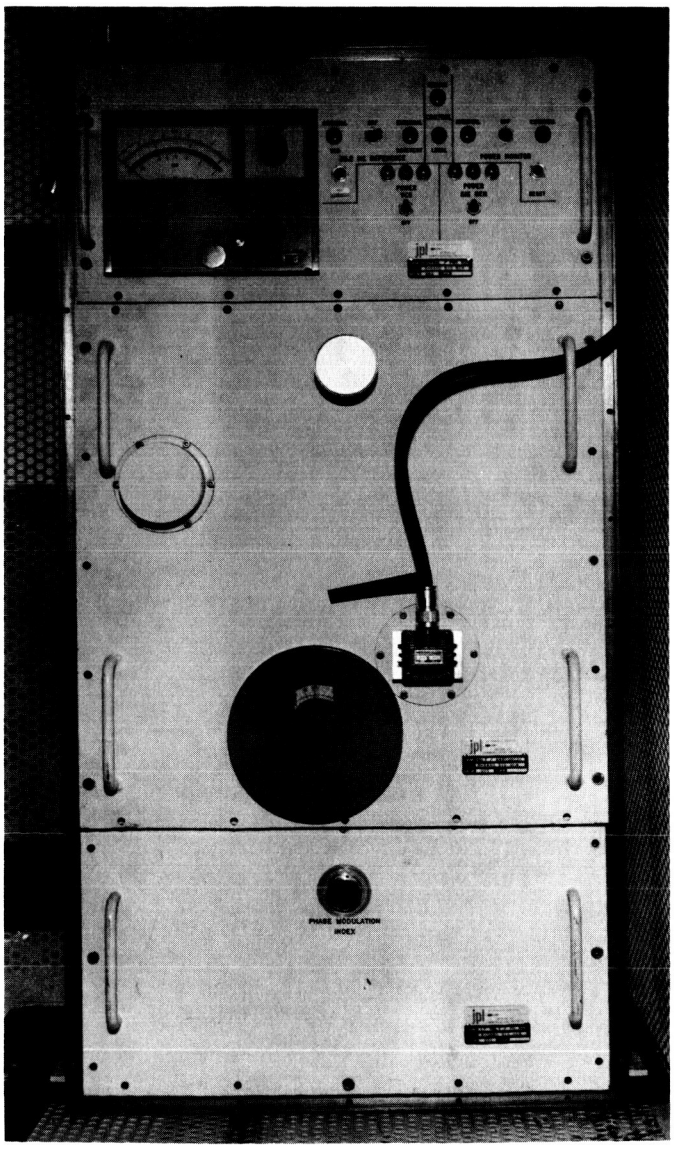

Fig. 5. 8.4-Gc signal generator

Assembly and test of the signal generator has been completed and the equipment has been installed in the cage of the 30-ft antenna (Fig. 5). A temporary coaxial line, having a loss of 5.1 db, connects the output of the signal generator to the 40-db directional coupler at the input to the receiver, so as to provide calibrated signals ranging between −90 and −190 dbm. The temporary line will be replaced by a permanent waveguide later when the signal generator will be set to provide calibrated receiver inputs between −80 and −180 dbm. RF gasketing of the inner compartments has not been completed and will have to be installed later. As a result, leakage into the receiver feed is too high to permit standby operation of the signal generator during the receive mode.

3. ×4 *Multiplier to X-Band*

As reported in *SPS 37-31*, Vol. III, p. 53, these multipliers, as originally procured, were not acceptable because of insufficient bandwidth, and restricted dynamic range. These deficiencies in performance have been corrected by a redesign of the input matching circuits and by application of self-bias to the multiplying varactor.

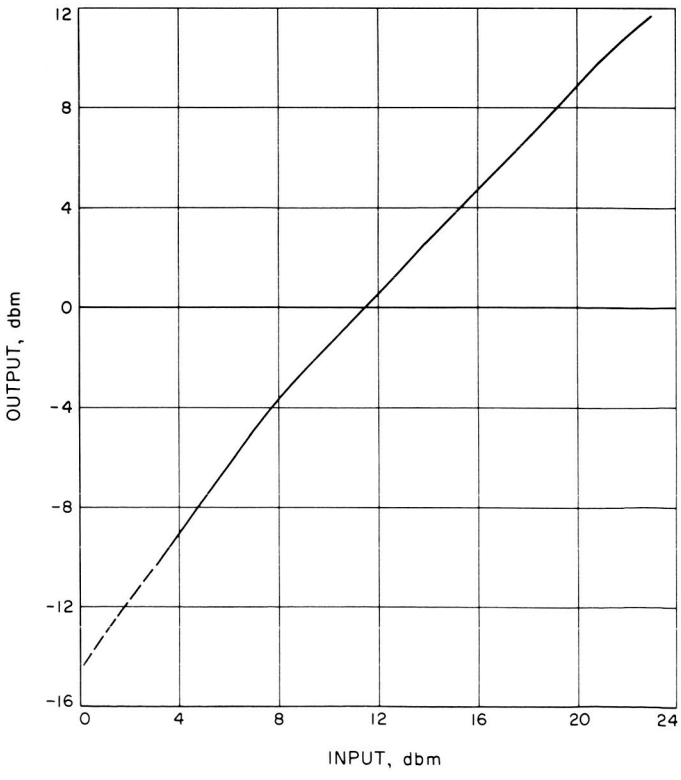

Fig. 6. Input–output characteristic ×4 multiplier to X-band

Documentation necessary for procurement of replacement S-band multipliers to meet design requirements is under way, but as an interim measure, the local oscillator injection, transmitter exciter, and signal generator multipliers have been modified for use in the equipment. Electrical tests indicate that the 1- and 3-db bandwidths at the output frequency are typically 30 and 54 Mc, and that the input–output characteristic is essentially linear over a wide dynamic range, as shown in Fig. 6.

E. Venus Station Operations

1. Experimental Activities

a. Summary. During the past 2 mo the spectrum analysis and ranging experiments being conducted with Mars and Mercury were completed. Additional measurements of the thermal temperature of Mars were made, and several measurements (at 2388 Mc) were made of temperatures of various radio star sources.

In continuing support of the Venus Station's commitment to support the *Mariner* Mars 1964 spacecraft upon demand, several additional command link lockups, as well as additional doppler testing, were accomplished. Also, the installation of the *Mariner* receiving system was completed and tested, and, commencing June 12, Venus Station provided prime receive capability for reception of telemetry data during a planned 4-day shutdown on Pioneer's (Station 11) maser. The receiver worked perfectly during this time, and good telemetry data were received and transmitted to SFOF via the microwave link and the demodulation unit at Pioneer Station.

Activities at the Venus Station during this period are summarized in Table 1.

2. Subsystem Performance

a. 100-kw transmitter (operation). The R&D transmitter for this reporting period was operated in conjunction with Mars and Mercury tracking experiments from April 13–27, during which time the transmitter was on 382 filament hr and 305 beam hr.

The transmitter lost 2 hr, 40 min of tracking time due to failures, the major contributing ones being caused by the crowbar and exciter adjustments.

Table 1. Venus Station activity (April 13–June 16, 1965)

Activity	Hours	Percent
Primary experiments		
Planetary radar		
Mars	50	3.3
Mercury	75	4.9
Secondary experiments		
Radio source temperature measurement	33	2.2
Black body (Mars)	9	0.6
Mariner Mars 1964		
Transmitter		
Water load testing	173	11.0
Transmitting to spacecraft	73	4.7
Receiver		
Receiving from spacecraft	49	3.1
Testing, calibration, construction, installation, and maintenance (scheduled)	539	34.6
Down time (equipment failure, includes unscheduled maintenance)	43	2.6
Holidays	24	1.5
Nonscheduled time (not on 24-hr operation)	492	31.5
Total	1560	100.0

b. Mariner 100-kw transmitters. *Mariner* transmitters have operated on the spacecraft and in the water load for testing a total of 160.5 filament hr and 85 beam hr on Amplifier 1 and 219.4 filament hr and 160.8 beam hr on Amplifier 2. The transmitters have operated on the spacecraft for a total of 72 hr, 45 min, with an *off*-time of approximately 1 hr. Failure causes and time lost were:

Failure causes	Time lost, min
Heat exchanger fans control (over-temperature)	35
Body current	7
Vacion pump	3
Crowbar logic tripped by body current	17

The heat exchanger fan control failure was in the thermostatic control system and has been repaired. The body current kickoffs were caused by a defective body current instrumentation meter.

c. System improvements and modifications. The eddy current coupling for the high-voltage motor generator was removed, repaired, and reinstalled.

Two items were installed: (1) a new drive motor on the DC water load and drive control in UD-10 control panel, and (2) a new series limiter box in the cone storage area for use in test area with high-voltage interlock on door for safety.

The warning light system was modified to operate with both the R&D and *Mariner* cones.

The 1-Mw solid-state rectifier is being used in the system for all operations and, so far, has required no maintenance except cleaning the oil.

d. Digital equipment. The Mod III stored program controller (SPC) completed its most successful term of operating, running substantially error-free for 7 mo with the operational failures confined to a 2-wk period at the end of tracking.

Failures fell into two classes: outright catastrophic component failure (transistors), and machine errors ultimately assigned to alignment and timing problems.

In the first instance, all noted failures occurred in one unit, the digital-to-analog converter frame associated with the auxiliary rack and with the Moseley X-Y plotter and Sanborn stripchart recorder installed there. Since neither of these units was programmed in either of the two major routines in use during the experiment, failure was not serious and repairs were postponed until the end of the mission, at which time three blown transistors and two diodes were removed from this unit. Similar problems have occurred in this unit recently, therefore, failures were tentatively assigned to excessive heating due to insufficient airflow around and through the unit. During the recent short repair period, the auxiliary rack was rearranged to permit greater circulation around the equipment, and some of the equipment was moved to the adjacent rack. As in the past, bottoms were cut from both racks and exhaust fans added to the tops. This brings Mod III SPC to five racks, all of which have been treated in this manner. It is significant that since this modification was performed on the computer mainframe (*SPS 37-31*, Vol. III, p. 81) no further errors attributable to heating have occurred there.

Errors which did occur came during the closing period of the experiment just concluded. These errors were random in nature and impossible to trace. Programs ran properly but occasional functions would fail to occur on time, or the inverse of a function would occur, or the complement of a number. Often, the problems would be self-healing or reloading the program would effect a cure. No single register or block function could be assigned as the cause of these recurring failures, and, with almost continuous 24-hr tracking in progress, little diagnostic work could be attempted.

The master clock system was selected as the possible source of the problems, and, during a brief outage elsewhere on site, the computer was taken off-line and the master clock system overhauled and realigned. A brief description of this system is in order.

Mod III SPC is constructed almost entirely of "T-Pacs," so-called "synchronous" or "dynamic" logic packages manufactured by the Computer Control Co. Each logic card is clocked by an external 1-Mc pulse delivered from a clock buss within each logic bloc. There are 32 logic cards to a bloc, each bloc with its slave-clock-amplifier card; 11 blocs to a rack frame, and 3½ frames to the computer main frame. This gives a total of 1200-odd cards driven by this clocking system. Decisions are made synchronously throughout the machine at this 1-Mc rate; it can be seen that the preservation of synchronism and coincidence of pulses is of the utmost importance.

A typical clock pulse as delivered has an amplitude of 2.5 to 3.0 v and a pulse width nominally of 0.2 μsec. Since the width is adjustable, it is held to less than 10% variation between blocs. During the adjustment period referred to, it was discovered for the first time that there existed between individual slave-clock cards a delay time *through* the card varying as much as 0.3 μsec relative to the master clock pulse. As a short-term repair, all slave-clock cards in the machine were sorted into groups of roughly equivalent delay times and assigned to a particular frame as a group. The master timing of the frame was then adjusted so that all four frames were reasonably coincident. Upon restart, the computer proceeded to operate without error.

In view of the length of the successful operation period, it would seem reasonable that the next increase in Mod III SPC reliability will be obtained by rework–rebuild of the clock system and its modular units. In the immediate future it is planned to:

(1) Construct a 1-Mc crystal VCO that will isolate Mod III from changes in input timing, shape, and amplitude.

(2) Isolate causes of varying time delay through slave-clock cards and to justify timings.

(3) Render clock timings independent of temperature change, perhaps through the use of silicon logic.

(4) Investigate the hard-wiring of time delays to render readjustments unnecessary.

During the repair period, opportunity was also taken to continue easing congestion in the vicinity of the input–output frame. Relay input–output was removed to the fifth rack, where meticulous isolation of grounds and shields was carried out and terminal block fanouts rearranged for easier access and greater flexibility.

e. Mod IV receiver. Extensive changes made on the Mod IV receiver included module relocation, and cabling and instrumentation changes. These modifications were made to provide the capability of operation on both X- and S-band frequencies. In some modes this operation can be simultaneous.

S-band portion. All the antenna cone-mounted equipment has been installed and checked out. A test transmitter has also been installed in the cone for use in receiver calibration; it can operate on its own internal reference oscillator or on an externally supplied signal.

A new one-bay cabinet, which contains local oscillator components, has been installed in the control room. When used with the S-band portion of the Mod IV receiver, this cabinet makes up the *Mariner* encounter receiver. A full description of this receiver is contained in *SPS 37-33*, Vol. III, p. 58.

X-band portion. The Mod IV receiver now provides two open-loop channels for use at X-band frequencies. Basically these channels are made up of the old S-band AM and ranging channels. Separate control functions are provided on the Mod IV receiver for both X- and S-band. However, mixer crystal current is the only function monitored remotely in the X-band front end.

All the X-band antenna-mounted equipment has been reinstalled in the 30-ft antenna and checked for proper operation. Installation included the use of new interconnecting cables and modification of the antenna junction box to insure the hardware compatibility of the X- and S-band receiving systems.

The new X-band signal generator was installed in the 30-ft antenna. During checkout of the generator, the internal reference 35.2-Mc oscillator failed and was removed for repair. The generator is now operating on a coherent reference signal being supplied by the central frequency synthesizer. Preliminary performance evaluation discloses a possible low-level leakage problem; evaluation is continuing.

Both the X- and the S-band receivers have been used during this period. The X-band was used in its open-loop mode in Moon experiments, and the S-band was used in its closed-loop mode, receiving signals from the *Mariner* spacecraft. Testing and evaluation of both systems is continuing.

The digital phase modulator has been returned to the Laboratory for rework and modification by the project engineer.

f. Central frequency synthesizer (CFS). Two module failures occurred. A 1-Mc distribution amplifier introduced excessive phase jitter into the 30.455- and 31.44-Mc reference loops. The amplifier was replaced, and operation is now normal. The second failure was that of a 35.2-Mc distribution amplifier, which was replaced.

Evaluation of the present standby battery system was completed and the information forwarded to the Laboratory project engineer.

A 1- to 4-Mc multiplier was installed in the CFS by Laboratory personnel. The output of the multiplier will be used in the programmed local oscillator.

g. Programmed local oscillator (PLO). *Digital control subsystem.* The down-loop VCO control potentiometer was found to be introducing noise into the PLO, resulting in unstable operation (the most likely cause is a worn or rough resistive element or wiper contact). The potentiometer could not be disassembled, so the unit was replaced, and normal operation was restored.

Two other failures appeared, both concerned with the external (synchronous) indicator; both were corrected by replacement of a faulty logic card and indicator lamp driving unit. The digital portion of the PLO is presently set up for Moon experiments; to change it for other experiments involves only a gear ratio change in the control potentiometer drive unit.

RF portion. The Montronics frequency synthesizer was reinstalled in the PLO and tested. Operation of the PLO was normal in the S- but not the X-band mode. Substitution of a different synthesizer restored normal operation to both modes. The Montronics has been returned to the Laboratory, and an H-P 5100A frequency synthesizer is being used.

A 35.44-Mc mixer has been installed in the PLO. This frequency could be utilized in the *Mariner* encounter receiver in the PLO-assisted closed-loop mode.

Another minor change involved the relocation of the *Mariner* receiver main VCO acquisition voltage supply to the receiver auxiliary cabinet. This change was made to facilitate receiver operation during acquisition of the spacecraft.

h. Preparation for X-band lunar experiment. At the conclusion of the advanced antenna system (AAS) ½-scale model feed tests, the 30-ft antenna was stripped of all test equipment in preparation for the X-band radar lunar mapping experiment. Since the hyperbolic reflector and quadripod used in the AAS ½-scale tests were found to be suitable for work in the X-band region, they were not replaced by the quadripod and reflector used in the previous X-band experiment. The cone and feed, however, were removed and replaced with the X-band cone and feed. Installation of the X-band equipment in the antenna equipment cage was facilitated by the availability of parts and mounting bracketry from the previous X-band experiment. Arrangement of equipment in the cage was practically identical to the former configuration with the following exceptions:

(1) A signal generator not previously available was added.

(2) The helium and nitrogen loads were relocated to provide additional access to transmitter components.

(3) The transmitter water load was relocated.

(4) The nitrogen and helium pressurization system was redesigned so that the gas containers are now at ground level. This change, plus the fact that the system now incorporates multiple gas containers in parallel, eliminates down time due to the replacement of spent nitrogen and helium containers.

(5) The routing of one waveguide run was changed to conform to the new location of the nitrogen and helium loads (Fig. 7).

Other work accomplished in preparation for the lunar mapping experiment included:

(1) Installation of maser instrumentation in the control rooms.

(2) Rework and pressurization of the waveguide runs between the antenna and the control room.

(3) Installation of additional cables and check out of existing cables.

(4) Overhaul and optimization of the television system.

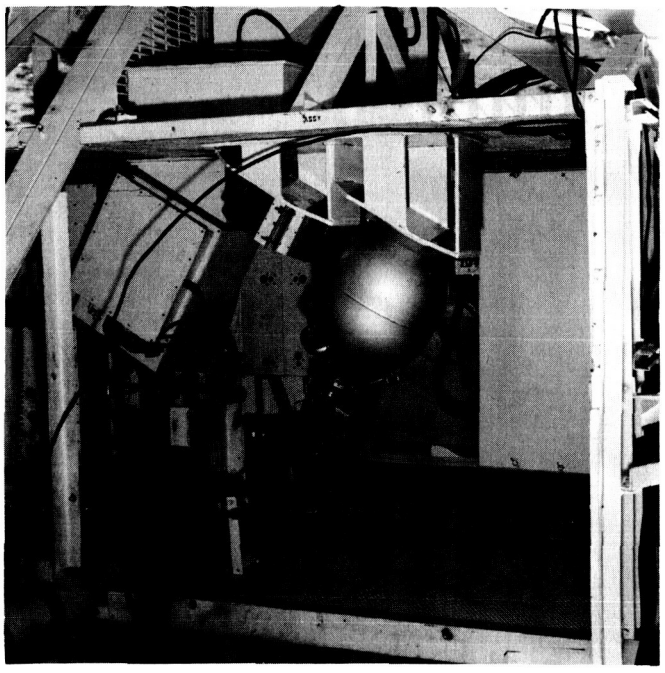

Fig. 7. X-band equipment layout in 30-ft antenna cage

(5) Reactivation and connection of the cooling water system to the antenna-mounted transmitter.

Because this work was accomplished ahead of schedule, there was additional time for equipment checkout.

F. Frequency Generation and Control: S- and X-Band Central Frequency Synthesizer

A 35.2-Mc frequency synthesizer has been developed to supply the input required by a 35.2-Mc phase locked loop (*SPS 37-33*, Vol. III, p. 92).

The frequency synthesizer consists of solid-state circuitry on terminal boards housed in a machined and gold-plated cavity-type chassis. (Fig. 8.) A combined series of multipliers, amplifiers and crystal filters constitutes the frequency conversion from 200 kc to 35.2 Mc (Fig. 9).

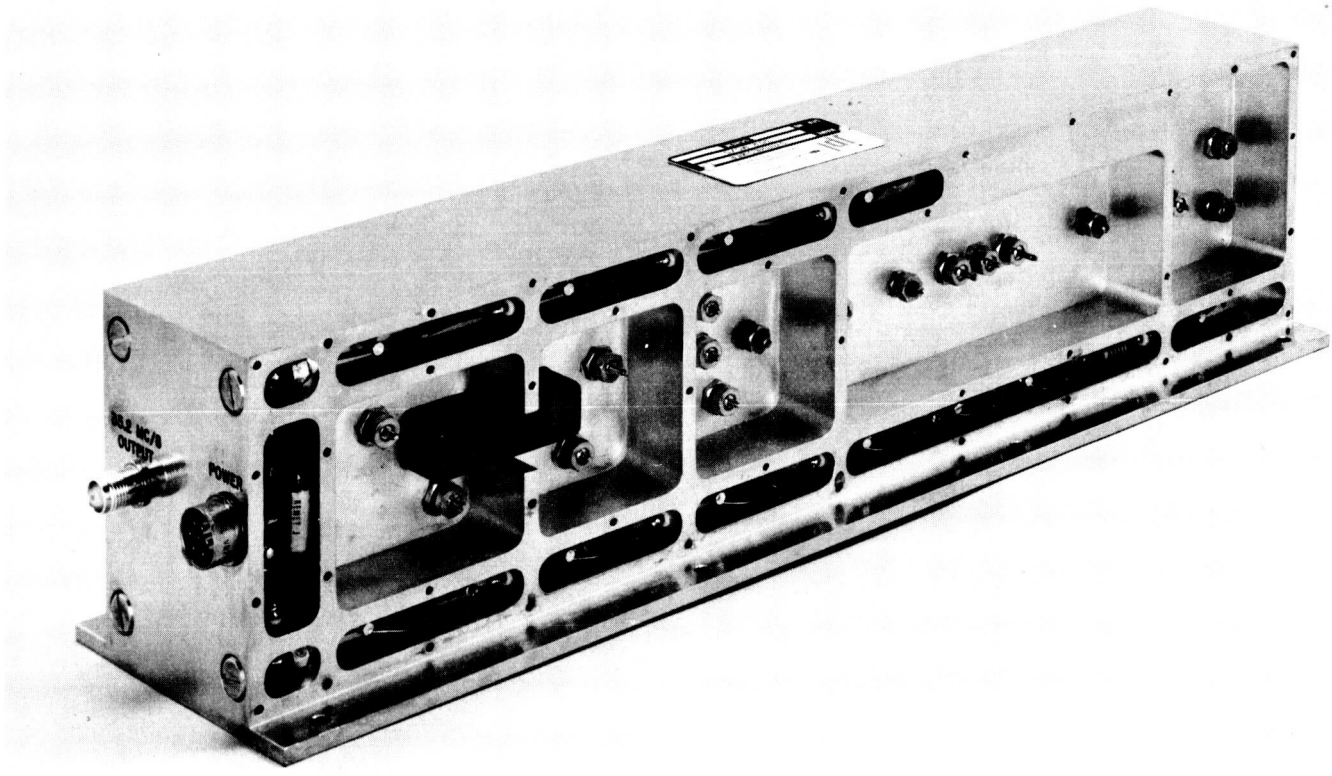

Fig. 8. 35.2-Mc frequency synthesizer

Performance features are: output level of +13 dbm, −0 db, +3 db, into 51 Ω; a power drain of 1.14 w from a +30-v DC supply; input impedance of 51 Ω ±10% for ±3 db at +10-dbm input level; and isolation from output to input > 60 db at any frequency.

The bandwidth of the synthesizer, which is determined by the crystal filter, is ±23.5 kc at 35.2 Mc. The bandpass characteristic is flat over this range. The 200-kc input amplifier-limiter has a bandwidth of ±135 cycles. The output spectrum contains no measurable internally generated spurious signals. Second harmonic distortion of the 35.2-Mc signal is 0.70%.

The RF leakage of 0.2-, 4.4-, 8.8- and 35.2-Mc was checked at the output terminals (TNC connector), the power line, and all external mechanical junctions. All leakage signals are ≤0.1 μv. With input terminal shorted, 3 μv of 35.2 Mc appears on the output connector.

The limiting characteristics are viewed in Fig. 10. An input signal loss of 31 db can still provide the required +13-dbm level.

Power supply variations versus the 35.2 Mc output level are shown in Fig. 11. A DC-supply loss of 20% can still provide the +13-dbm output.

The synthesizer was subjected to a temperature environment from 0 to 50°C with results shown in Fig. 12.

G. Efficient Data Systems

1. Evaluation of the DSN Teletype Communications System

a. Introduction. The DSN teletype communications system is used to send messages from the Goldstone Space Communications Station to all DSN stations using the NASCOM communications processor at the Goddard Space Flight Center. The system consists of teletype equipment at each location and some internal coding to guard against errors in transmission. In addition, in

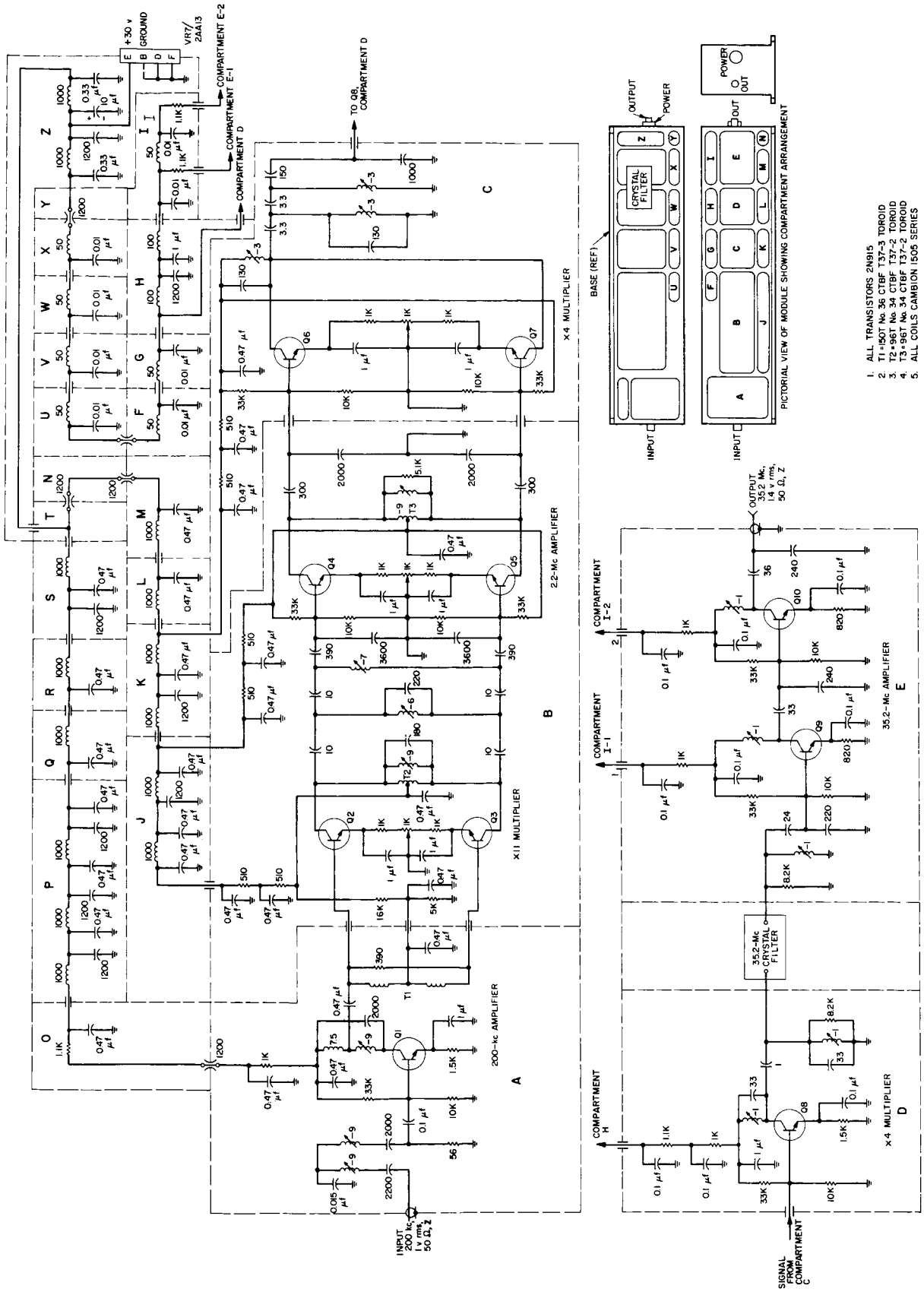

Fig. 9. 35.2 synthesizer central frequency synthesizer

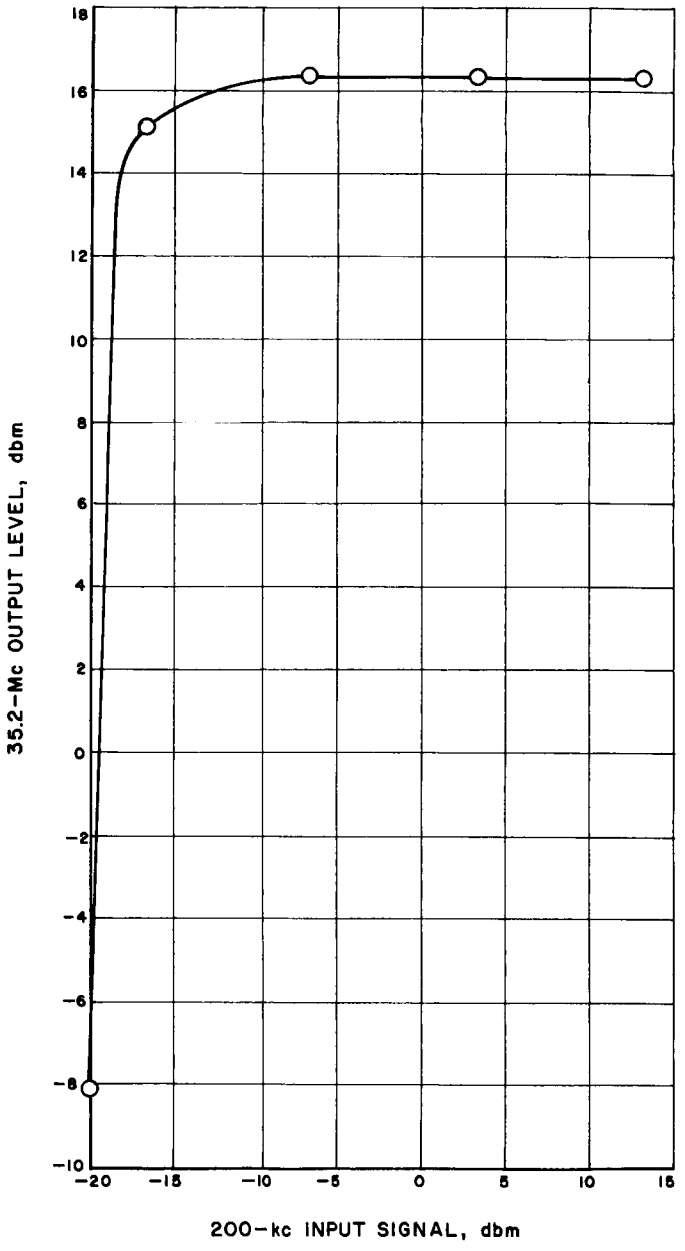

Fig. 10. Limiting characteristics

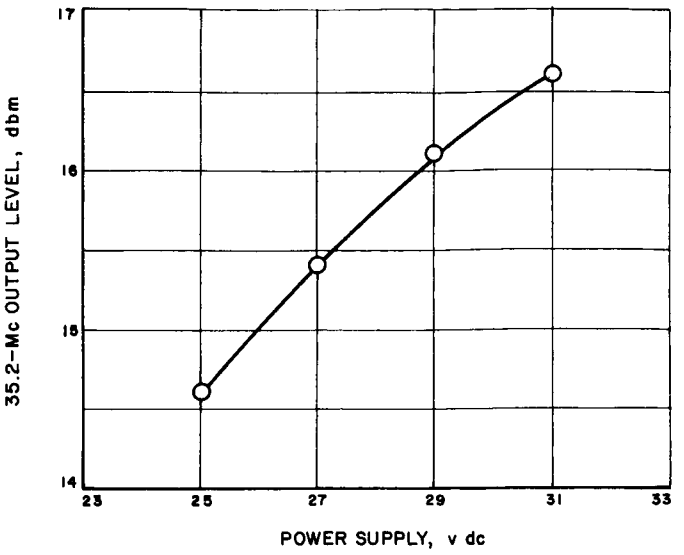

Fig. 11. Power supply variations versus 35.2-Mc output

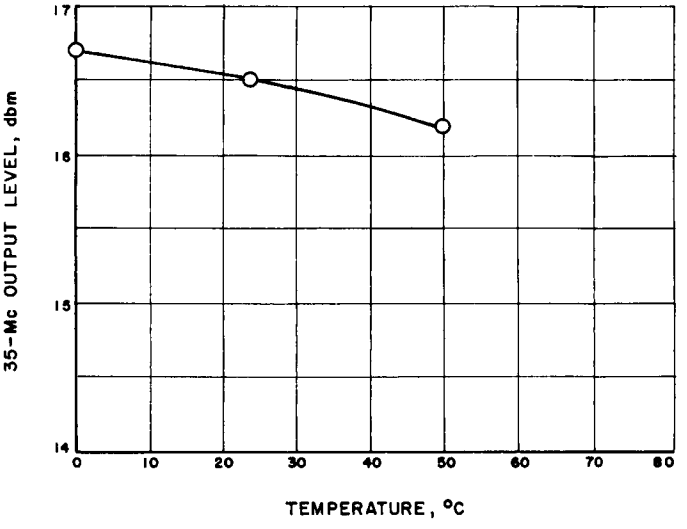

Fig. 12. Temperature versus output

the loop from the Space Flight Operations Facility to the Johannesburg Tracking Station, there is a phase when messages are sent by high-frequency radio; transmission is generally believed to be least reliable over this link.

An experiment was designed to test the operation of this system, since adequate information concerning its operation was not available. The only input available was a string of teletype symbols, so a tape of 3200 teletype symbols was prepared using a pseudonoise shift register of degree 23. The information on this tape, fed into the system daily through the Goldstone communications center, was interpreted as a message and was sent to all DSN stations. The phase of the experiment reported here used mission circuits, not NASCOM circuits. The information on the received tapes was transmitted back to Goldstone, and the tapes were returned by air freight. The one-way tapes (those mailed to Goldstone) and the two-way tapes (information transmitted back) served as the output of the teletype machine. An understanding of its operation was obtained by examining these outputs.

b. Examination of the output tape. Ideally, the output tape of the teletype machine should correspond exactly

to the input tape. A computer program to compare the two tapes was written, and the output tapes were examined. Preliminary results of this examination were given in *SPS 37-33*, Vol. III, pp. 109–110. A total of 127 output tapes was compared with the input tape, and only 17 corresponded exactly. A major difference between the input tape and all of the remaining 110 output tapes was the exchange of one teletype symbol for another; however, another type of error caused 38 of these tapes to be placed into a special category to be examined subsequently. The interchanges of teletype symbols may actually have been physical exchanges in the message, but more likely were caused by a change in some of the five levels of binary bits that make up the teletype symbol. Error patterns in 1, 2, 3, 4, and 5 of these levels were noted in the output tapes. The number of error patterns of each kind that occurred is given below:

Type of pattern	Number of occurrences
Single	1682
Double	33
Triple	19
Quadruple	8
Quintuple	1

Changes that occur in the various levels can be of two kinds: a $0 \rightarrow 1$ change or a $1 \rightarrow 0$ change. The number of patterns for each of these changes is:

Type of pattern	Number of occurrences	
	$0 \rightarrow 1$	$1 \rightarrow 0$
Single	1522	185
Double	21	17
Triple	3	10
Quadruple	1	4
Quintuple	0	0

The totals of the error patterns given here are different than those given in the first table, which indicates that some of the error patterns included there are of a mixed type; i.e., in the pattern of errors of some symbols, some errors are of the $0 \rightarrow 1$ type and some are of the $1 \rightarrow 0$ type. There are nine tapes in all that have multiple error patterns with errors split between the $0 \rightarrow 1$ and $1 \rightarrow 0$ types.

The error patterns are broken up into the various levels in which they occur in the following table:

Type of change	Number of occurrences in indicated level					Total number of occurrences
	1	2	3	4	5	
$0 \rightarrow 1$	135	121	84	603	634	1577
$1 \rightarrow 0$	29	22	32	88	94	265

The $0 \rightarrow 1$ errors are the most frequent; in fact, there are 38 tapes that have only $0 \rightarrow 1$ errors, whereas only 3 tapes that have only $1 \rightarrow 0$ errors. Also, of the 31 tapes that have errors of each type, in 17 cases the errors of the $0 \rightarrow 1$ variety predominate, while in 2 cases the $1 \rightarrow 0$ errors are the most frequent. The other 12 cases are fairly even as to types of errors.

There were 38 tapes (and possibly 3 others) with a special kind of error. This error appears to be of a type which was totally unexpected. When the tapes were examined, it seemed that about half of the bits were in error from some point on to the end of the tape. This phenomenon was due to an insertion or deletion of a teletype symbol in the message. Since the bits were formed in a degree 23 shift register, if some bits are deleted (or inserted) at any position in the tape, the correlation from that point on is essentially zero. Hence, half of the bits would appear to be in error.

c. Analysis of the communications system. The synchronization problem caused by the insertion and deletion of symbols was totally unexpected. However, corrective action is possible by various synchronization and coding techniques.

A noticeable feature is the heavy accumulation of errors in the fourth and fifth levels of the teletype symbols. Teletype experts feel this is due to a "surging effect"; since the fourth and fifth levels are punched in the teletype tape last, any accumulation of error is concentrated in these levels.

Another feature apparently due to the mechanics of the teletype machine is the larger proportion of $0 \rightarrow 1$

errors. It seems the machine will more often *punch* the wrong thing than *not punch* the wrong thing.

As a final observation, the average over-all teletype character error rate for all tapes not having synchronization errors is about 0.005. The one-way equivalent of this error rate is about 0.003.

d. Use of the communications system. It is desirable to send spacecraft and other operational messages through the system in strict binary format; but, since certain errors seem to occur in transmission, error-correction techniques must be employed. A computer program is being written to encode and subsequently decode messages with sufficient structure so that errors made in transmission will be corrected. This program will correct the $0 \rightarrow 1$ and $1 \rightarrow 0$ errors, as well as the errors caused by insertion and deletion of one symbol. The running time for encoding is milliseconds; for decoding, the time is less than 1 sec for a 3-sec word (15 teletype characters, including check and synchronization characters). The running times are based on a Scientific Data Systems, Inc., 900-series machine. The data show that, by using this code on the channels, the desired performance will be achieved.

e. New experiments. A new series of experiments is being run to test NASCOM circuits. As explained in *SPS 37-33*, the test message will have the fifth channel be odd parity on the first four for NASCOM compatibility. In fact, the error-correcting code chosen will have the same format: a code over the 16-element field with 8 information symbols (including 1 synchronization symbol) and 7 check symbols. The total rate (ratio of information bits to total bits) is therefore $(4 \times 7) / (15 \times 5) = 0.3733$. This low rate is suitable for command links from the Space Flight Operations Facility to the DSIF stations; the return link for monitor data could use a higher-rate code since reliability is not as necessary, but is still desirable.

The NASCOM tests are to be one-way only, with the tapes being returned every week by air freight. After the completion of these tests, the next tests should be with actual encoding and decoding.